NASA CONTRACTOR REPORT

NASA CR-2757

A COMPARISON BETWEEN NIMBUS 5 THIR AND ITPR TEMPERATURES AND DERIVED WINDS WITH RAWINSONDE DATA OBTAINED IN THE AVE II EXPERIMENT

James E. Arnold, James R. Scoggins, and Henry E. Fuelberg

Prepared by
TEXAS A&M UNIVERSITY
College Station, Tex. 77840
for George C. Marshall Space Flight Center

NATIONAL AERONAUTICS AND SPACE ADMINISTRATION • WASHINGTON, D. C. • OCTOBER 1976

1. REPORT NO.	2. GOVERNMENT ACCESSION NO.	3. RECIPIENT'S CATALOG NO.
NASA CR-2757		

4. TITLE AND SUBTITLE	5. REPORT DATE
A Comparison between Nimbus 5 THIR and ITPR Temperatures and Derived Winds with Rawinsonde Data Obtained in the AVE II Experiment	October 1976
	6. PERFORMING ORGANIZATION CODE
7. AUTHOR(S)	8. PERFORMING ORGANIZATION REPORT #
James E. Arnold, James R. Scoggins, and Henry E. Fuelberg	M-180
9. PERFORMING ORGANIZATION NAME AND ADDRESS	10. WORK UNIT NO.
Center for Applied Geosciences Texas A&M University College Station, Texas 77840	11. CONTRACT OR GRANT NO. NAS8-26751
	13. TYPE OF REPORT & PERIOD COVERED
12 SPONSORING AGENCY NAME AND ADDRESS	Contractor
National Aeronautics and Space Administration Washington, D. C. 20546	14. SPONSORING AGENCY CODE

15. SUPPLEMENTARY NOTES

Prepared under the technical direction of the Aerospace Environment Division, Space Sciences Laboratory, NASA, Marshall Space Flight Center

16. ABSTRACT

During the period of May 11 and 12, 1974, NASA conducted its second Atmospheric Variability Experiment (AVE II) over the eastern United States. In this time interval, two Nimbus 5 orbits crossed the AVE II area, providing a series of ITPR soundings as well as THIR data. Horizontal temperature mapping of the AVE II cloud field is examined using two grid print map scales. Implied cloud top heights are compared with maximum radar-echo top reports. In addition, shelter temperatures in areas of clear sky are compared with the surface temperatures as determined from 11.5 micrometer radiometer data of the THIR experiment.

The ITPR sounding accuracy is evaluated using interpolated radiosonde temperatures at times nearly coincident with the ITPR soundings. It was found that mean differences between the two data sets were as small as 1.3°C near 500 mb and as large as 2.9°C near the tropopause. Specific differences, however, were much larger. The differences between ITPR and radiosonde temperatures at constant pressure levels were sufficient to induce significant differences in the horizontal temperature gradient.

Cross sections of geostrophic wind along the orbital tracks were developed using a thermal wind buildup based on the ITPR temperature data and, as a check, the radiosonde temperature data. Since the data spacing for both the ITPR and the radiosonde data was approximately the same, differences between the radiosonde and ITPR geostrophic winds could be explained on the basis of differences in the ITPR and radiosonde temperature gradients.

17. KEY WORDS	18. DISTRIBUTION STATEMENT
	Category 47

19. SECURITY CLASSIF. (of this report)	20. SECURITY CLASSIF. (of this page)	21. NO. OF PAGES	22. PRICE
Unclassified	Unclassified	83	$4.75

For sale by the National Technical Information Service, Springfield, Virginia 22161

AUTHORS' ACKNOWLEDGMENTS

The authors wish to express their appreciation to a number of people who provided assistance in the research and the preparation of this report. We wish to acknowledge the help of Mr. Gregory S. Wilson in processing a portion of the AVE related data and Ms. Nancy Fucik for her help in preparing and drafting the figures used in this report. We are also indebted to Ms. Kay Dobbins for typing the text.

TABLE OF CONTENTS

LIST OF FIGURES

LIST OF TABLES

1. INTRODUCTION

Atmospheric temperature profiles are computed from Nimbus 5 data from a combination of experiments onboard the satellite. Under optimum conditions the most accurate satellite-derived profile is one which makes use of the Infrared Temperature Profile Radiometer (ITPR), the Nimbus-E Microwave Spectrometer (NEMS), and the Selective Chopper Radiometer (SCR). Under certain conditions an abbreviated solution may be used such as a combination between the NEMS and the SCR experiments (Solution 1) or the ITPR and SCR experiments (Solution 2). If all consistency checks are satisfied in the development of the ITPR+SCR and NEMS+SCR profiles, an ITPR+NEMS+SCR (Solution 3) profile is determined.

Previous studies comparing Nimbus 5 temperature profiles with radiosonde profiles indicated that reasonable temperature cross sections could be developed using the satellite-derived information. Smith and Woolf (1974) found that standard deviations between radiosonde observations (RAOB) and Nimbus 5 temperatures, on the basis of cross section analyses, were a maximum in the low troposphere below 850 mb and near the tropopause with mean deviations of 2.6°C and 3.6°C, respectively. In the mid-troposphere (700 to 400 mb), the mean standard deviation between ITPR and RAOB temperatures was approximately 1.6°C. Temperature gradients evaluated along the orbital track proved more accurate than individual temperatures. Gradient errors of 1.7 and 1.8°C/3°lat were found in the lower and upper troposphere. Smaller errors in the gradient of temperature rather than in individual temperatures were due to an apparent bias in the Nimbus temperature soundings at similar levels. For example, large differences between the RAOB and Nimbus temperatures were found consistently near the tropopause due to the satellite reduction technique which makes use of climatological radiance data to obtain the initial minimum information solution in determining the profile.

Cross sections of thermal and geostrophic winds were computed from satellite-derived cross sections of temperature by Smith and Woolf (1974), and by Shen, Smith, and Woolf (1975) along the Nimbus orbital track. Both studies produced encouraging geostrophic wind fields developed from the satellite-derived thermal fields. In particular, jet stream maximums were defined and agreed better with the apparent double jet indicated in satellite photographs than did an analysis based on RAWIN data only.

Use of satellite-derived temperature profiles to develop geostrophic wind fields has been explored on a hypothetical basis by Togstad and Horn (1974) in

a study which examined the influence of sensor error and distance over which the gradient was determined on the derived geostrophic wind field. It was found that the use of a 2°lat distance to evaluate the temperature gradient provided the greatest resolution without undue problems due to sensor inaccuracies in the evaluation of specific temperatures. Detail in the pattern of geostrophic wind was gradually lost as the distance increased over which the horizontal gradient was evaluated. In addition, maximum wind values decreased from those determined over smaller gradient distances. The horizontal gradient of temperature evaluated over 4°lat produced a satellite-derived geostrophic wind field which was much like that depicted using RAWIN data.

The development of a geostrophic wind profile or cross section requires a tie-on wind somewhere in the profile to which thermal winds between layers can be added. Smith and Wolf (1974) appear to use 1000 mb while Togstad and Horn used 700 mb. Duncan and Kays (1974) suggest that the tie-on wind might be in the mid troposphere, perhaps a 500-mb wind forecast. Without the tie-on wind the thermal wind buildup will produce a relative wind profile only.

Studies of winds derived from ATS cloud vectors provide an encouraging source of tie-on winds in data-sparce areas. Hubert and Whitney (1974) and Poteat (1973) indicate low-level winds derived from cloud motion and high-level winds derived by cirroform cloud motion are reasonably representative of the actual wind field at cloud level. If the cloud level can be further specified by measuring cloud-top temperatures to more accurately place the observed cloud features being tracked, even better tie-on wind values may be determined.

The second Atmospheric Variability Experiment (AVE II) undertaken by NASA was run for a 24-h period in May 1974. Its purpose was to provide data to study short-period variability of meteorological phenomena using the conventional rawinsonde network east of 105°W Longitude from soundings at 3-h intervals. During this time period, two orbits of Nimbus 5 passed across the AVE II network. The first overpass occurred at approximately 1700 GMT on 11 May 1974 with the second overpass occurring at 0600 GMT on 12 May. The presence of ITPR and RAOB vertical temperature profiles taken at approximately the same time provide an opportunity for a comparison between the two data sources.

When AVE II was run in May 1974, the Nimbus 5 radiometer systems had been aloft almost 2 1/2 years. By this time the ITPR scan mirror drive had failed, and the ITPR radiometer was operating in the nadir mode only. This confined the sounding points to positions along the orbital track. Although the nadir mode of operation severely limits the area of coverage for temperature profiles, it still permits the construction of atmospheric temperature cross sections along the orbital track.

In this study, the temperature differences between Nimbus 5 and radiosonde soundings will be evaluated along the cross section of each orbit over the AVE II area. Differences between ITPR and RAOB temperature gradients will be evaluated in the cross section, and the corresponding geostrophic wind differences illustrated. A tie-on wind at 500 mb will be used to develop the geostrophic wind field. This level was chosen primarily because it resulted in a minimum absolute error since maximum gradient errors occur at extreme ends of the thermal wind buildup.

The Nimbus 5 sounding system provides total liquid water for each sounding. The total liquid water amounts determined from the Nimbus 5 ITPR experiment over the AVE II area are compared with those determined from radiosonde soundings. Such a comparison has previously been made over the AMTEX area by Shen, Smith, and Woolf (1975) on a day-by-day basis. Generally, they found fair agreement between values of total liquid water obtained from ITPR and RAOB data although the ITPR amounts were slightly less than the RAOB totals.

In addition to the ITPR data and the computed geostrophic winds, temperature mapping of the surface and/or cloud tops can be accomplished using the 11.5 micrometer sensor of the THIR experiment. Under ideal conditions, this will provide contour maps of the cloud tops as reflected in their temperature field. Cloud-top temperature mapping and implicit cloud-top heights are briefly examined in this study using grid print maps of 1:10,000,000 and 1:2,000,000 scale. THIR equivalent black body temperatures of the surface determined from the 1:10,000,000 mapping data are compared with shelter temperatures.

2. THE DATA SOURCES

The AVE II data set consisted of rawinsonde data acquired at 3-h intervals from 1200 GMT on 11 May 1974 to 1200 GMT on 12 May 1974 for all the United States radiosonde stations east of 105°W Longitude. The data were processed at each contact of the radiosonde baroswitch by techniques described by Fuelberg (1974). Twenty-five mb data from the special rawinsonde data set have been published by Scoggins and Turner (1974). Because of the more frequent time periods in the AVE data, near simultaneous data from satellite and RAOB sources occur. Actual spatial separation between the Nimbus 5 sounding points and RAWIN soundings were less than 2°lat and averaged 1.2°lat on the daytime orbit (6932), and 1.8°lat on the nighttime orbit (6939).

Comparisons between the Nimbus 5 and the RAOB-measured temperatures were carried out by interpolating the RAOB temperature values at levels corresponding to those at which the Nimbus 5 sounding temperatures were determined. This was accomplished by making a temperature analysis on constant pressure maps at the levels corresponding to the ITPR temperature levels--920, 850, 700, 500, 400, 300, 250, 200, 150, and 100 mb. In all cases this reduced the difference between the individual RAOB temperature profiles and the satellite temperature profiles.

The Nimbus 5 soundings were processed by The Goddard Institute of Space Sciences and provided by NASA in reduced form which included solutions from the ITPR+SCR (Solution 1), NEMS+SCR (Solution 2) and ITPR+NEMS+SCR (Solution 3). Comparisons between RAOB and Nimbus 5 soundings were made using Solution 3 profiles when available. Ten of the twelve soundings which fell in the AVE II area were generated using the Solution 3 technique, while the remaining two Nimbus 5 profiles were generated using Solution 2 techniques. Details of the Nimbus 5 sounding reduction techniques have been described by Smith et al. (1974).

Mapping of surface temperatures was accomplished in this study using the 11.5 micrometer channel of the THIR experiment. Grid print maps of temperature on Mercator projections of 1:10,000,000 and 1:2,000,000 scales were provided by NASA over the AVE area. The 1:10,000,000 maps were used to determine general cloud-top temperatures over large regions as well as to compare THIR temperatures with reported shelter temperatures in clear areas. The 1:2,000,000 mappings were used primarily to examine small areas of particular interest.

ATS III photographs as well as supportive National Weather Service information were used to define the overall meteorological situation. Service C and A teletype data as well as radar summaries including representative echo top heights were used to further define the synoptic situation and convective conditions. In addition, selected radar scope photographs at individual stations were used for correlation with cloud-top temperatures.

3. SYNOPTIC FEATURES

In choosing a time to conduct the data collection phase of AVE II, it was desirable to have a synoptic situation with a broad spectrum of metecrological phenomena occurring. In particular, it was desirable to have an advancing cold front with associated frontal weather, convective activity in the form of thunderstorms, stratiform cloud cover over some of the area, and a significant region which was free of clouds. About equal amounts of skill and luck went into the decision to initiate the 24-h experiment at 1200 GMT on 11 May 1974. Fortunately, all desired conditions were observed.

The upper-level flow had been dominated by a trough over the western United States for several days prior to the experiment. On May 10 the southern end of the upper-level trough separated from the main trough and began a slow northeastward drift as a cut-off low. By the time the AVE II observation period began, this upper-level low was approaching the Gulf Coast at the southern end of the AVE II network, while a cold front at the surface was advancing toward the western boundary of the network. At the first observation period, 1200 GMT on 11 May 1974, the frontal system which had been advancing from the west had moved into the western part of the network and extended southward from a low center over Minnesota through northern Missouri, central Oklahoma, and into northwest Texas. A strong southerly flow of warm, moist air was taking place over the eastern Gulf Coast associated in part with the surface reflection of the upper-level low now in the northern Gulf of Mexico. A retreating cold air mass covered the northeastern portion of the United States.

By midday on 11 May the eastward moving cold front had moved well into the AVE II network (see Fig. 1) and was accompanied by extensive cloud cover along the frontal boundary with imbedded rain showers and limited thunderstorm activity. The southern low pressure center had moved over the Gulf Coast bringing widespread cloud cover and rain. The ATS III photograph taken at 1800 GMT on 11 May, and shown in Fig. 2a, reveals the extent of cloud cover present over the eastern United States. The clearing trend behind the frontal band is evident in the central United States and the cyclonic configuration of the cloud mass associated with the upper-level low over the central Gulf Coast is seen dominating the southern portion of the AVE network.

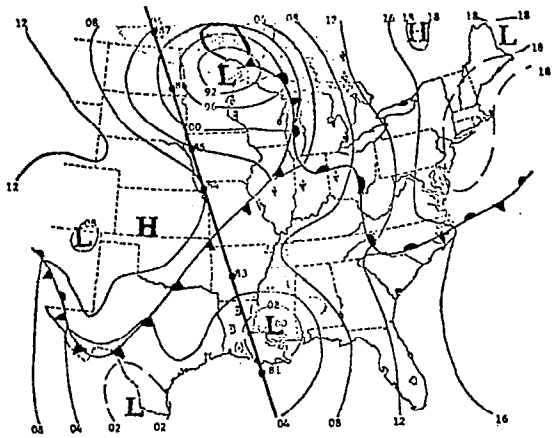

a) Surface

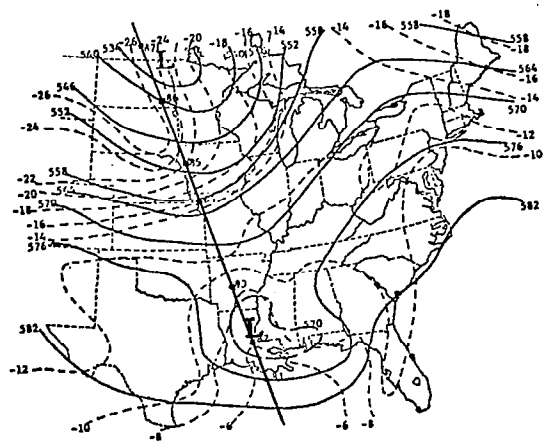

d) 500 mb

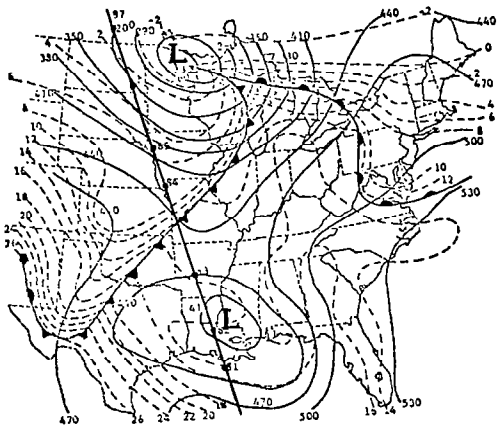

b) 850 mb

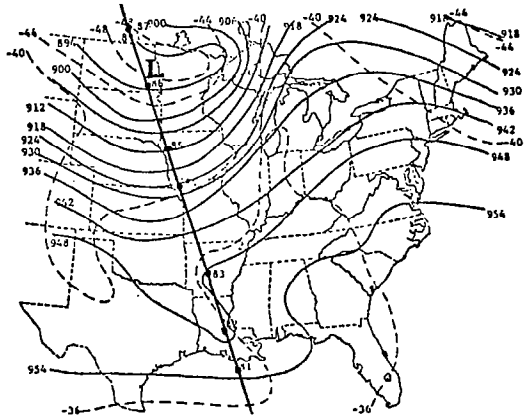

e) 300 mb

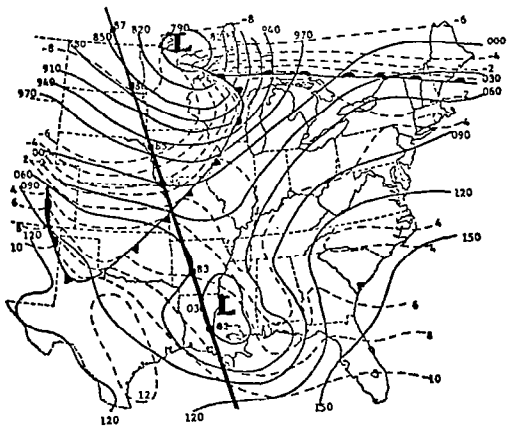

c) 700 mb

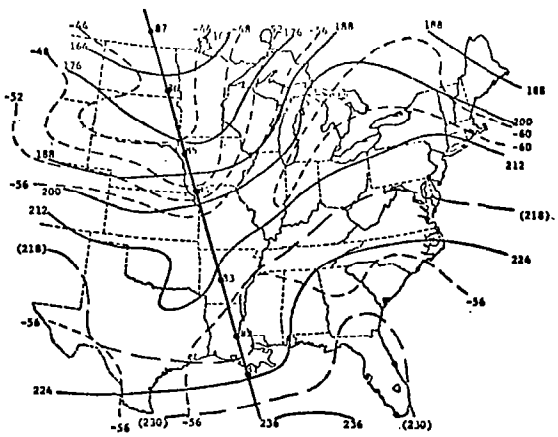

f) 200 mb

Fig. 1. Surface and constant pressure analysis of the synoptic situation at 1800 GMT on 11 May 1974. The Nimbus 5 orbital track and associated ITPR data points for Orbit 6932 are shown on the charts.

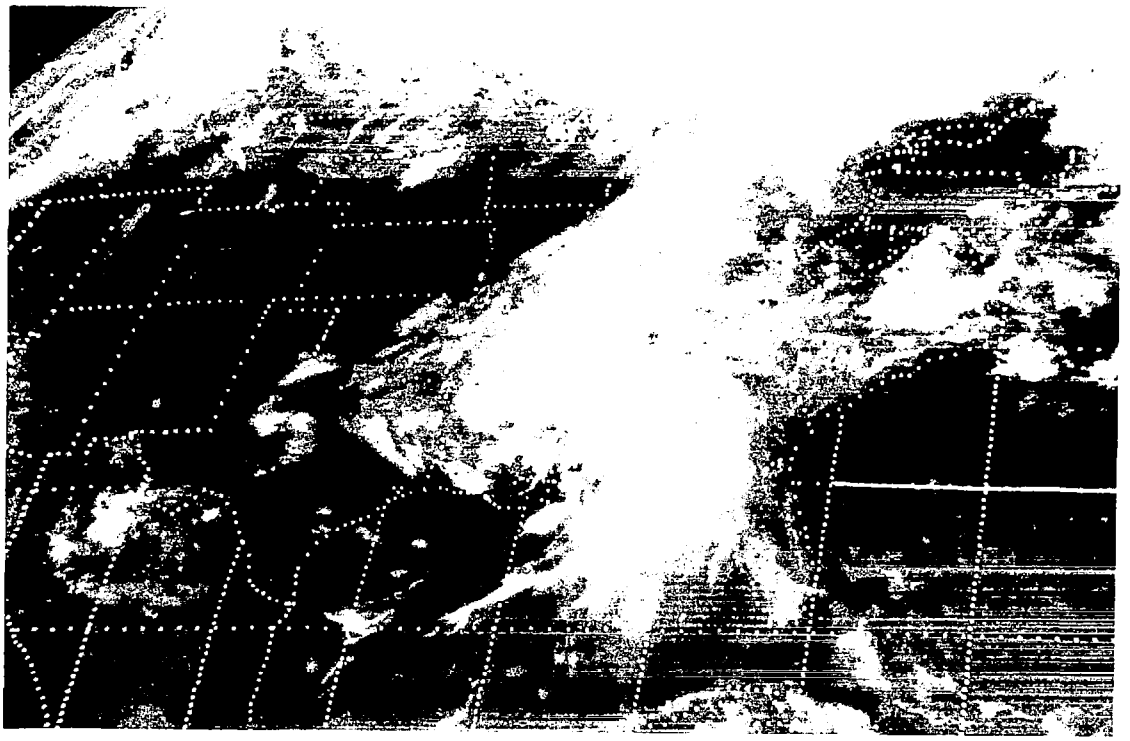

a) 1800 GMT on 11 May 1974

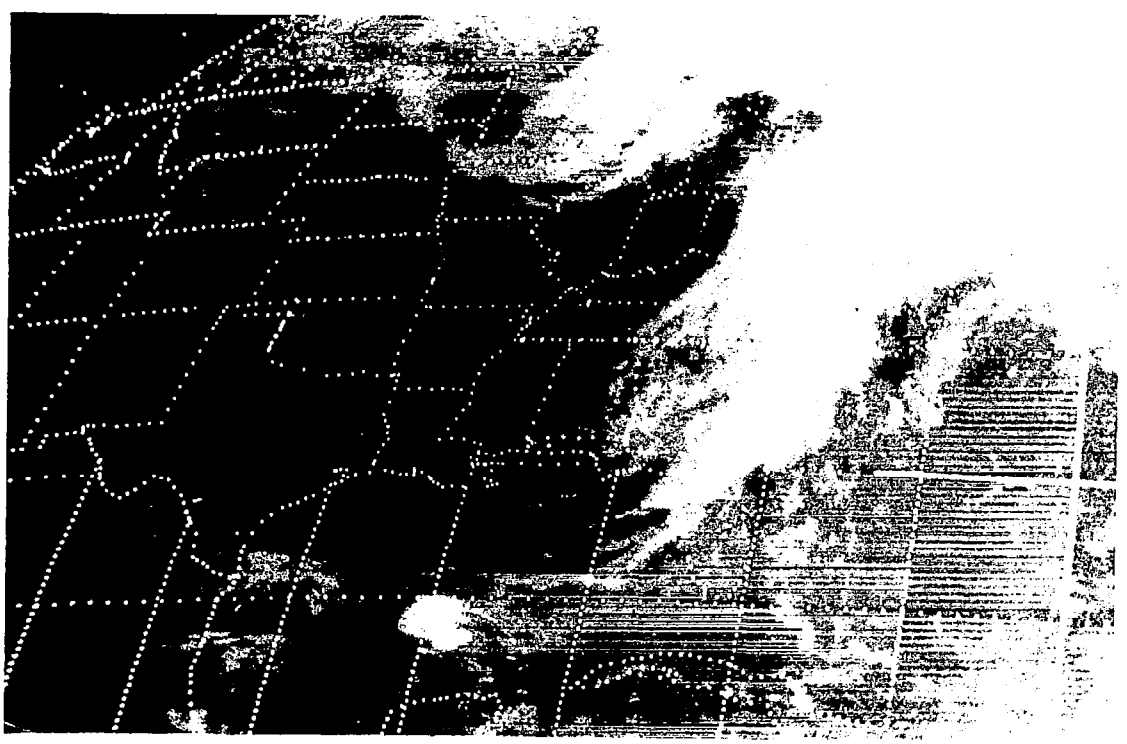

b) 1300 GMT on 12 May 1974

Fig. 2. ATS III photographs of the eastern United States showing the AVE II data area.

As the experiment progressed, the cold frontal system moved eastward while the upper-level low in advance of the cold front moved northeastward. By the morning of the 12th, the frontal band and the cloud mass associated with the northward moving low had merged into an extensive cloud shield over the eastern United States. This is illustrated in the ATS III photograph shown in Fig. 2b taken at 1300 GMT on 12 May after the end of the observational period. During the period of AVE II, the central part of the data network experienced a clearing trend as the frontal system moved eastward.

Orbit 6932 of the Nimbus 5 satellite passed over the AVE II network from 1711 to 1717 GMT on 11 May only slightly before the actual release time of the radiosonde balloons from the surface stations. The orbital track and the ITPR sounding points are illustrated on the 1800 GMT constant pressure charts shown in Fig. 1. The orbital track itself lies essentially along the trough line being slightly to the west of the trough at lower levels and slightly east of the trough in the upper troposphere. The orbit crossed the frontal zone between sounding points 83 and 84. Isotherms were almost normal to the orbital track throughout the troposphere in the northern half of the orbit, while along the southern portion of the orbital track the isotherms tended to parallel the track in the cold pool of air associated with the low pressure center over Mississippi.

Orbit 6939 passed over the AVE II network between 0613 and 0619 GMT on 12 May. By this time the cold front at the surface had moved to the Texas Gulf Coast and the orbital track lay almost entirely within the region bounded by the surface cold front. The constant pressure charts for 0600 GMT and the associated track of Orbit 6939 are illustrated in Fig. 3. The ITPR data points lie to the west of the trough line in cloud-free air with the exception of the northern two points which occur near the occluded frontal low over Lake Superior. For the most part, the orbital track is perpendicular to the isotherms as well as the geostrophic flow indicated by the contour field.

The distribution of the total liquid water across the AVE II network at the time of the satellite overpasses was considered typical of the prevailing synoptic situation. Figure 4 illustrates the distribution of total precipitable water as determined from radiosonde observations at the time of each orbit. At 1800 GMT the satellite track extended from a zone of maximum precipitable water, about 4.5 cm, across the frontal zone and into a zone of low precipitable water, about 1.5 cm. By 0600 GMT the drier polar air dominated the region covered by the track of Orbit 6939 reducing the range of precipitable water amounts at the

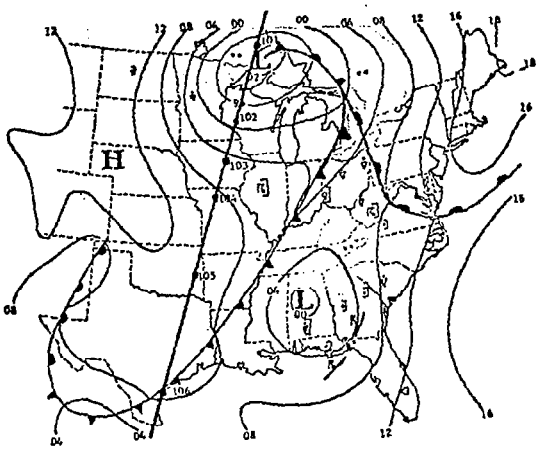

a) Surface

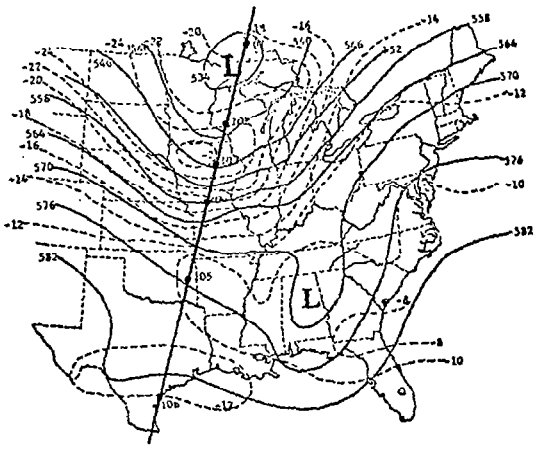

d) 500 mb

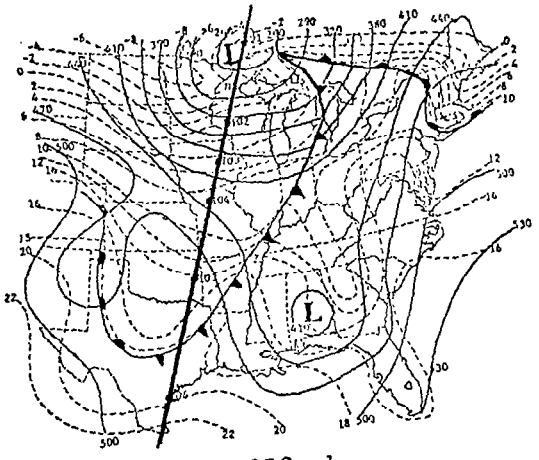

b) 850 mb

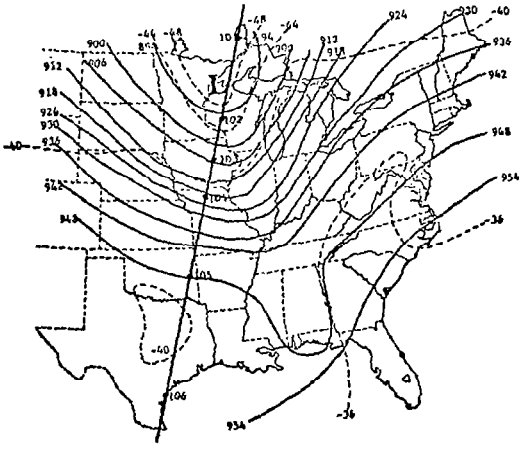

e) 300 mb

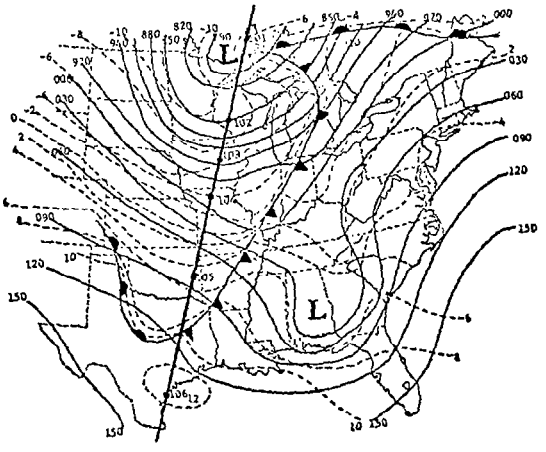

c) 700 mb

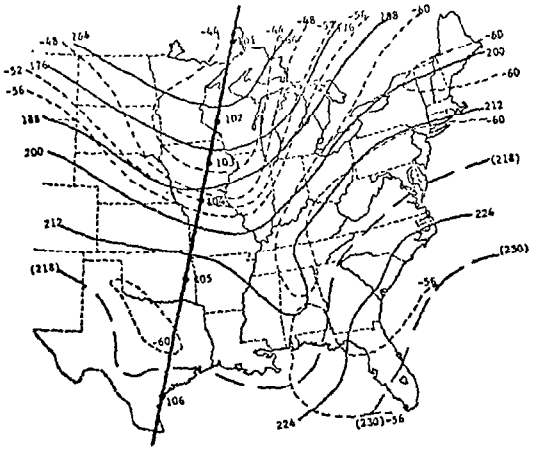

f) 200 mb

Fig. 3. Surface and constant pressure analysis of the synoptic situation at 0600 GMT on 12 May 1974. The Nimbus 5 orbital track and associated ITPR data points for Orbit 6939 are shown on the charts.

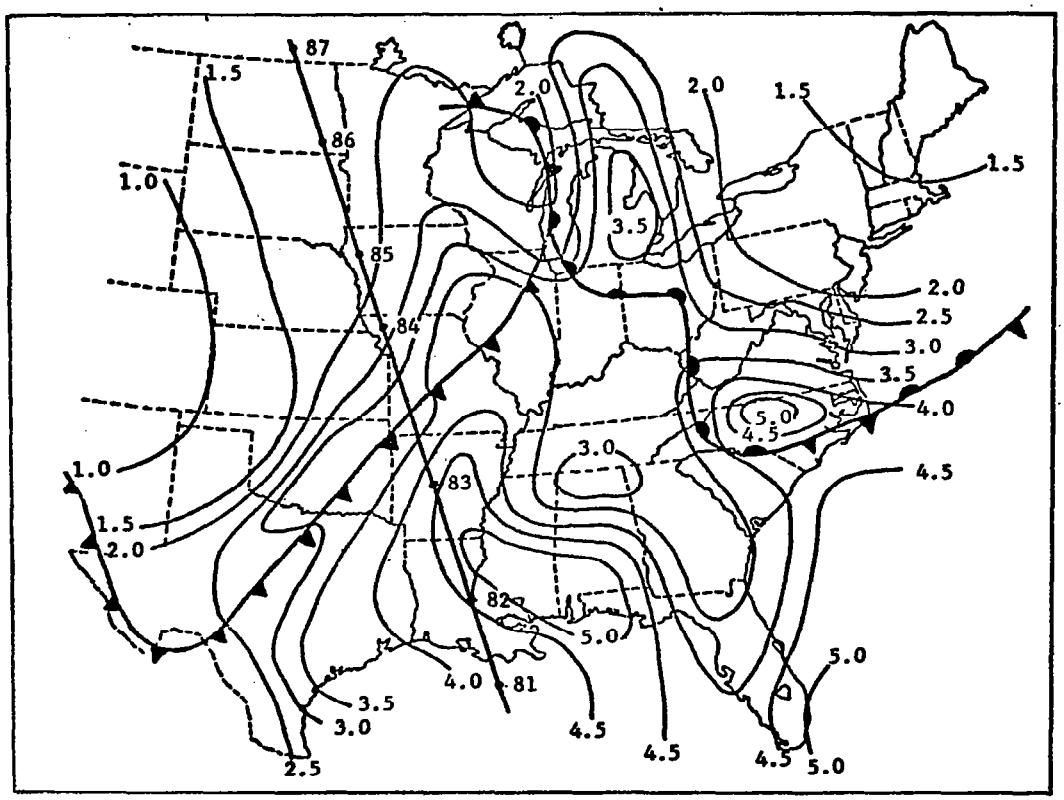

a) 1800 GMT on 11 May 1974

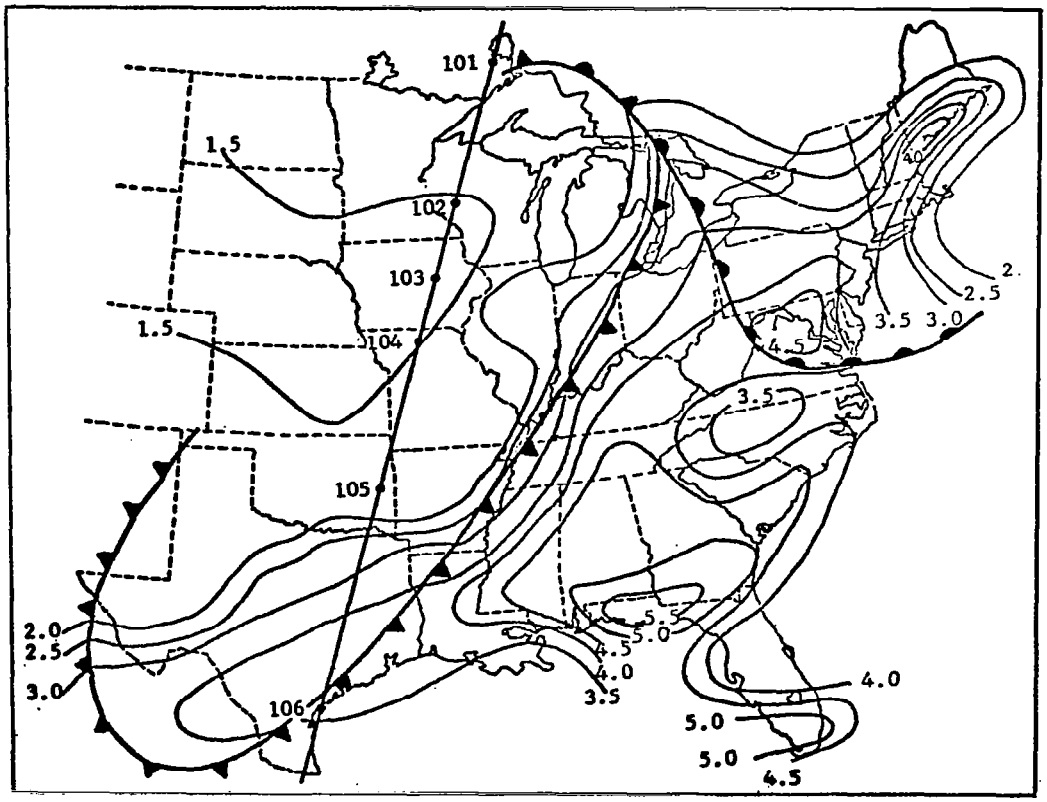

b) 0600 GMT on 12 May 1974

Fig. 4. Total precipitable water (cm) determined from the radiosonde data.

ITPR soundings points along the track. At both times, the moist tongue extended northward from the Gulf of Mexico in front of the cold front and across the warm front into the retreating polar air. A maximum of precipitable water at both observation times was associated with the northward drifting low center in front of the polar frontal zone.

Isolines of echo tops were analyzed over the AVE II network using National Weather Service radar summaries and are illustrated in Fig. 5 for the two time periods coincidental with the Nimbus 5 orbits over the network. Near Orbit 6932 at 1735 GMT, Fig. 5a, most echo tops along the frontal zone were on the order of 30,000 ft (9100 m) while echo tops associated with the low over the Gulf Coast ranged from 35,000 ft (10,670 m) in southern Mississippi to 45,000 ft (13,720 m) in the Gulf of Mexico off the Florida panhandle. Along the orbital track itself, only the southern portion contained any significant activity with reporting echo tops ranging from 20-30,000 ft (6100-9100 m). Using the 0530 GMT radar summary charts corresponding to Orbit 6939, significant areas of deep convection were present over the southeastern United States (Fig. 5b) with tops ranging from 30-50,000 ft (9100-15,250 m). This activity, however, was well east of the track for Orbit 6939. Along the orbital track itself, only limited activity is indicated on the basis of the radar charts and this is confined to the northern part of the track in the vicinity of ITPR sounding points 102 and 103.

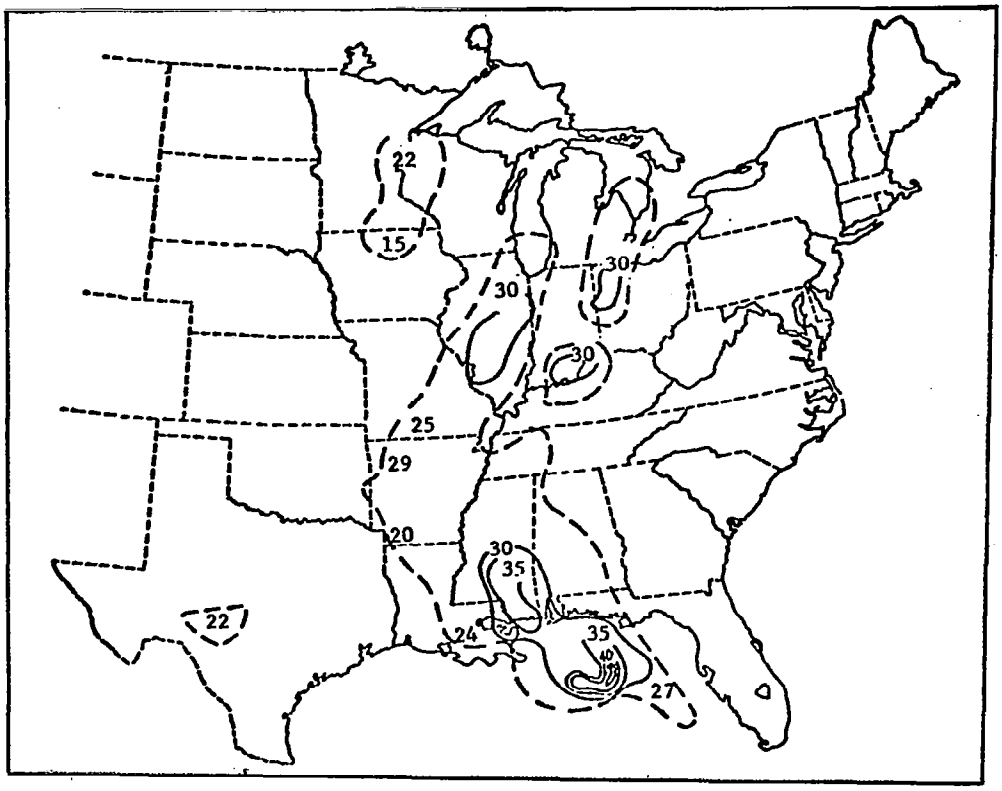

a) 1735 GMT (1800) on 11 May 1974

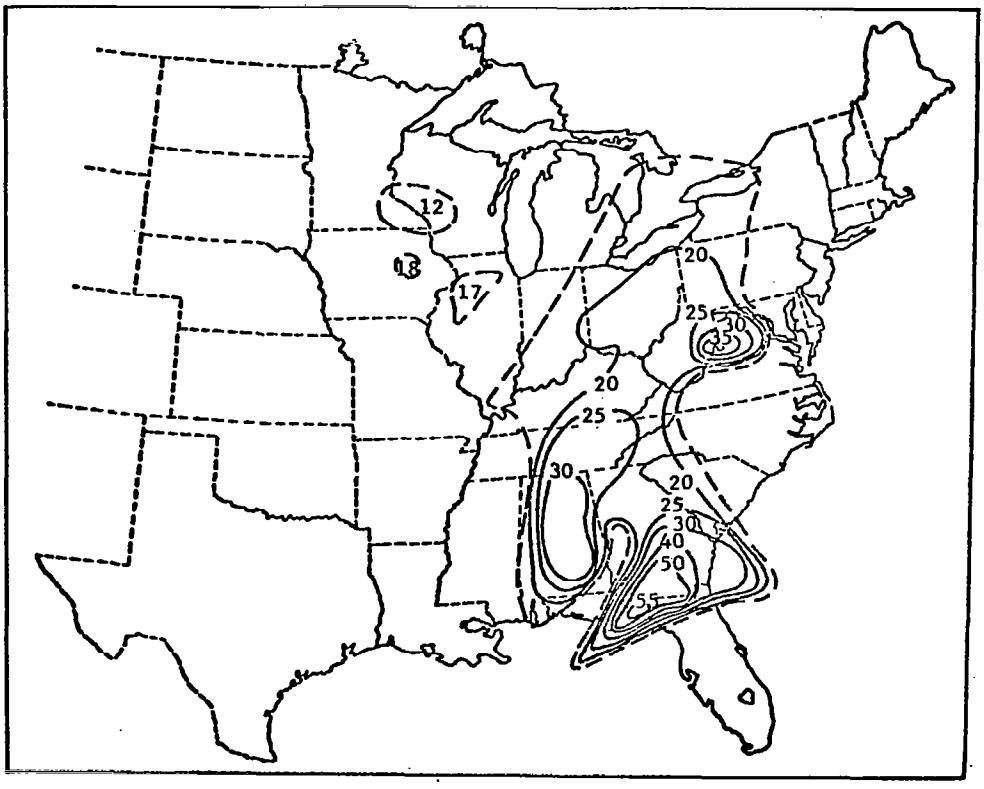

b) 0530 GMT (0600) on 12 May 1974

Fig. 5. Analysis of radar echo tops as reported in the National Weather Service radar summaries. Isolines of cloud tops are labeled in thousands of feet. Dashed lines delineate the general boundary of the radar echo regions.

4. THIR CLOUD TOP MAPPING

Temperature mapping of the surface and/or cloud tops can be accomplished using the 11.5 micrometer sensor of the THIR experiment if, among other things, it is assumed that the surfaces emitting the radiation received by the radiometer are radiating as if they were black bodies. From a practical aspect, the emissivity of clouds and particularly that of middle- and high-level clouds may differ considerably from unity (Platt, 1975; Allen, 1971). In many instances it is also possible that the field of view of the radiometer is not completely filled by a uniform temperature field. This would be the case with convective towers, or with scattered or broken cloud conditions where more than one emitting layer was contributing to the total radiation received by the radiometer. If it is assumed that the problem of non-unity emissivity and multiple layer sources can be temporarily disregarded, a map of the cloud and ground temperatures can be produced. If the temperature profile is known, cloud temperatures converted to cloud heights can be used to obtain a three-dimensional picture of the cloud-top distribution.

Using the 1:10,000,000 grid print maps on a Mercator projection, the temperature field derived from 11.5 micrometer data was analyzed for the southeastern portion of the United States during the orbits crossing the AVE II region. Comparison of the temperature field on 11 May (Fig. 6) with the cloud distribution shown in the ATS III photograph for the AVE area (Fig. 2a) indicates the general relationship that would be expected between cloud areas and cold radiation temperatures. The main mass of clouds in the central and southeastern part of the United States is associated with cloud-top temperatures on the order of 210 to 230 K. Although the exact height correlation with temperature varies from region to region on the map, the 250 K isotherm corresponds approximately to a height of 30,000 ft (9100 m), 230 K to 34,000 ft (10,360 m), and 210 K to 45,000 ft (13,700 m). Using this information, cloud-top temperatures can be relabeled as cloud-top contours. The extension of the main cloud mass from Illinois through Oklahoma and Texas is characterized by scattered and broken cloud cover at all levels with resulting non-representative cloud-top temperatures along this axis of the cloud band associated with the cold front in the central United States.

A comparison of the distribution of cloud-top temperature and, in particular, the associated heights with the contour chart of maximum echo tops on 11 May shown in Fig. 5a, reveals that the implied height field from the radiation data corresponds well with the radar-echo top information. In particular, echo tops of 30,000 ft (9100 m) in Illinois agree favorably with implied cloud-top heights

based on the radiation data. The echo height approaching 45,000 ft (13,700 m) off the Florida panhandle agrees well with the implied cloud tops of 45-50,000 ft (13,700-15,250 m) determined from radiation data in the 1:10,000,000 mapping.

By use of the 1:2,000,000 grid print mapping, the portion of the temperature field enclosed in the box over southern Illinois and eastern Missouri in Fig. 6 was reanalyzed and the result shown in Fig. 7. The corresponding area in the ATS III photograph (Fig. 2a) can be located by referring to the outlines of states. The great detail and small-scale variation in the temperature field apparent in Fig. 7 is not present in the 1:10,000,000 mapping shown previously. The warm tongue, A-B, present in the southeastern portion of Fig. 7 appears to be associated with the "clear" zone in the same area visible in the ATS photograph. In the far northwestern portion of Fig. 7 the warm radiation temperatures coincide with the clear sky conditions in the northwestern portion of the AVE II area. Between these two identifiable zones is an area of extensive cloud cover associated with the frontal system extending through this portion of the United States. The colder cloud-top temperatures can be relabeled as cloud heights by using the Peoria and Salem, Illinois, soundings. The areas with temperatures of 228 K and 232 K correspond to radiating cloud tops at approximately 33,800 ft (10,300 m) and 32,100 ft (9800 m), while the 224 K temperatures are associated with clouds at approximately 35,300 ft (10,750 m). Using these temperature-height relationships, the band of cold temperatures, C-D, northwest of the clearer zone corresponds to a cloud line with tops approximately 32-34,000 ft (9750-10,350 m). Behind this cloud band is a second warm band, E-F, followed by another cloud band, G-H, with tops about the same as that found further east. In fact, three cloud bands, C-D, G-H, and I-J, can be identified in the cloud-top temperature field before the main clear zone to the west is encountered. The cold temperatures in the far southeastern portion of the chart correspond to heights near 35,200 ft (10,730 m) and are associated with the low along the Gulf Coast.

Figure 7 is characterized by a cloud field which is predominantly cirroform with embedded thunderstorm systems associated with the cold front. The associated surface data and the radar presentation at St. Louis are shown in Fig. 8. The radar presentation shows a line of activity extending northeast-southwest across St. Louis with rain showers and thunderstorm activity reported in the surface data. Some indications of the second cloud band interpreted from the radiation data are also apparent in the radar display. The two surface stations reporting thunderstorm activity in the past hour, St. Louis and Decatur,

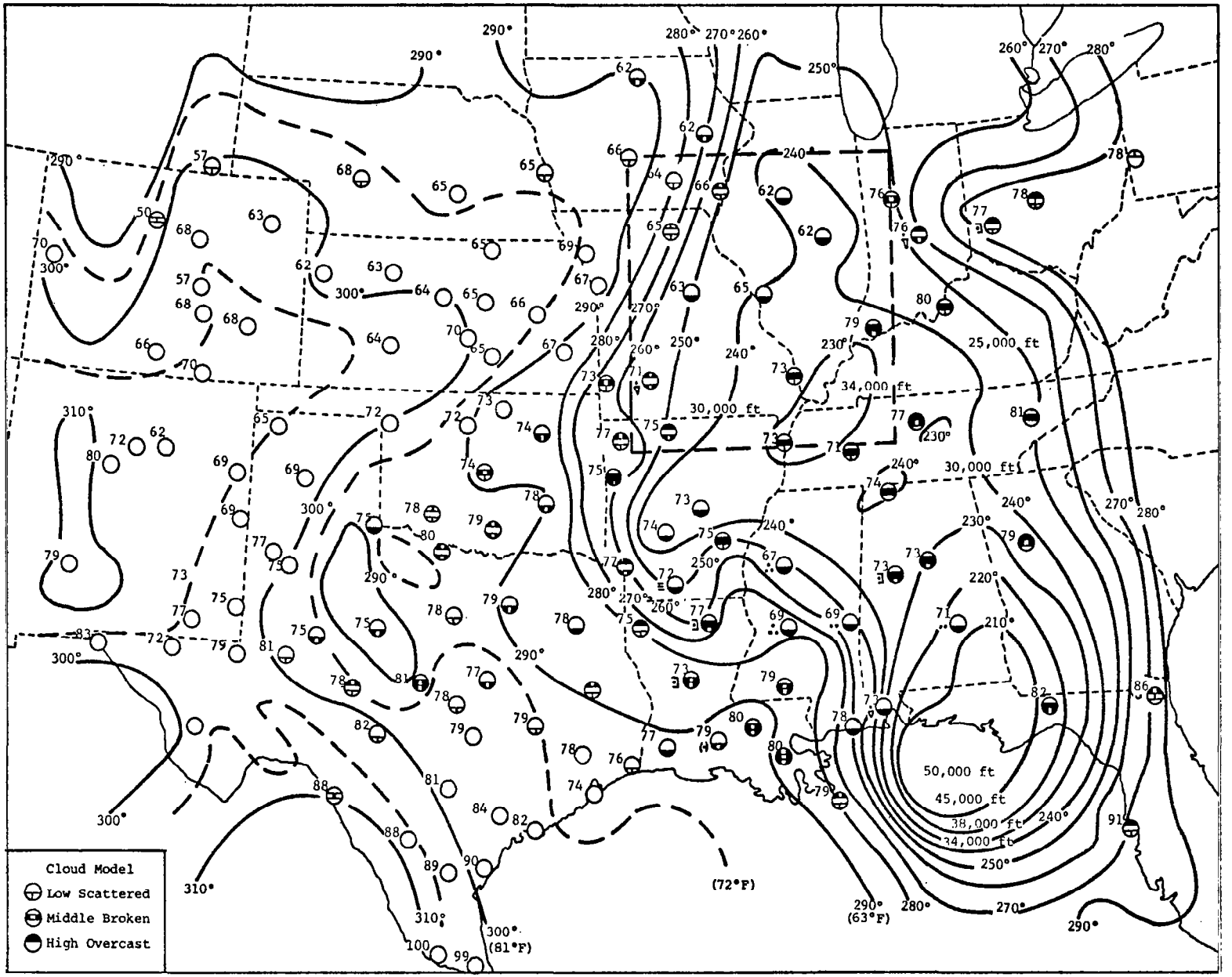

Fig. 6. THIR 11.5 micrometer equivalent black body temperature analysis for 1711 GMT (Nimbus Orbit 6932) on 11 May 1974. The analysis is from the 1:10,000,000 grid print map. Surface reports of temperature and cloud cover are for 1800 GMT. Representative cloud top heights corresponding to temperatures have been determined from associated RAOB data and are labeled on appropriate isotherms.

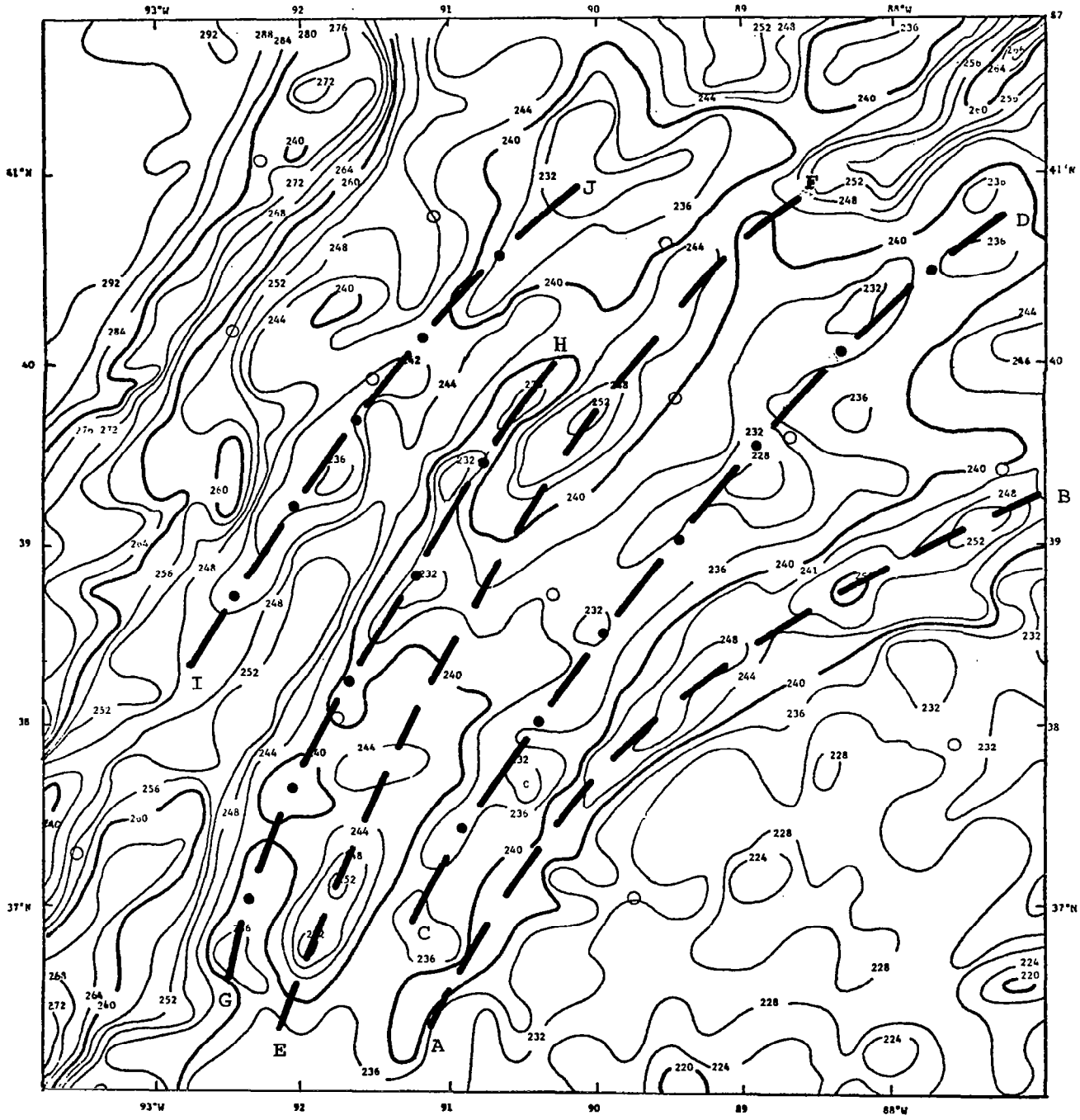

Fig. 7. THIR 11.5 micrometer equivalent black body temperature analysis using the 1:2,000,000 grid print mapping at 1711 GMT on 11 May 1974 for the region covered by the St. Louis, Missouri, radar. Dashed and dash-dot lines designate warm and cold temperature bands.

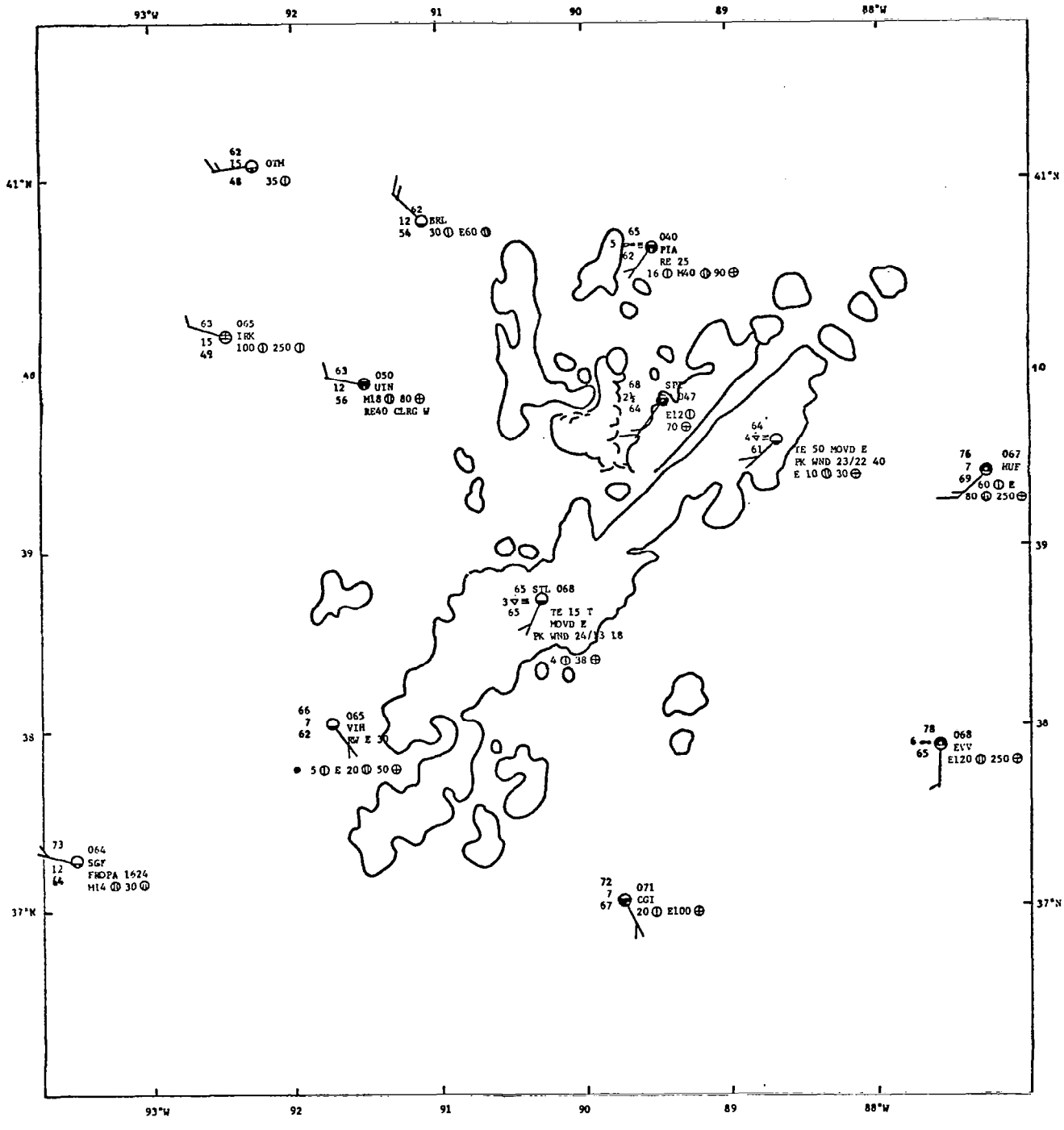

Fig. 8. St. Louis, Missouri, radar echo presentation and accompanying surface data at 1700 GMT on 11 May 1974.

Illinois are near regions of cloud-top maxima as interpreted from the radiation data and lie within the echo line observed from the St. Louis radar. Other cold spots in the THIR mapping do not necessarily occur coincidentally with radar echoes although as previously pointed out many do occur in lines which might be interpreted as bands of convective activity.

Accurate temperature mapping of the cirroform cloud cover present in Fig. 7 is complicated by the problem of varying emissivities for cirroform clouds. Emissivity measurements of cirrus clouds indicate that although dense patches or areas of cirrus have an emissivity approaching unity, a high percentage of cirrus is characterized by a much lower emissivity. For example, Platt (1975) found that the mean emissivity of jet stream cirrus was 0.28, while Allen (1971) estimated cirroform clouds to have an emissivity of about 0.35. In both studies there was an almost linear relationship between the number of cases and emissivity values. If it is assumed that the cirrus coverage is fairly uniform in Fig. 7, but that the actual emissivity varies across the cloud layer such as might be expected with embedded thunderstorms, an induced temperature gradient will be observed which has nothing to do with cloud-top height. If a second cloud layer is present under the cirrus with tops at approximately -10°C (about 17,000 ft or 5200 m), an assumption not out of line with surface cloud reports and radiosonde humidity values, an emissivity of the cirroform clouds of 0.35 would increase the apparent cloud-top temperature to 253 K or about that temperature observed for the warmer cloud-top temperatures. In reality, knowing the temperature field as depicted by the THIR radiometer is only a first step in defining the cloud-top height distribution. In cases such as presented here with extensive cirrus, cloud emissivities and coverage information are necessary additional ingredients which must be known before top contours can be adequately reproduced.

By the time Orbit 6939 on 12 May occurred, the major cloud systems had moved to the eastern portion of the United States leaving the central United States free from significant cloud cover. The temperature field derived from the 1:10,000,000 mapping of the 11.5 micrometer channel of the THIR experiment is presented in Fig. 9. The ATS III photographs (Fig. 2) reveal that the main cloud mass has a predominant north-south alignment. Over northern Florida the cloud tops should be at approximately 39,000 ft (11,900 m) based on the 220 K temperature. Convective tops slightly in excess of 50,000 ft (15,250 m) are indicated from the radar data (Fig. 5b). The 1:2,000,000

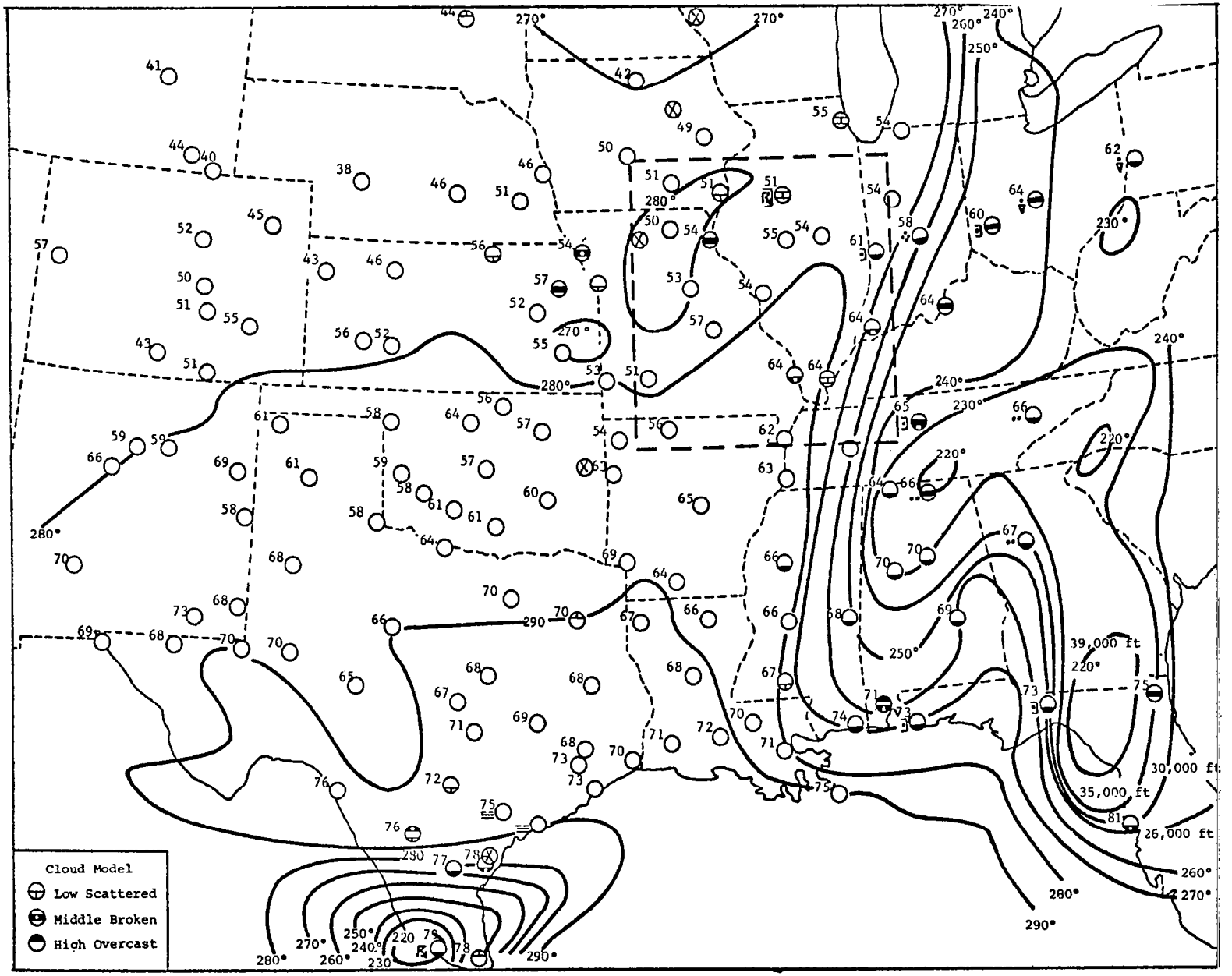

Fig. 9. THIR 11.5 micrometer equivalent black body temperature analysis for 0610 GMT (Nimbus Orbit 6939) on 12 May 1974. The analysis is from the 1:10,000,000 grid print map. Surface reports of temperature and cloud cover are for 0600 GMT. Representative cloud top heights corresponding to temperatures have been determined from associated RAOB data and are labeled on appropriate isotherms.

mapping data in this region indicate minimum cloud-top temperatures on the order of 209 K which at unit emissivity would correspond to top heights of approximately 46,000 ft (14,000 m), still somewhat below that indicated by the radar observations. Two factors probably contribute to the difference in THIR inferred heights and radar-top heights, viz, the relatively small size of the convective tops or turrets may not fill the area from which the resultant cloud-top temperature was determined, or the emissivity of the cloud top was considerably different from unity. The latter would be true if the upper cloud layer was primarily cirroform but does not seem likely if actual convective cloud tops dominated in the area; a combination of both effects probably are present. Over much of the remainder of the major cloud mass, inferred cloud-top heights from the THIR data agree reasonably well with radar-echo tops when viewing angle and area smoothing are considered.

It is of interest to reexamine the St. Louis area using the data from Orbit 6939. The THIR, 11.5 micrometer film strip over the AVE area is shown in Fig. 10 with the area to be illustrated in the synoptic and radar data as well as in the 1:2,000,000 mapping of the 11.5 micrometer THIR data outlined. A band of clouds can be seen extending southwestward through the small area to be considered. Figure 11 shows the synoptic reports over the region as well as the radar display at 0600 GMT. In this case the radar return seemed to be primarily ground clutter and anamolous propogation. A subsynoptic feature in the form of a wind shift line appeared to be moving through the area and is reflected in the wind shift reported at Springfield, Illinois. What cloud cover that did exist was primarily at Quincy, Illinois, in the form of an overcast middle cloud layer and the remains of thunderstorm activity at Peoria, Illinois.

It becomes apparent when the THIR temperature field is compared in detail with the synoptic reports, that the major percentage of the cloud band so apparent in the THIR data shown in Fig. 12 misses all the synoptic stations with the exception of Peoria, Illinois. St. Louis lies just on the eastern side of the band and remains clear for several hours after the time of Orbit 6932. The overcast reported at Quincy, Illinois, is west of the THIR cloud band but is in a region which is slightly cooler than the surrounding area. The Service A reports for Quincy indicate that the station went from clear at 0400 GMT to a layer of scattered clouds at 10,000 ft (3000 m) and broken

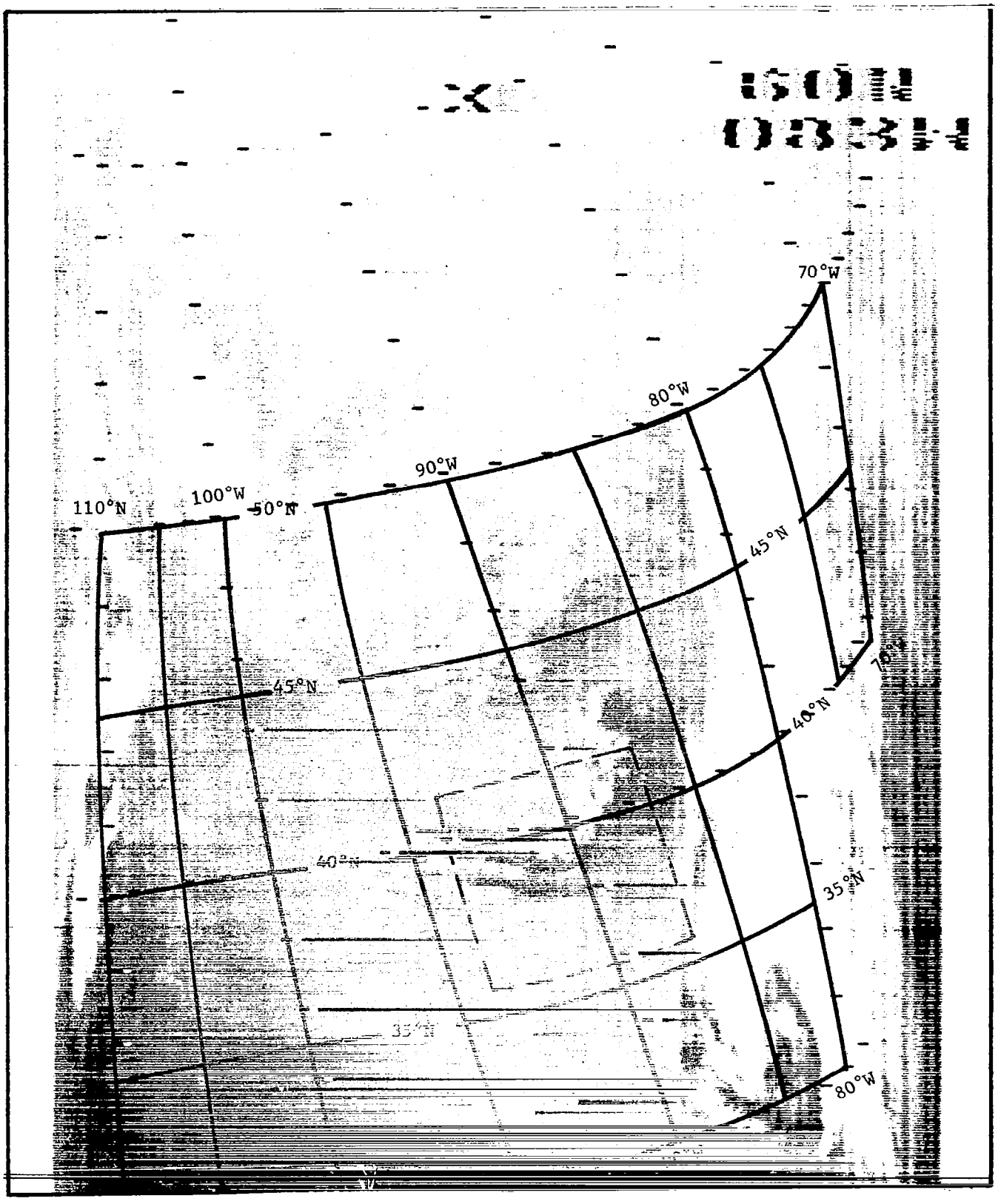

Fig. 10. Nimbus 5, 11.5 micrometer, THIR film for 12 May 1974 at approximately 0610 GMT. The dashed box in the center of the picture outlines the geographic area presented in Figs. 11 and 12.

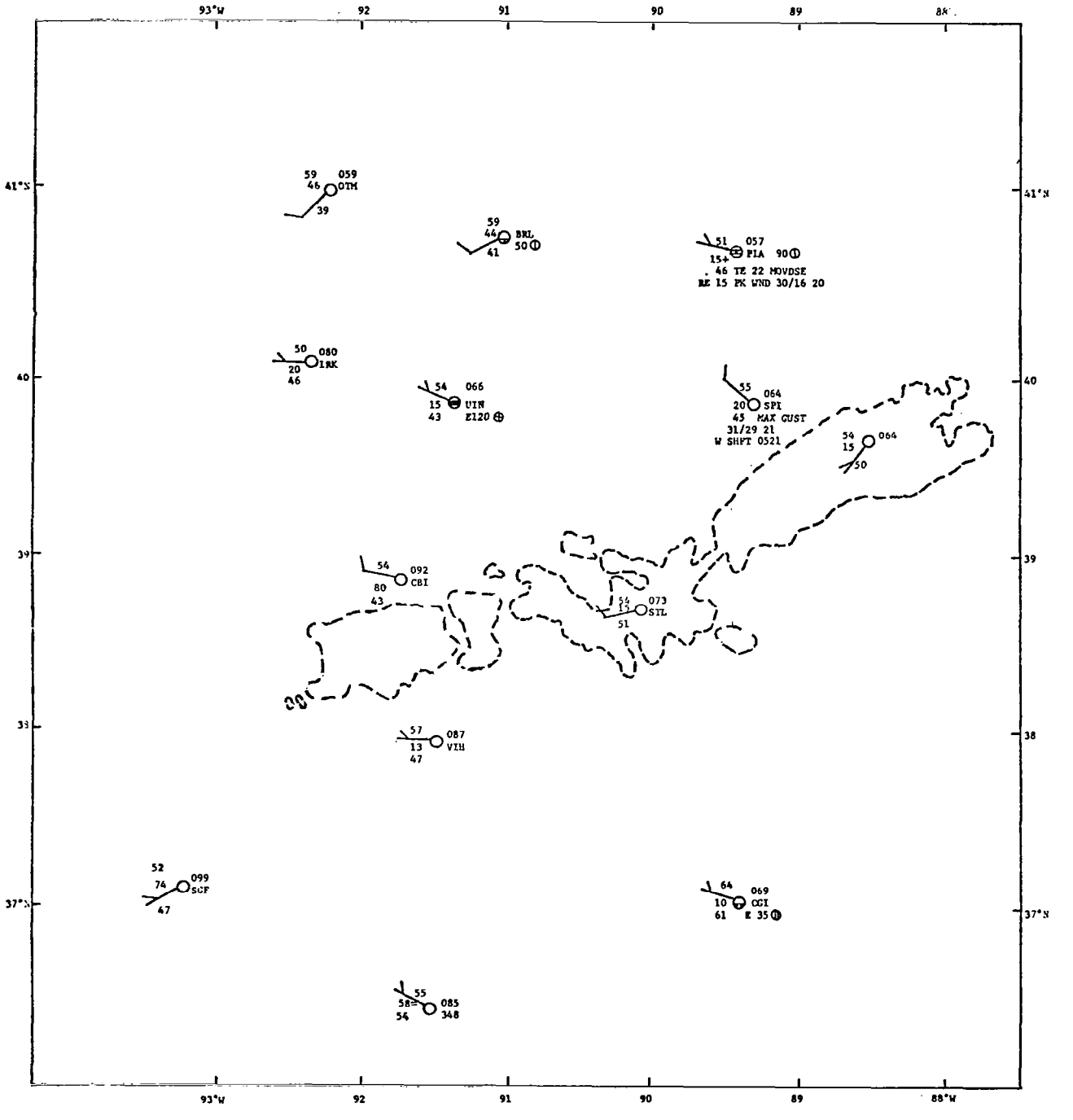

Fig. 11. Accompanying surface data at 0600 GMT on 11 May 1974 for the region illustrated in Fig. 12. Dashed echo outline delineates ground clutter rather than convective echoes.

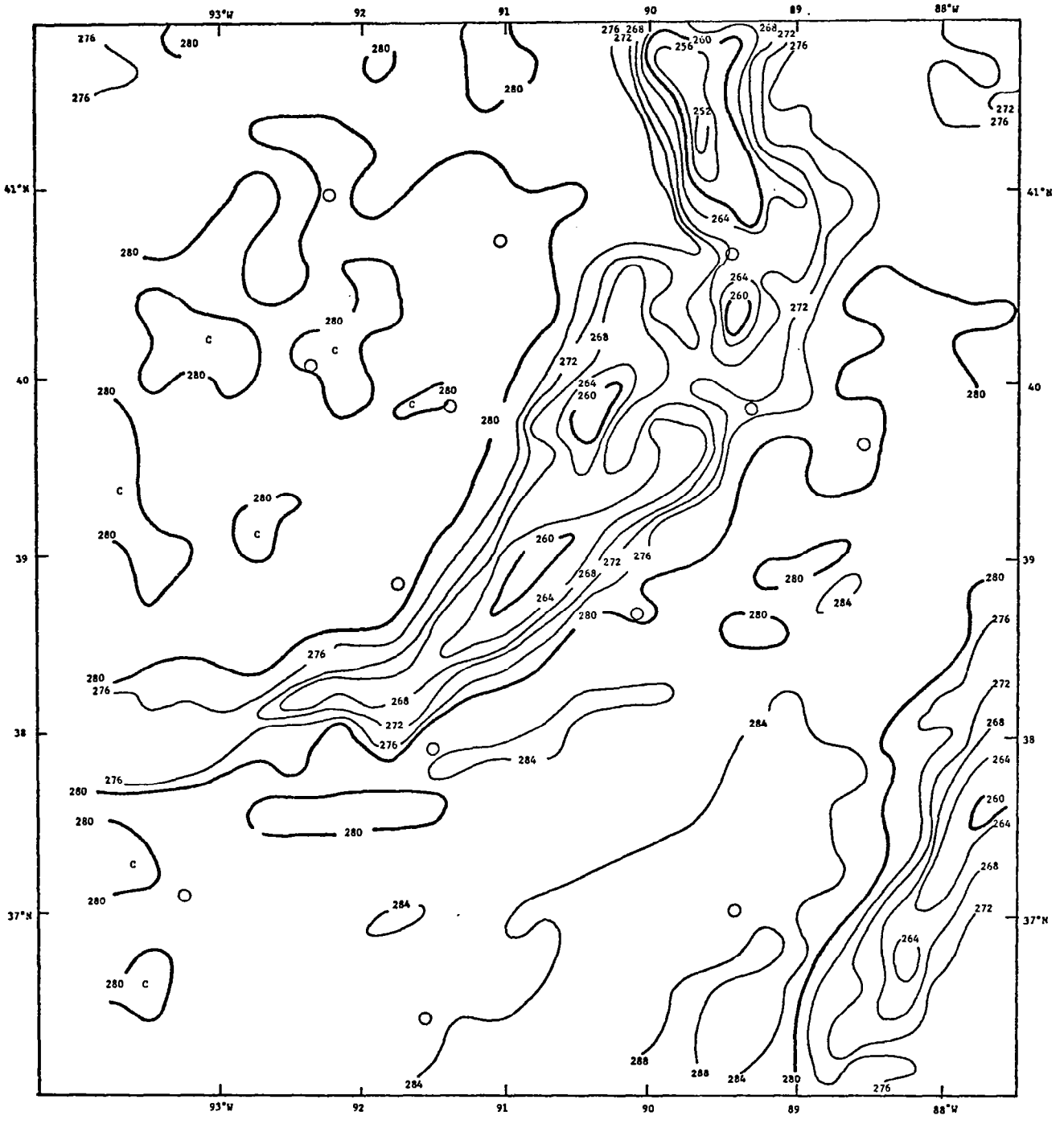

Fig. 12. THIR 11.5 micrometer equivalent black body temperature analysis using the 1:2,000,000 grid print mapping at 0610 GMT on 12 May 1974 for the region covered by the St. Louis, Missouri, radar.

at 25,000 ft (7600 m) at 0500 GMT, to 12,000 ft (3650 m) overcast at 0600 GMT and back to scattered by 0700 GMT. It is possible that the overcast reported at this station is not associated with the main cloud mass but with a smaller patch of clouds west of the main cloud mass. Springfield, which reported clear at the time of the THIR data, went to a middle scattered condition at 0700 GMT with bases reported at 12,000 ft (3650 m).

If it is assumed that the middle cloud layer is overcast in the vicinity of the coldest cloud-top temperatures and that the emissivity of the clouds approaches unity, the tops are at approximately 17,000 ft (5200 m) MSL. Actually, there is a considerable north-south temperature gradient causing the 260 K isotherm to be close to 20,000 ft (6100 m) in the southern end of the line and nearer 14,000 ft (4250 m) at the northern end. Using the apparent radiation temperature of the background, as determined from the clear sky conditions in the area and a cloud-top temperature of 260 K, the effect on the apparent cloud-top temperature by going from overcast to 0.5 coverage is to increase the apparent cloud temperature to apprxoimately 270 K, and with 0.2 cloud cover to an effective temperature of 275 K. Since the area in question is near the orbital track these are probably realistic estimates of the effect of changing cloud cover on apparent temperature. Since the emissivity of middle clouds tends to be fairly high (Allen, 1971) the cloud height corresponding to the height of the 260 K isotherm is probably a good estimate of cloud tops.

In summary, comparisons between the THIR patterns and the cloud field as seen in the satellite photographs and radar presentations revealed about what would be expected. In general, there was good agreement between the cloud pattern and cloud top estimates based on the THIR data and radar cloud top reports. Specific problems in the interpretation of the THIR temperature data stemmed from the possibility of variable emissivities of cirroform clouds and features below the resolving power of the 1:2,000,000 grid print mapping. Specific features in the radar patterns were found to be only loosely associated with the pattern of temperature at the cloud top as portrayed by the 1:2,000,000 THIR data.

5. POINT COMPARISON OF ITPR AND THIR DATA WITH SURFACE INFORMATION

Comparisons of THIR radiometer temperature with surface shelter temperature were carried out using the 1:10,000,000 grid print maps on a Mercator projection. These comparisons were made if the radiometer data points were over surface reporting stations and if the stations were reporting clear sky conditions at the time of the satellite overpass. The restrictions of clear sky conditions as well as data points coincident in space with surface stations greatly reduced the number of points that could be compared directly. The AVE II area experienced a clearing trend during the observation period such that more nighttime comparison points were available than daytime points.

The results of the point-by-point comparison are presented in Fig. 13. Here the points from Orbit 6932 are plotted as X's while those from Orbit 6939, the nighttime case, are plotted as circles. Typically the temperature comparisons for the daytime orbit averaged about 9C warmer than the corresponding shelter temperature while nighttime comparisons over the same area averaged about 4C colder than the corresponding shelter temperature. It is also of interest to note the scatter of data points associated with each orbit. During the daytime orbit the scatter is quite large ranging from radiometer temperatures 18C too warm to 5C too cold with essentially no trend in differences versus temperature. On the nighttime orbit the scatter of the data points is much less than observed on the daytime orbit, and a rather uniform difference of approximately 4C is noted over the entire temperature range. The extreme differences between radiometer and shelter temperatures in this latter case ranged from approximately 2 to 10C.

Interestingly, when the ITPR surface data points are plotted on the same chart (⊗ for Orbit 6932 and □ for Orbit 6939), the points are clustered in with the 1:10,000,000 data points. With two exceptions, differences on the daytime orbit were on the order of about 5C too warm; while on the nighttime orbit, ITPR surface temperatures were approximately 3C too cool. The two major exceptions occurred at data points 81 and 82 from Orbit 6932 in which the daytime ITPR temperatures were approximately 4C cooler than the estimated shelter temperatures. It should be noted that data point 81 occurred over water and data point 82 occurred where low and middle broken clouds were reported. On the other hand, the largest positive departure occurred at data point 83 which was overcast with low clouds as determined from surface data. Checks of differences between shelter temperatures and radiometer temperatures from the 1:2,000,000 mapping showed differences similar to those found for the 1:10,000,000 data.

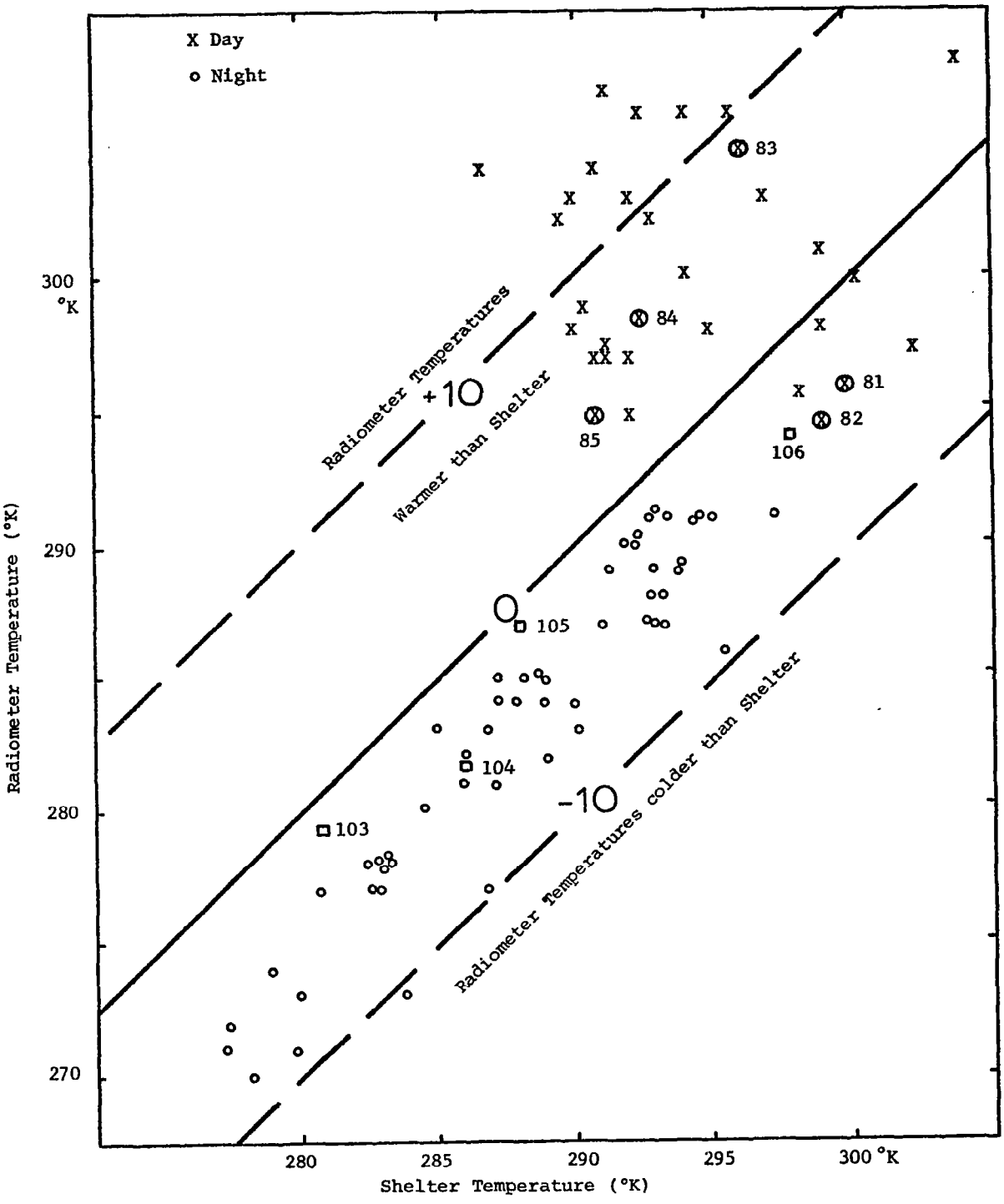

Fig. 13. Nimbus 5, 11.5 micrometer radiometer temperatures versus shelter temperature observed under clear sky conditions. Data from Orbits 6932 (day) and 6939 (night) on 11-12 May 1974 were used for the comparison. Radiometer temperatures were determined from 1:10,000,000 grid print maps (x and o data points), and from ITPR surface temperature values (□ and ⊗ data points).

A second comparison carried out using the ITPR data was that between the total precipitable water as determined from the radiosonde data and that determined from the ITPR information. Figure 14 shows the results of this comparison for the two orbits over the AVE II area. The ITPR sounding measurement of precipitable water was lower than that determined from the radiosonde data in all cases. There was a general trend for the difference to increase as the amount of precipitable water increased, although the percentage difference is not greatly different.

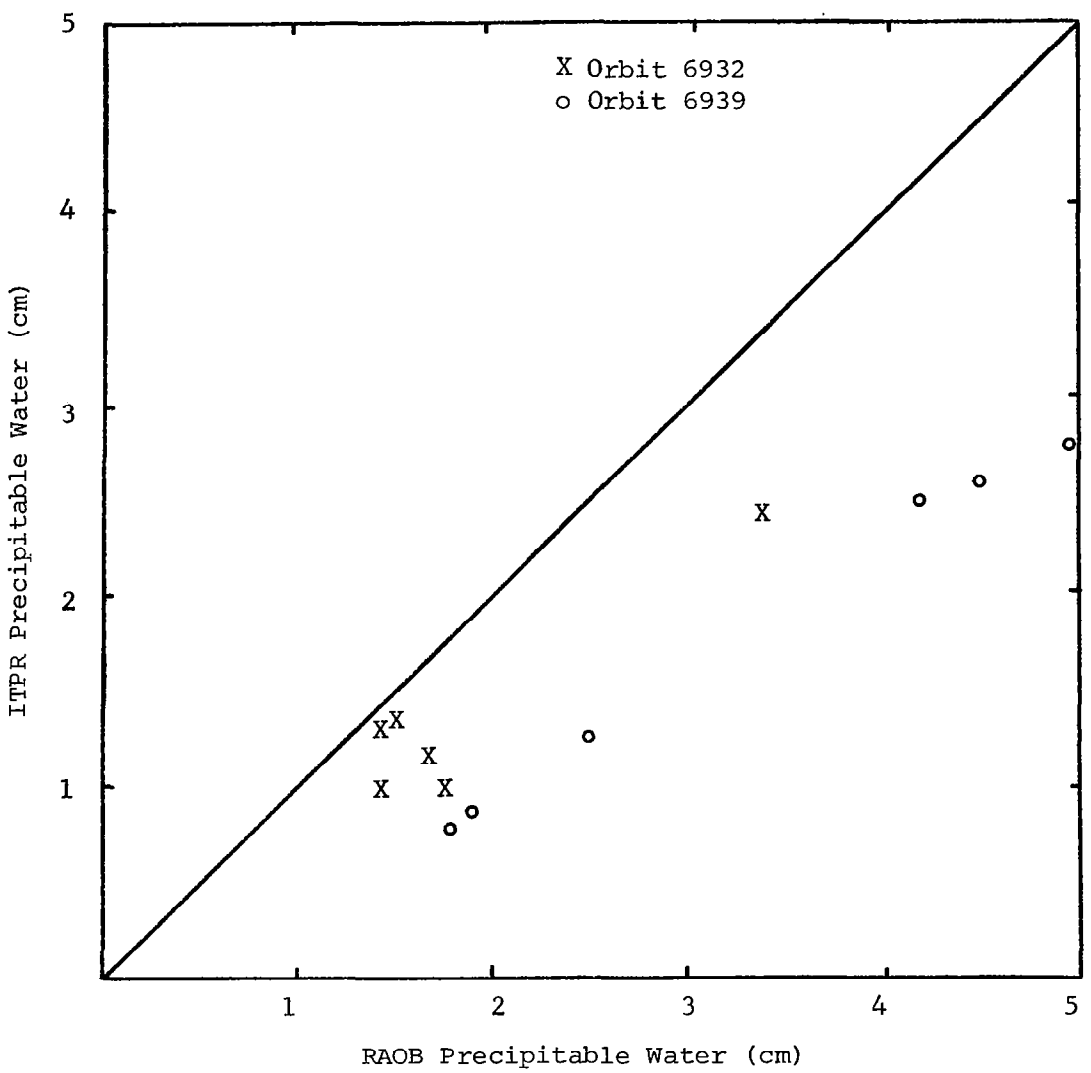

Fig. 14. Comparison between precipitable water as determined from the Nimbus ITPR Sounder and that measured from RAOB soundings. The difference in time between ITPR and RAOB soundings was approximately 30 min.

6. NIMBUS 5 ITPR COMPARISONS WITH RADIOSONDE DATA

The spatial and temporal coincidence of the Nimbus 5 ITPR soundings and the radiosonde soundings during the AVE II period provided an excellent opportunity to compare temperature soundings from the two sources. The ITPR soundings used were those derived from the combination of the Nimbus 5 ITPR, NEMS, and SCR experiments using regression equations relating temperatures to radiances. One of the six soundings in each orbit, however, consisted of an abbreviated solution using only the NEMS and SCR inputs.

For all practical purposes, the ITPR and RAOB observations used in this comparison were obtained at the same time. Although spatial separation between the two data sets were small, additional data interpolation for pressure surfaces corresponding to the levels at which ITPR temperatures were determined was performed and used in the actual temperature comparisons. In all cases, the interpolation processes brought the radiosonde temperature closer to the satellite sounding value.

The Nimbus 5 orbital tracks which passed over the AVE II observation area are illustrated in Fig. 15. Both orbits passed over the central United States with Orbit 6932 crossing at midday, 1711-1717 GMT on 11 May 1974, while Orbit 6939 crossed the area near midnight, 0613-0619 GMT on 12 May 1974. The ITPR sounding points lie along the solid line with individual soundings numbered as in the solution output furnished by NASA. The rawinsonde stations used in the comparisons are indicated with X's on the track charts and are connected with a dashed line.

Temperature profiles from the ITPR, the nearest radiosonde, and radiosonde soundings interpolated to the ITPR sounding points are illustrated in Figs. 16 and 17 for Orbits 6932 and 6939, respectively. There is of course, significant detail in the individual soundings which is lost in the ITPR soundings as well as in the interpolated radiosonde soundings. Although such detail is important, it is below the resolution possibilities of the ITPR sounder. In this study we are concerned with features and temperature differences which are within the resolution possibilities of the ITPR sounder. Temperature comparisons at ITPR data levels are made with the vertically smoothed and horizontally interpolated radiosonde temperature profiles.

Radiometrically determined horizontal temperature distributions over

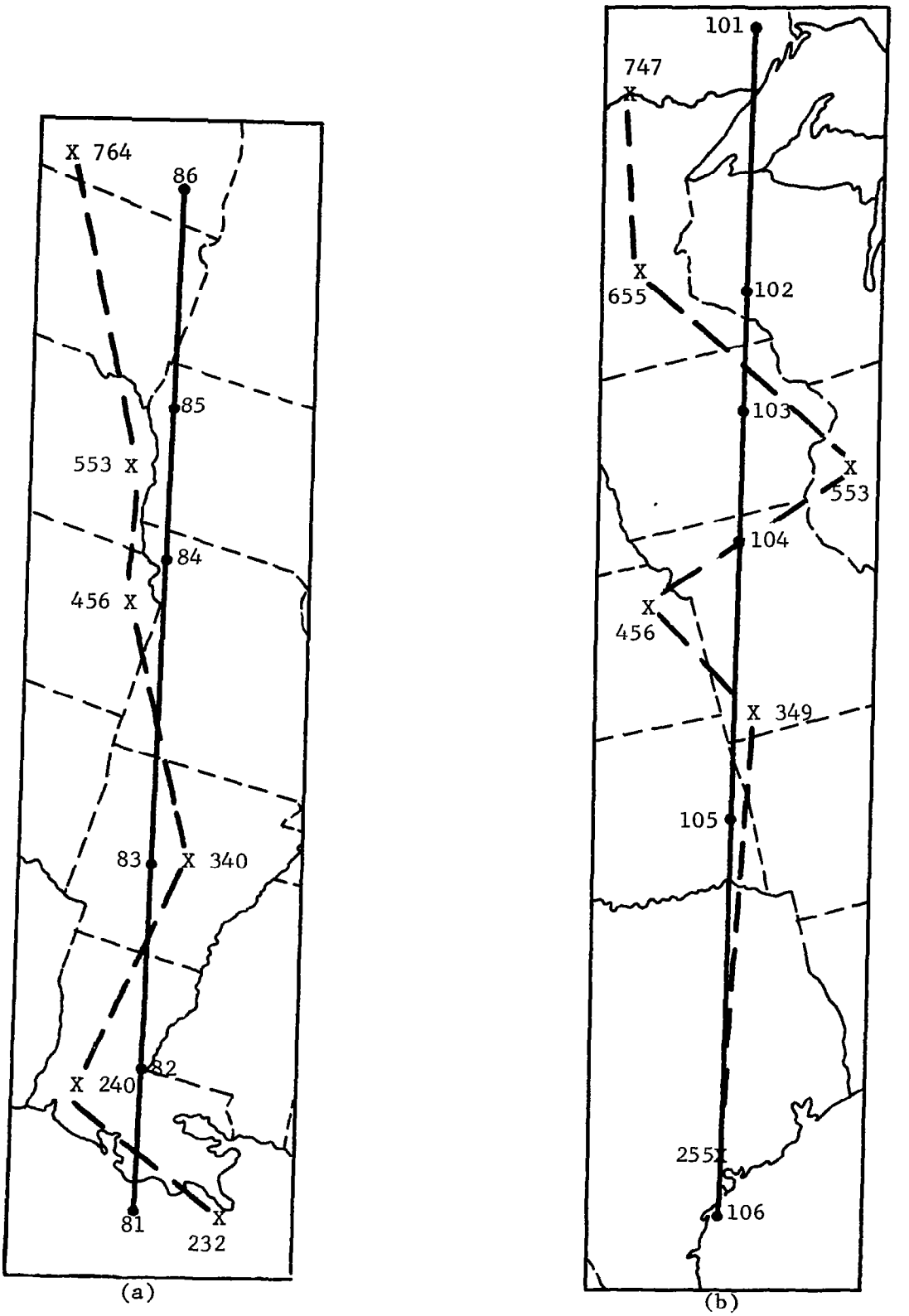

Fig. 15. Nimbus 5 orbital tracks over the AVE II area. (a) Orbit 6932 at 1711-1717 GMT on 11 May 1974. (b) Orbit 6939 at 0613-0619 GMT on 12 May 1974. ITPR sounding numbers and rawinsonde stations used for comparisons are shown.

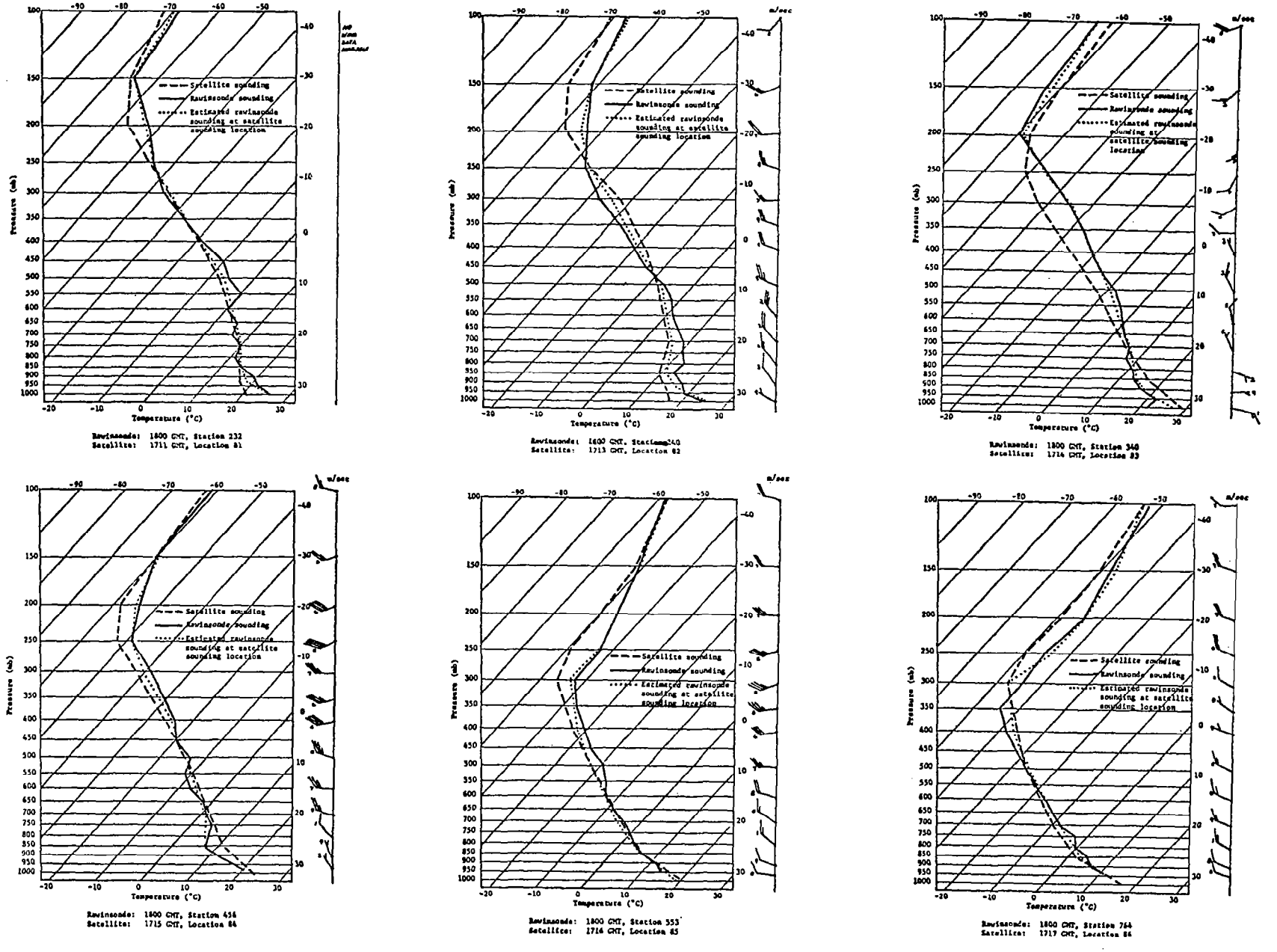

Fig. 16. Temperature profiles at individual sounding points within the AVE II network on 11 May 1974. Satellite profiles were taken at approximately 1715 GMT. All are Solution 3 profiles with the exception of sounding 83 which was a Solution 2 profile. RAOB profiles were taken at 1800 GMT. Estimated radiosonde profiles were determined by interpolation from surrounding stations.

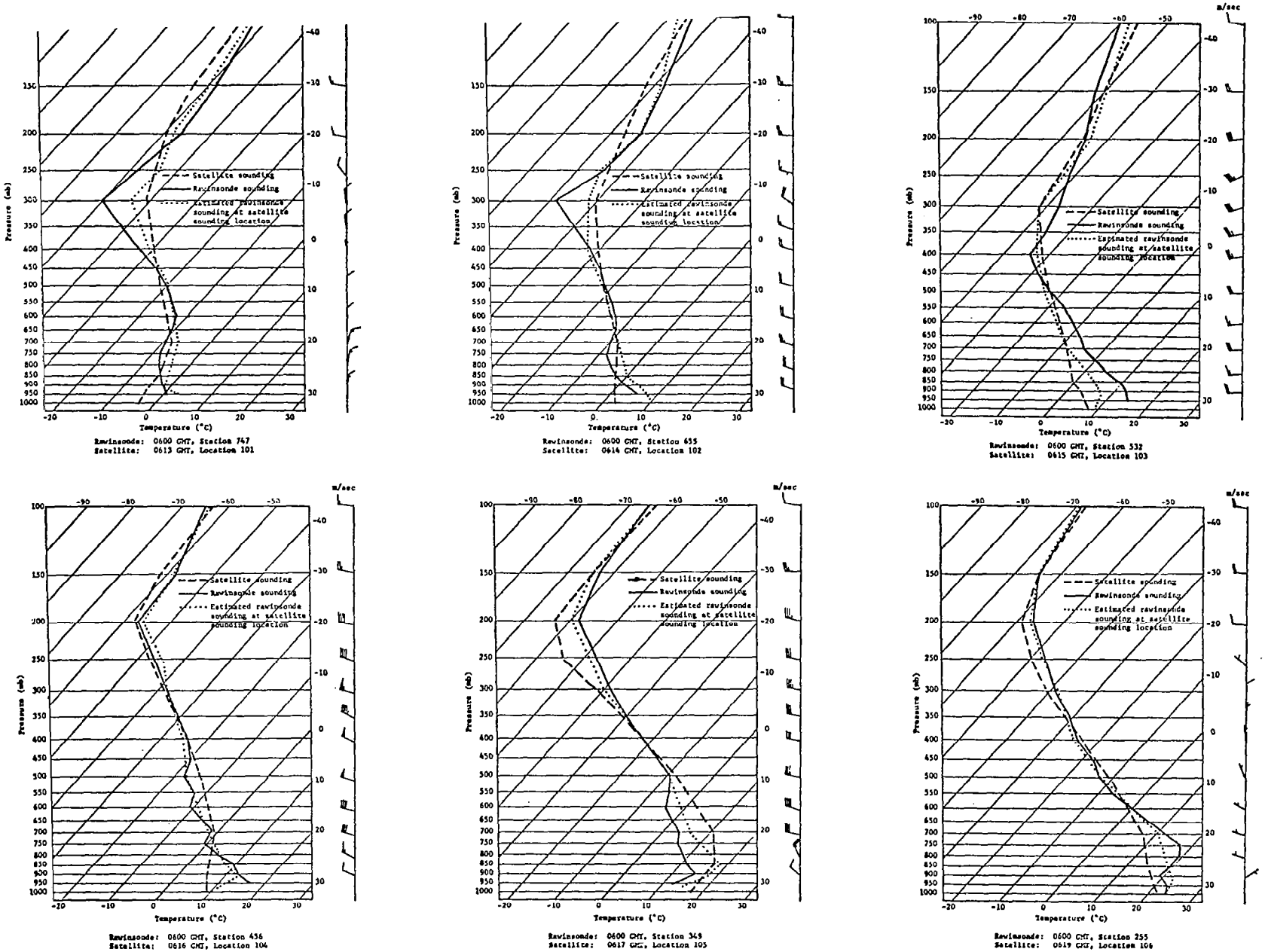

Fig. 17. Temperature profiles at individual sounding points within the AVE II network on 12 May 1974. Satellite profiles were taken at approximately 0615 GMT. All are Solution 3 profiles with the exception of sounding 105 which was a Solution 2 profile. RAOB profiles were taken at 0600 GMT. Estimated radiosonde profiles were determined by interpolation from surrounding stations.

one degree latitude-longitude boxes centered on the individual ITPR data points are presented in Figs. 18 and 19. The temperature fields were constructed from the 1:2,000,000 grid print maps using the 11.5 micrometer channel of the THIR experiment. The THIR temperature fields about the ITPR data points taken on Orbit 6932 reveal that at four of the points temperatures were essentially surface values, although there was generally at least a three degree temperature variation over the field near the data points. Two of the ITPR soundings occurred in the vicinity of significant clouds. Data point 83, one of the abbreviated solutions, occurred where the effective cloud-top temperature in the THIR data corresponded approximately to a pressure of 330 mb. The ITPR profile solution for effective cloud amount placed 1% cloud cover at 700 mb, 9% at 500 mb, and 58% at 300 mb. Data point 86 was taken in an area where the effective THIR cloud-top temperature corresponded to that near 730 mb on the rawinsonde sounding. The ITPR effective cloud amounts for the same point totaled 19% at 850 mb, 44% at 700 mb, and 6% at 500 mb.

The THIR temperature fields about the ITPR data points on Orbit 6939 are presented in Fig. 19. Four of the six ITPR points were taken in areas where the THIR temperature field indicated either clear skies or relatively low cloud conditions. Two of the data points occurred in areas of significant cloud cover. On the basis of the THIR temperature field, the effective cloud-top temperature at sounding point 101 corresponds to that at approximately 580 mb. For this same data point, the ITPR solutions for clouds specified an 18% cloud cover at 500 mb, and a 12% cover at 300 mb. At ITPR data point 102, the THIR temperature field indicated the top of the cloud cover near 750 mb where the ITPR solution indicated a coverage of 16% at 850 mb, 30% at 700 mb, 13% at 500 mb, and 5% at 400 mb. In the ITPR solutions, two of the data points, which had good agreement between ITPR surface temperatures and THIR temperatures, indicated significant cloud amounts in the profile solution. At point 104, where the difference between THIR and ITPR surface temperatures was less than 2°, clouds in the amount of 11% at 850 mb, 1% at 700 mb, 15% at 500 mb, 6% at 400 mb, and 1% at 300 mb were determined from the ITPR profile. At data point 106 where the difference between THIR and ITPR surface temperature was about one degree, clouds in the amount of 1% at 700 mb, 1% at 300 mb, 24% at 250 mb, and 9% at 200 mb were determined from the ITPR profile solution.

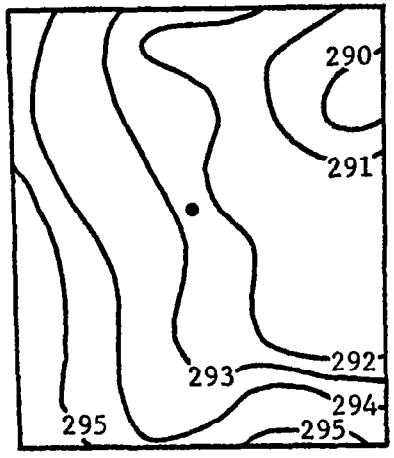

81 ITPR SFC 295°K

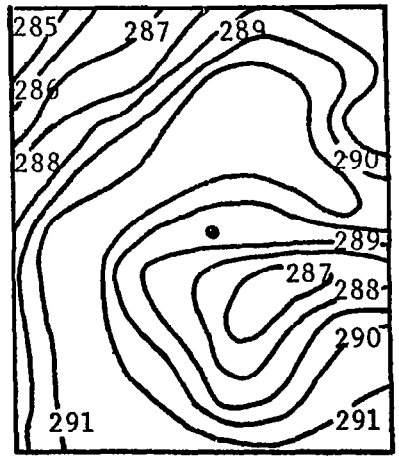

82 ITPR SFC 294°K

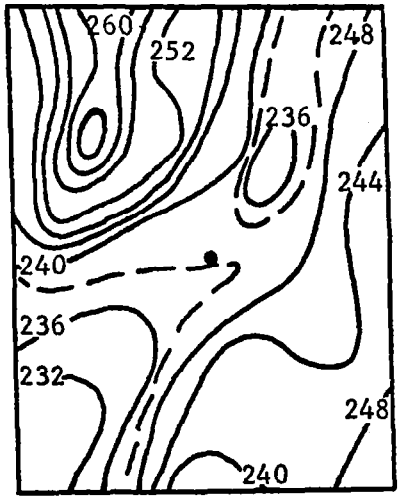

83 ITPR SFC 305°K

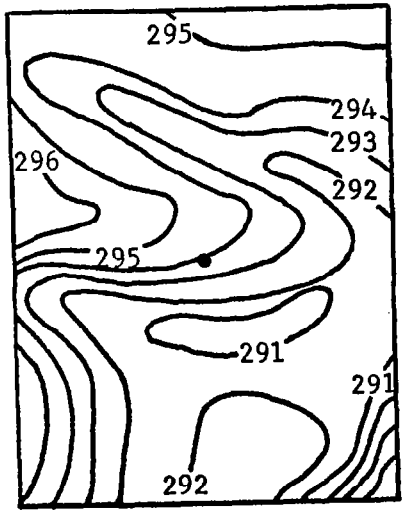

84 ITPR SFC 298°K

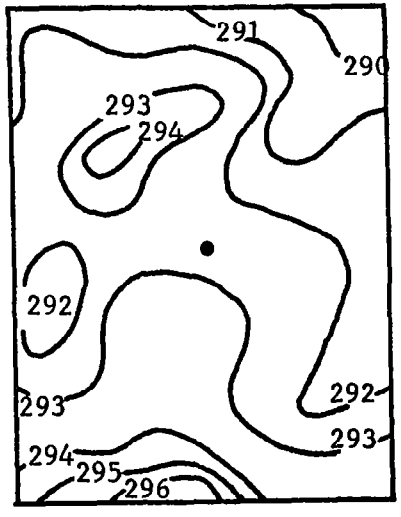

85 ITPR SFC 295°K

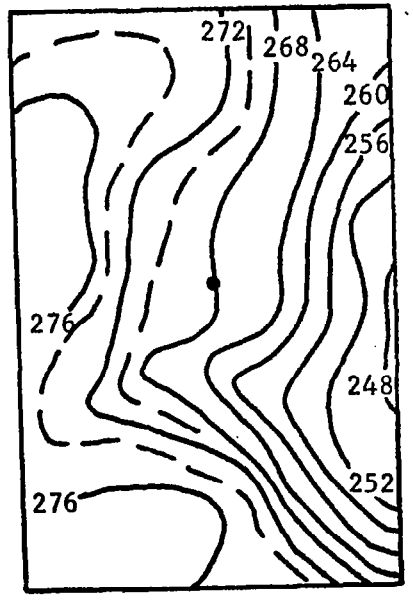

86 ITPR SFC 295°K

Fig. 18. THIR 11.5 micrometer temperature field from the 1:2,000,000 grid print maps for one degree latitude-longitude boxes about the sounding points on Orbit 6932. ITPR surface temperatures are given for the ITPR data point within each box.

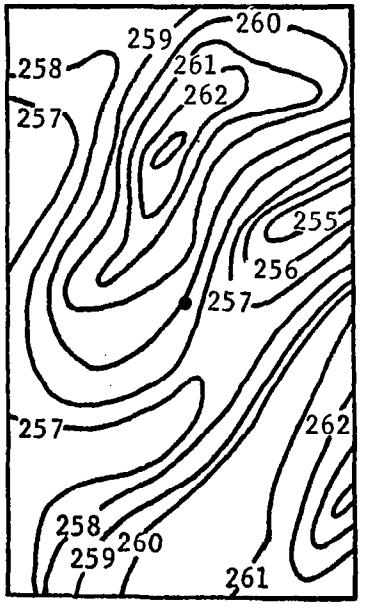

101 ITPR SFC 268°K

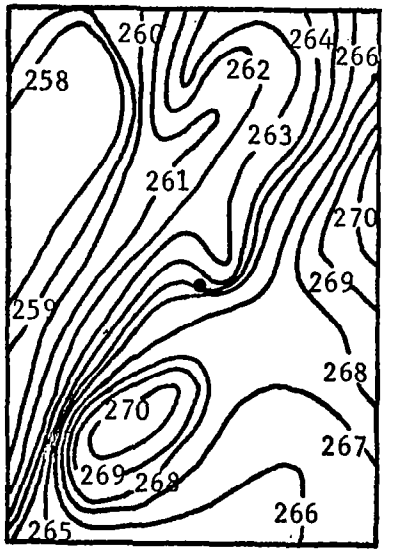

102 ITPR SFC 275°K

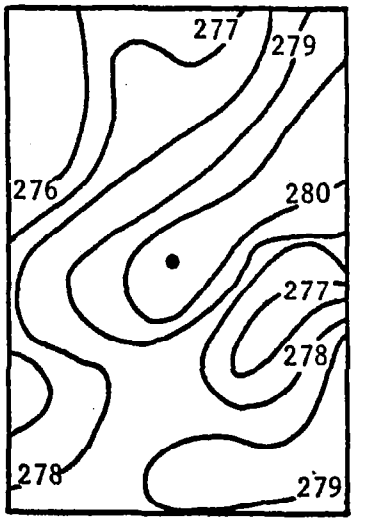

103 ITPR SFC 280°K

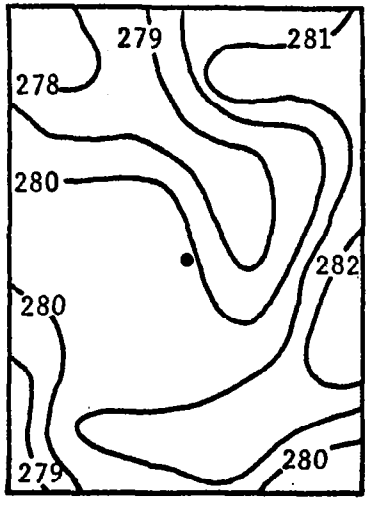

104 ITPR SFC 282°K

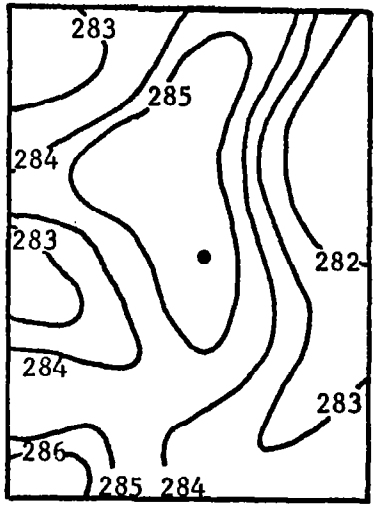

105 ITPR SFC 287°K

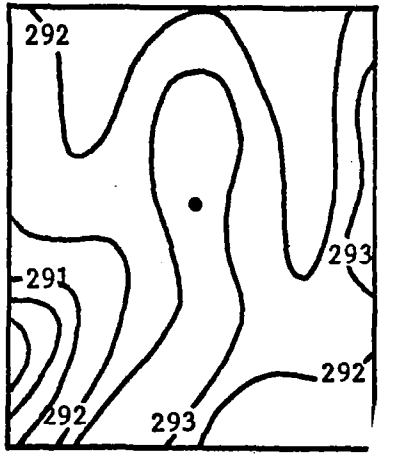

106 ITPR SFC 294°K

Fig. 19. THIR 11.5 micrometer temperature field from the 1:2,000,000 grid print maps for one degree latitude-longitude boxes about the ITPR sounding points on Orbit 6939. ITPR surface temperatures are given for the ITPR data point within each box.

Prior to comparing ITPR and radiosonde temperatures, the degree of comparison which might be expected under the conditions present is examined. In an actual comparison between ITPR and RAOB temperature profiles, some difference between the two profiles should be expected due to measurement errors in each technique. Results of error analyses carried out in the 1960's for the RAOB temperature data indicated errors from 0.7°C (Case, 1962) to 1.4°C (Hodge and Harmantas, 1965). Based on this information, Fuelberg (1974) assigned a realistic error of 1°C to the AVE II temperature data. Studies by Lenhard (1970, 1973), however, indicate that the current temperature measuring system in the RAOB instrument package is capable of much greater accuracy than indicated in the earlier studies. This more recent work indicates RMS errors in the temperature data of approximately 0.2°C. Lenhard attributes the much smaller error found in the more recent evaluations to improved instrumentation.

Regardless of the actual sensor accuracy, the spatial separation between comparison points, in this case the RAOB and ITPR data points, will influence the observed differences between the two observation techniques. During AVE II, the RAOB and ITPR soundings were separated by at least 100 km. To improve the chances of a reasonable comparison, the RAOB data were interpolated to the satellite sounding points. Although this should minimize the problem of spatial separation between the two data sources, the total effect of the separation is probably not eliminated. In an effort to better understand the significance of differences between the RAOB and ITPR profiles due to spatial temperature differences, data from five NSSL rawinsonde stations in Oklahoma were analyzed. These stations are separated by distances ranging from 42 km to 108 km. Although such a comparison will not give an estimate of instrument error, it will provide a numerical value for difference or error possibility when making data comparisons where the two comparison points are separated by small but uncertain distances. Such an evaluation includes both sensor error as well as spatial variation. Under normal conditions we would expect the spatial variation to change with synoptic situation and pressure level. In the case of the Oklahoma stations, the mean spatial separation of the stations was approximately 65 km or about one half a degree of latitude.

Layer thickness and differences in thickness (m km^{-1}) between stations

corresponding to pressure intervals in the ITPR soundings were determined rather than evaluating specific temperature values and differences between stations. The resultant mean thickness differences for all the NSSL stations through the AVE II period are shown in Table 1. The differences in thickness ranged from 5.5 m km^{-1} in the 1000-920-mb layer to 2.3 m km^{-1} in the 400-300-mb layer. The comparatively large difference at low levels is probably due to greater spatial variation of temperature, a feature which may be inferred by examining the synoptic charts shown in Figs. 1 and 3. The corresponding temperature difference required to provide the observed thickness differences are also shown in Table 1. These values range from 1.6°C near the surface to 0.5°C in the 400-300-mb layer.

Table 1. Mean layer thickness differences and corresponding mean temperature differences between the NSSL Oklahoma stations during the AVE II period. The average station spacing was 65 km.

Pressure Interval	Observed Thickness Differences	Corresponding Mean Temperature Difference
1000-920 mb	5.5 m km^{-1}	1.6°C km^{-1}
920-850	5.5	1.5
850-700	3.1	.9
700-500	4.6	1.2
500-400	2.5	.6
400-300	2.3	.5
300-250	3.0	.7
250-200	3.1	.7
200-150	3.1	.7
150-100 mb	3.1 m km^{-1}	.7°C km^{-1}

Errors associated with the ITPR sounding system are basically associated with the regression coefficients used in the minimum information solution of the profile radiance values measured by the sounding system. Retrieved ITPR temperature profiles would be fairly good as long as more or less ideal conditions are present, i.e. clear sky, prescribed atmospheric gas composition, and climatological means which closely approximate the conditions actually present at the time of the ITPR sounding. Such ideal conditions are not frequently present so that a certain amount of error is induced into the ITPR temperature profiles due to nonrepresentative

regression coefficients used to retrieve the temperature profile. The estimated RMS temperature error for a NEMS+SCR+ITPR derived profile of temperature as a result of regression coefficient errors for the layers used in this study was taken from Smith et al. (1974) and is presented in the second column of Table 2. This temperature error is associated with a corresponding thickness error which is illustrated in the third column of Table 2. Using the mean thickness difference found in the NSSL data as an estimate of the RMS thickness error due to interpolation of the RAOB data to the ITPR data points, a hypothetical combined error or difference in thickness between the ITPR- and RAOB-derived values at what is supposed to be the same point is illustrated in the fourth column of Table 2 (RMS of Col. 2, Table 1, and Col. 3, Table 2). The error in temperature associated with the thickness error or difference is presented in the fifth column of Table 2. This last column, the combined temperature error, presents an estimate of temperature difference between RAOB and ITPR values.

Table 2. Thickness and mean layer temperature error resulting from a combined error in the ITPR reduction method and the RAOB error.

Pressure Interval	ITPR Temperature Error (RMS) due to Regression Analysis (30-60°N) Smith et al. (1974)	Thickness Error Based on RMS Errors in ITPR Temperatures	Combined RAOB and ITPR Error	Combined Mean Temperature Error
1000-920 mb	1.9°C	6.6 m km^{-1}	8.6 m km^{-1}	2.5°C
920-850	2.0	7.1	9.0	2.5
850-700	1.9	6.7	7.4	2.0
700-500	1.4	5.4	7.1	1.8
500-400	1.4	5.5	6.0	1.5
400-300	1.7	7.0	7.4	1.7
300-250	1.8	8.0	8.5	1.9
250-200	1.9	8.5	9.0	2.0
200-150	1.8	8.3	8.8	1.9
150-100 mb	1.6°C	7.1 m km^{-1}	7.8 m km^{-1}	1.7°C

Figure 20 presents the differences in calculated thicknesses between the ITPR sounding data and the interpolated rawinsonde data. In general, the thickness difference is greatest at low and upper heights with a minimum difference in the mid-troposphere. A thickness error of

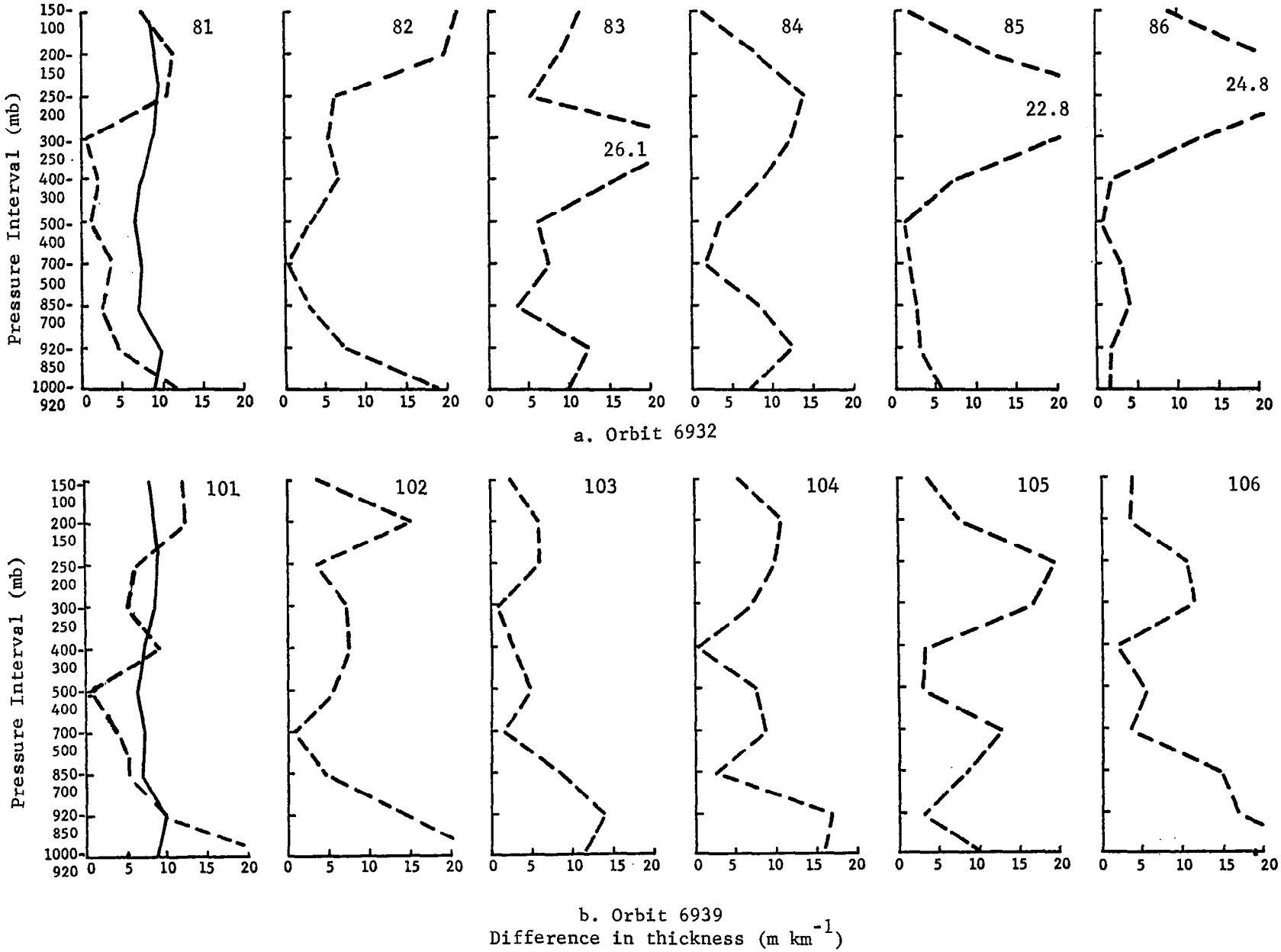

Fig. 20. Differences in layer thickness (m km^{-1}) between ITPR soundings and interpolated radiosonde soundings for Orbits 6932 (a) and 6939 (b). The solid curve on soundings 81 and 101 is the thickness error possible due to inherent radiosonde and ITPR sounding errors (Table 2).

5 m km^{-1} in these diagrams corresponds to an error in mean temperature of about 1.24°C, the exact amount depending on the pressure. This is slightly less than the difference given in Table 2 between 500 and 400 mb. In most instances a thickness difference approaching 10 m km^{-1} would be necessary before the difference exceeded that which might be expected due to the errors illustrated in Table 2. For convenience the combined RAOB-ITPR error extreme (listed in Table 2 for the combined error) is superimposed upon individual thickness difference curves in Fig. 20 for the ITPR sounding points on the two orbits. It should be remembered when comparing the curves that the error curves contain the influence of horizontal temperature gradients present in the Oklahoma network.

The differences between interpolated radiosonde profiles and the ITPR profiles shown in Fig. 16 for Orbit 6932 are presented in cross section form in Fig. 21. These differences result from error in the ITPR system, different degrees of vertical smoothing, errors in radiosonde data, and interpolation errors. It should be recalled that there is an inherent difference between radiosonde and ITPR profiles on the order of 2°C (see Table 2).

Figure 21 reveals an apparent dependence on pressure of the difference of the ITPR and RAOB data, with the maximum difference occurring near 200 mb in the vicinity of the tropopause. Radiosonde temperatures in this area are up to 6°C warmer than the corresponding ITPR temperatures. Near the surface, during this daytime orbit, there is a pronounced area where the ITPR temperatures are warmer than the RAOB temperatures. In the mid troposphere, the differences are relatively small. The distribution of temperature differences versus height illustrated in Fig. 21 bears at least a partial relationship in relative magnitudes to that expected on the basis of Table 2.

In the vicinity of data points 82 and 83 some rather significant ITPR-RAOB temperature differences are present which vary significantly along the pressure surfaces. The sounding generated at point 83 consisted of the NEMS and SCR data only (Solution 2 profile), and as such is of a different nature than the other profiles in the cross section. The maximum difference between this profile and the corresponding RAOB profile occurs near 300 mb and is negative (radiosonde temperature warmer than the ITPR temperature) while a maximum difference of opposite sign

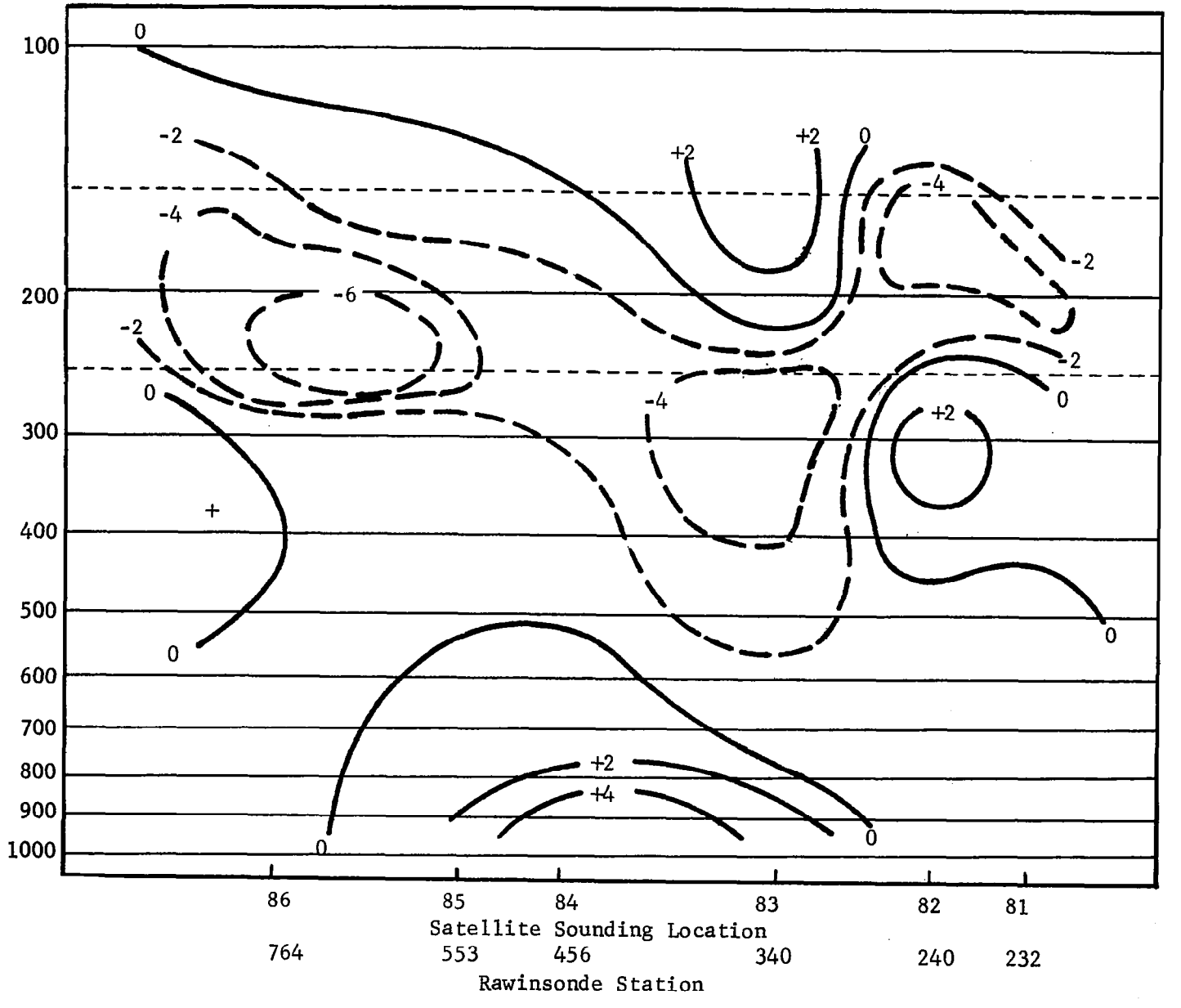

Fig. 21. Temperature differences between the ITPR soundings and the interpolated radiosonde soundings (ITPR temperatures minus RAOB temperatures) for Orbit 6932 at 1800 GMT on 11 May 1974.

occurs at approximately 150 mb in the same profile. Comparison of the cloud-top temperatures in this area, Fig. 18, with the temperature profiles, Fig. 16, reveals that the cloud tops must have been at about 300 mb. The ITPR sounding at data point 82 also contains a maximum and minimum temperature difference near and above 300 mb with the maximum positive difference (ITPR temperature warmer than radiosonde temperature) at the same level as the maximum negative value at data point 83. The THIR temperature field about this point in Fig. 16 indicates that, at least on the basis of these temperatures, this maximum positive difference occurs well above the cloud tops, which are probably near 900 mb.

Figure 22 provides some additional insight into possible contributing factors toward the temperature differences. Although the ITPR cloud amounts are not meant to specifically represent actual cloud amounts, it is of interest to note in Fig. 22c that the amount of cloud calculated from the satellite profile over point 82 was on the order of 32% at 300 mb and 22% at 400 mb. On the basis of the measured relative humidity by the corresponding radiosonde sounding (Fig. 22b), these satellite interpreted cloud amounts seem high. Likewise, near the surface (900 mb), ITPR cloud amounts are almost negligible while surface reports and RAOB humidities indicate an overcast near 900 mb. On the other hand, cloud amounts over data point 83 were estimated as 58% in the ITPR data at 300 mb, and on the basis of radiosonde relative humidity, Fig. 22b, and THIR cloud-top temperatures, this seems to be a reasonable amount for that level. The radiosonde also indicated a significant cloud cover near 900 mb at station 83 which was not indicated in the satellite data. Near the tropopause, maximum negative temperature differences usually occurred in regions where the vertical increase of atmospheric stability was the greatest. This can be seen by comparing Fig. 22a with Fig. 21. These two figures also show that negative temperature differences tended to follow the stable zone. The region of positive temperature differences near the surface across the interval from point 83 to point 85 seems to be associated with the clear sky conditions in that area. The tendency for the ITPR surface temperature calculations in the sunlight orbit to be warmer than the actual surface by approximately 4°C as shown in Fig. 11, seems also to be reflected in the temperature profile.

Finally, with respect to Orbit 6932, it should be noted that cloud amounts on the order of 44% at 700 mb were estimated from the ITPR data

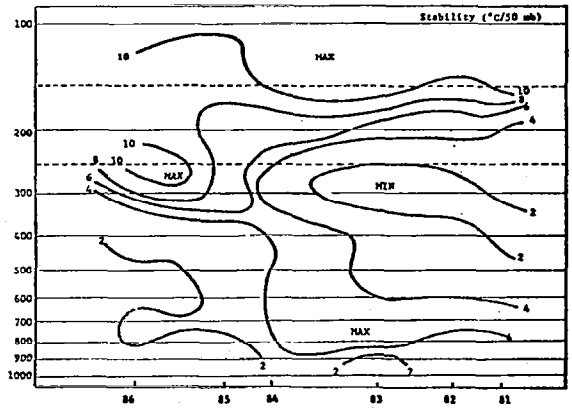

a) Potential stability, $-\frac{\partial \theta}{\partial p}$, (°C/50 mb) based on radiosonde soundings through the AVE II area on 11 May 1974 at 1800 GMT. Data points at the same pressure level as ITPR data were used in the analysis.

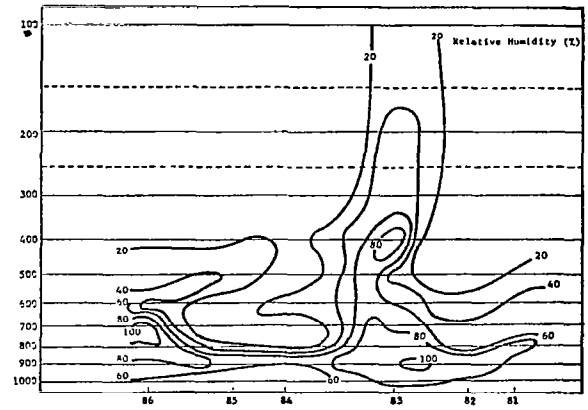

b) Radiosonde relative humidity along the cross section in a).

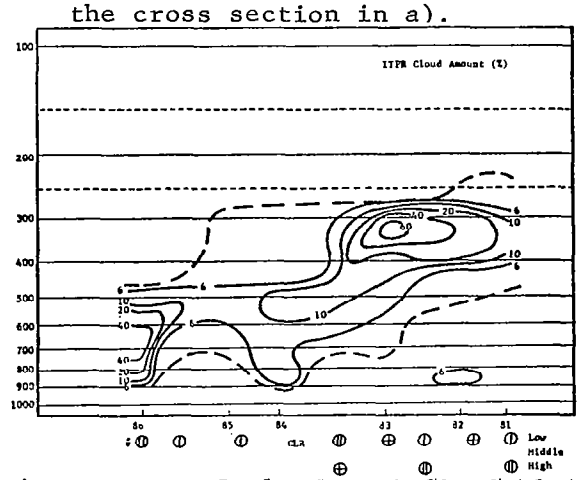

c) Percent of cloud at individual levels along the cross section in a) as specified by the ITPR experiment. Cloud amounts reported by surface stations are also specified.

Fig. 22. Cross-sections along the orbital path for Orbit 6932.

at data point 86. At this location a saturated layer near 700 mb was observed in the RAOB data, surface reports of middle broken clouds were present, and mean cloud-top temperatures based on the THIR data near 700 mb were determined. Correspondingly, there is almost no difference between the ITPR temperature data and the RAOB data. It is also of interest to note that data point 86 is essentially in a region where one cloud layer existed while data point 83 appears to have multiple layers of clouds in its vicinity. Data point 82 has a misplaced cloud layer in the ITPR data.

The differences between the interpolated radiosonde temperature profiles and the ITPR temperature profiles presented in Fig. 17 for Orbit 6939 on 12 May 1974 are shown in Fig. 23 in cross section form along the orbital track through the AVE II network. As was previously the case, differences between ITPR and RAOB temperatures were pressure dependent. A comparison between the difference patterns during Orbit 6932 (Fig. 21), and Orbit 6939 (Fig. 23), reveals similarities but also some significant differences. First of all, in the vicinity of the tropopause, above 300 mb, the tendency is for radiosonde temperatures to be warmer than the ITPR temperatures in both cross sections. In the mid troposphere, however, there is a significant region where a positive difference is present from simple reduction and comparison errors. In Fig. 23 near the surface, an extensive region along the track has appreciable negative temperature difference, i.e. radiosonde temperatures warmer than ITPR temperatures, rather than colder as in Fig. 21.

At the time Orbit 6939 cut through the AVE II area, the frontal system had moved to the Texas coast, and in the orbital cross section the front was located near the ground over location 106 and sloped upward to the tropopause over location 103. This is reflected in the stability analysis shown in Fig. 24a. Humidity values determined from the radiosonde information along the orbital track (Fig. 24b) indicate a zone of maximum humidity in the cross section at approximately 700 mb which extends from the southern end (right side of the diagram) to the central portion of the cross section. Between locations 103 and 102 a humidity maximum extends upward to 300 mb with a maximum in the cross section extending to the northern end in the 700-900-mb layer. The pattern of ITPR estimated cloud amounts shown in Fig. 24c departs considerably from

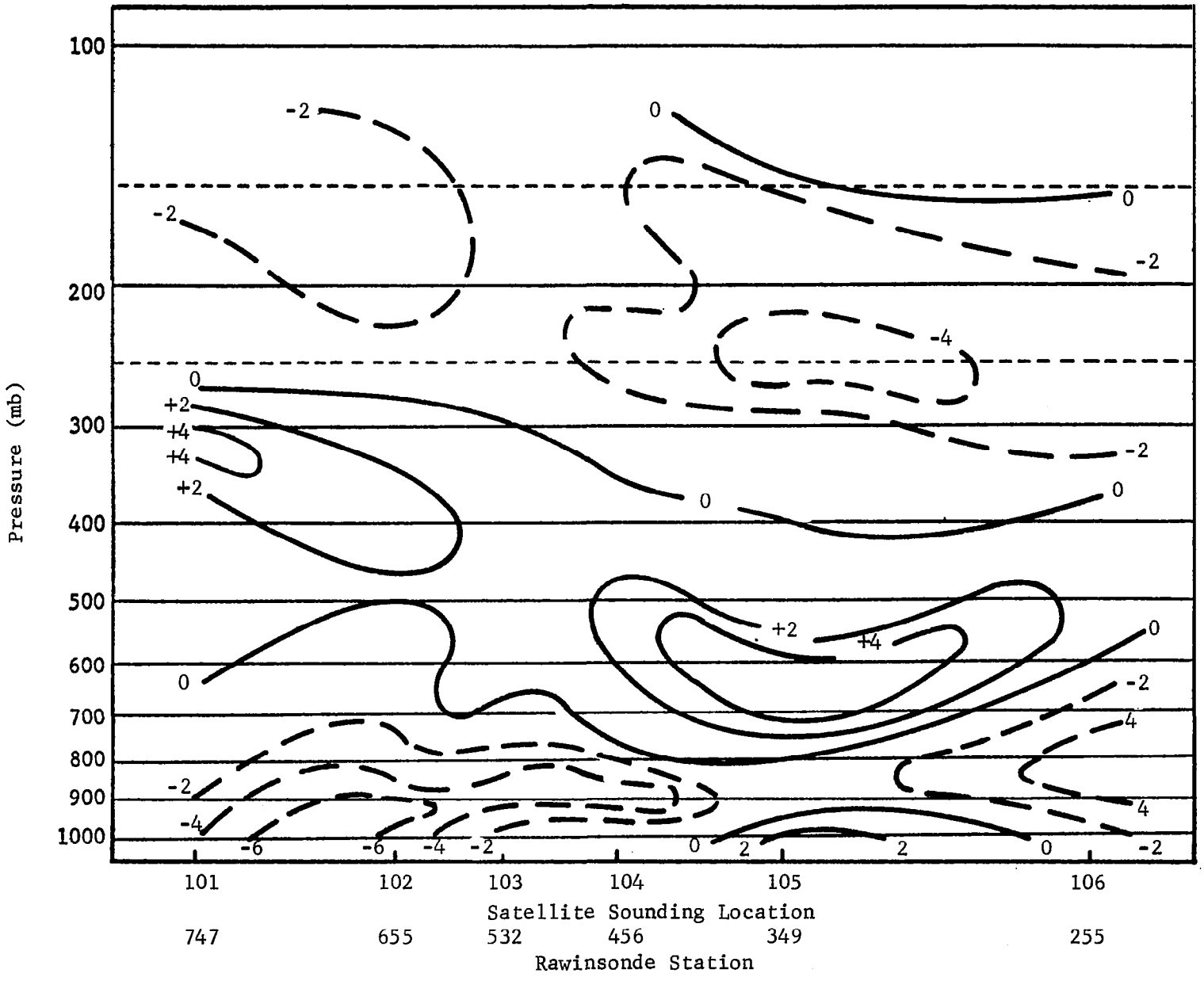

Fig. 23. Temperature differences between the ITPR soundings and the interpolated radiosonde soundings (ITPR temperatures minus RAOB temperatures) for Orbit 6939 at 0600 GMT on 12 May 1974.

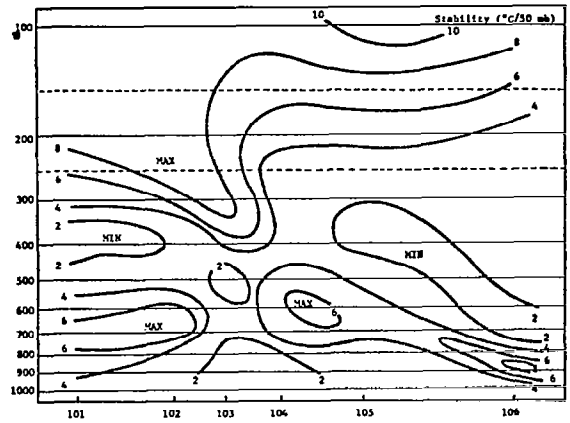

a) Potential stability, $-\frac{\partial \theta}{\partial p}$, (°C/50 mb) based on radiosonde soundings through the AVE II area on 12 May 1974 at 0600 GMT. Data points at the same pressure level as ITPR data were used in the analysis.

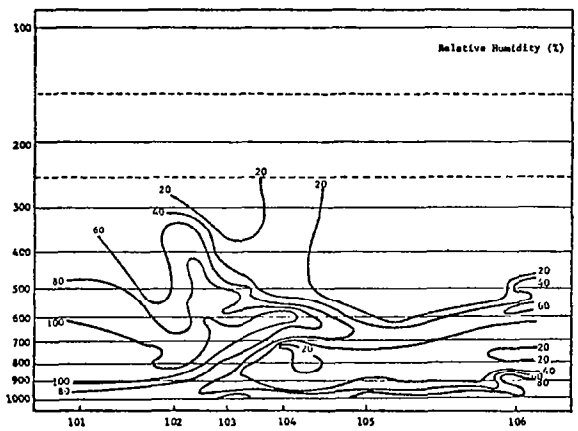

b) Radiosonde relative humidity along the cross section in a).

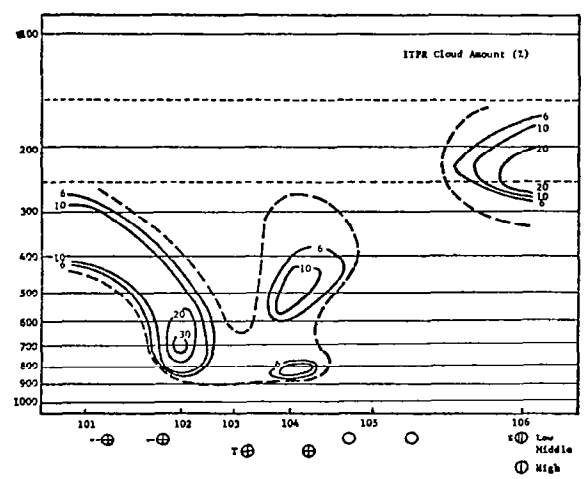

c) Percent of cloud cover at individual levels along the cross section in a) as specified by the ITPR experiment. Cloud amounts reported by surface stations are also specified.

Fig. 24. Cross sections along Orbit 6939.

that which would be expected from other data. On the basis of THIR temperatures (Fig. 19) and the radiosonde soundings (Fig. 17) the cloud tops should be at about 600 mb over location 101, decreasing to approximately 800 mb over location 104, and remaining at approximately that level to location 106 at the southern end. Actually, cloud reports from the surface shown at the bottom of Fig. 24 indicate that there is a region near location 105 where it is clear. In this cloud depiction, the only points where ITPR cloud maximums and indications of clouds from other sources coincide are over location 102 at 700 mb and over location 104 at 850 mb.

Comparison of the temperature differences in Fig. 23 with other features in the cross section shown in Fig. 24 reveals that over locations 105 and 106, the negative temperature differences take place in the area of maximum stability increase with height as was the case in Orbit 6932. On the other side of the cross section, over locations 101 and 103, however, there is a positive temperature anomaly in the area where the stability increases rapidly with height. Figures 24b and 24c show that this positive anomaly occurs near a region where there is a large vertical gradient of relative humidity and implied ITPR cloud amounts. It should be recalled that a similar temperature difference occurred above location 82 in Orbit 6932 under a similar condition. The large area of positive differences between the ITPR and the RAOB data at 600 to 700 mb in the cross section for Orbit 6939 can be attributed almost entirely to the sounding at location 105. Unfortunately, this sounding, as was sounding 82 in Orbit 6939, is a Solution 2 profile (NEMS+SCR) while all others were Solution 3 profiles (ITPR+NEMS+SCR).

The remaining significant feature in the difference field illustrated in Fig. 23 is the extensive band from 850 to 920 mb of negative temperature differences in which the ITPR temperatures are colder than the RAOB temperatures which extend along the entire cross section. It should be recalled that comparisons between ITPR as well as THIR surface temperatures and shelter temperatures on the nighttime Orbit 6939, and presented in Fig. 13, indicated that radiometer temperatures tended to be colder than the shelter temperatures by 3-5°C. That this cold radiometer temperature anomaly influenced the lower-level temperatures seems apparent in at least this collection of ITPR soundings.

Temperature differences between the ITPR solutions and the RAOB temperature data, as evaluated in this study for the two orbits crossing through the AVE II area, appear to be related to such factors as surface temperature determinations which produced radiometer temperatures significantly different than corresponding shelter temperatures, significant changes in lapse rate in the upper troposphere which were not reproduced in the ITPR profiles, and the cloud contamination problem.

So far, the ITPR soundings have been examined spatially along cross sections. For comparison with other studies, as well as the initial error analysis in this study, it is informative to examine the mean value of the difference at specific levels. Two types of error will be presented. In general, an absolute value of the differences between the ITPR and the RAOB data will be discussed. For some comparison purposes it is advantageous to present standard deviations of differences. Although the sample size is extremely small in this study, 6 data points at individual levels on each cross section, a standard deviation of differences in temperature for levels and layers is presented. Table 3 illustrates the mean of the absolute value of the difference in RAOB and ITPR temperatures as well as standard deviations present at the individual ITPR levels in both orbits. Although there are specific differences between the two

Table 3. Means of the absolute value of the radiosonde minus ITPR temperature ($T_{RAOB} - T_{SAT}$) differences at the temperature levels in the ITPR data. The standard deviation (σ_D) of the difference in temperature is also presented for each layer. Data are shown for the two individual orbits and for both orbits taken together.

Level	6932		6939		6932 & 6939 Combined	
	$\overline{\lvert T_{RAOB} - T_{SAT} \rvert}$	σ_D	$\overline{\lvert T_{RAOB} - T_{SAT} \rvert}$	σ_D	$\overline{\lvert T_{RAOB} - T_{SAT} \rvert}$	σ_D
920 mb	1.9°C	2.3°C	4.0°C	4.5°C	3.0°C	3.6°C
850	1.8	2.1	2.9	3.2	2.4	2.7
700	0.8	0.8	1.8	2.5	1.3	1.9
500	0.9	1.4	1.4	1.6	1.2	1.5
400	1.5	2.1	1.2	1.4	1.4	1.8
300	1.8	3.4	1.8	2.3	1.8	2.9
250	3.5	4.1	2.3	2.8	2.9	3.5
200	3.5	3.6	2.3	2.4	2.9	3.1
150	2.3	2.8	1.8	2.2	2.1	2.5
100 mb	1.5°C	2.1°C	1.5°C	1.5°C	1.5°C	1.8°C

orbits, an average difference for both orbits, level by level, has a systematic variation with pressure. At the lowest level, 920 mb, the temperature difference is a maximum (3.0°C) and decreases to a minimum (1.2°C) at 500 mb. There is a gradual increase in the mean difference up to 200 mb followed by a slight decrease at 100 mb. In general, the comparison between the ITPR temperature values and the interpolated radiosonde soundings is quite good, particularly in the mid-troposphere.

In addition to the differences in the layer thickness between the ITPR and RAOB data and the layer mean temperatures presented in Table 2, the layer differences in mean temperature are presented in Table 4. The mean temperature error or differences expected in the comparisons due to the error in determining the regression coefficients in the ITPR solution as well as the error in the RAOB temperatures are combined and presented in the second column. The layers are those between standard ITPR temperature levels. The third column in Table 4 presents the mean of the absolute value of the layer differences observed in the data from

Table 4. A comparison of the differences between the RAOB and ITPR temperatures. Mean layer temperatures were determined from the combined "error" in interpolating the RAOB data to the ITPR sounding location, as well as instrument and reduction error, and the ITPR regression analysis error (Table 2, Col. 5) with mean differences and standard deviations of differences, σ_D, (from Table 3, Col. 5 and 6) observed in Orbits 6932 and 6939. Standard deviations of ITPR and RAOB difference found by Smith and Woolf (1974) have been determined for comparable layers used here and are illustrated in the last column.

Layer	Expected Error due to the ITPR Solution and RAOB Errors	6932-6939		Smith and Woolf (1974)
		$\overline{\lvert T_{RAOB}-T_{SAT}\rvert}$	σ_D	σ_D
920-850 mb	2.5°C	2.7°C	3.1°C	2.3°C
850-700	2.0	1.9	1.8	2.1
700-500	1.8	1.3	1.4	1.6
500-400	1.5	1.3	1.5	1.9
400-300	1.7	1.6	2.2	2.2
300-250	1.9	2.4	2.9	3.1
250-200	2.0	2.9	3.0	3.6
200-150	1.9	2.5	2.7	3.5
150-100 mb	1.7°C	1.8°C	1.8°C	3.7°C

Orbits 6932 and 6939 over the AVE II area. It is of particular interest to note that the expected error or difference and the observed differences are practically the same up to the 300-250-mb layer. In the region near the tropopause, the observed difference is slightly greater than the expected error. This would indicate that in the mean, the ITPR soundings are about as good as could be expected with the present reduction system. The standard deviation of the layer mean temperatures estimated from results of Smith and Woolf (1974) are given in the fifth column of Table 4. In general these deviations are slightly greater than the mean temperature differences found in this study. This should not be entirely unexpected since the temporal as well as spatial separation between the ITPR and RAOB soundings were less in this study.

7. SATELLITE-DERIVED CROSS SECTIONS OF WIND

The temperature soundings obtained from the ITPR sounder provide information which enables the determination of the geostrophic wind component normal to the orbital track. This is accomplished using the thermal wind equation

$$\vec{V}_t = \vec{V}_g(P_2) - \vec{V}_g(P_1) = \frac{R}{f} \ln\frac{P_2}{P_1} (\vec{V}_D T \times \vec{k}) \qquad (1)$$

In the case of the ITPR data, the pressure surfaces P_1 and P_2 where $P_1 > P_2$ are determined by the vertical data spacing in the soundings. The horizontal temperature gradient is evaluated in the plane of the orbital track. In the temperature solutions for Orbits 6932 and 6939, the layers used were 920-850 mb, 850-700 mb, 700-500 mb, 500-300 mb, 300-250 mb, 250-200 mb, 200-150 mb, and 150-100 mb. The mean temperatures for the layers were determined by taking averages at the base and top of each layer. The horizontal gradients of the mean temperatures were determined between successive soundings along the orbital track, and subsequently a layer thermal wind was computed between each pair of pressure levels up to 100 mb. In the two cases treated here, a component geostrophic wind cross section along the United States portion of the two orbital tracks is developed using the measured 500-mb wind component normal to the cross section as a tie-on wind.

Three problems arise in the application of the above wind computation technique. First, the geostrophic wind and the actual wind may not be the same; second, errors in the temperature and consequently the temperature gradient will induce errors in the computed geostrophic wind; and third, a tie-on wind may not be known. The first problem, geostrophic versus actual wind values, is a classic problem and will be treated later. The question of a representative tie-on wind in areas where satellite-derived winds are the only data source can possibly be solved using wind values derived from cloud motion vectors and assigned a height corresponding to cloud temperature. The second problem, wind error induced by temperature gradients incorrectly determined from the ITPR data, can be examined for the two orbits under discussion by making use of data on temperature differences presented in the previous section.

From the thermal wind equation, errors in the thermal wind normal to the cross section due to errors in the cross section horizontal temperature

gradient between two levels can be specified by

$$\Delta V_{t(n)} = \frac{R}{f} \ln\frac{P_1}{P_2} \frac{\partial(\Delta T)}{\partial S} \qquad (2)$$

where $\Delta V_{t(n)}$ is the error in the thermal wind normal to the cross section resulting from an error in the mean temperature gradient $\frac{\partial(\Delta T)}{\partial S}$ where S is defined as positive toward the south and is distance measured in the section. The magnitude of the error in the computed geostrophic wind from a thermal wind error induced by a one degree error in the temperature gradient is presented in Table 5. In this table, the error in the thermal wind between successive ITPR data layers in presented. If the wind is assumed to be known at 500 mb, an error in the geostrophic wind at any other level will be the sum of the individual layer thermal wind errors from 500 mb to any other level. In the case of an error of 1°C over four degrees of latitude, an error of almost 7 m s^{-1} will result in the geostrophic wind at 200 mb. If the geostrophic wind had been built up from the lowest level (920 mb), this error would have been 11.62 m s^{-1}, the sum of the geostrophic wind error at 200 and 920 mb, or about 23 kts. An error of 2°C over four degrees of latitude would double the errors in Table 5.

Table 5. Induced thermal wind error and corresponding error in the geostrophic wind due to an error in the layer horizontal temperature gradient of 1°C/4°lat. The 500-mb level is assumed to be the level that the wind field is developed from.

Pressure Level (mb)	Thermal Wind ($m\ s^{-1}$) error	Geostrophic Wind ($m\ s^{-1}$) error
100		12.26
	3.09	
150		9.17
	2.19	
200		6.98
	1.70	
250		5.28
	1.39	
300		3.89
	2.19	
400		1.70
	1.70	
500		0.00
	2.56	
700		2.56
	1.48	
850		4.04
	0.60	
920		4.64

When errors in the temperature gradient are evaluated, a measure of the expected geostrophic wind error can be determined. Since in this study there is no assurance that the RAOB values of temperature are at the exact point of the ITPR data, the differences between the ITPR and RAOB gradients and geostrophic winds will be discussed rather than specific errors in the ITPR derived data. Although Togstad and Horn (1974) have shown that a gradient distance of 2°lat produces the optimum geostrophic wind field, ITPR sounding point spacings during AVE II do not permit the evaluation of the gradient over such short intervals. Since the average ITPR spacing is approximately 4°lat in this study, this distance will be used for gradient evaluation. Such a distance should produce a geostrophic wind field which approximates the wind field deduced from standard rawinsonde station spacing. The differences in temperature gradient as a result of differences between the RAOB and ITPR temperatures at sounding points are presented for Orbit 6932 in the cross section shown in Fig. 25 using a uniform interval of 4°lat. Gradient differences are relatively large at the tropopause level as well as near the surface, reaching 6°C between data points 82 and 83. This particular large difference, however, is induced by the solution profile of the data set and is probably not representative of what would have been found if all Solution 3 profiles had been available. There are other areas in the cross section where gradient differences as large as 4°C are found.

The differences between ITPR-and RAOB-derived geostrophic winds resulting from the temperature gradient differences in the cross section of Orbit 6932 are presented in Fig. 26. The maximum difference between geostrophic wind normal to the cross section occurs near 300 mb where the difference reaches a magnitude of 20 m s^{-1}. Since the sign of the temperature gradient difference changes with height across most of the cross section, the geostrophic wind difference usually increases to some maximum value and subsequently decreases.

If, as was the case in the preceding example, the distance over which the gradient is determined is not an optimum distance but a distance specified by sounding spacing along the orbital track, a slightly different difference distribution will result. Figure 27 illustrates the expected difference in the geostrophic wind if the thermal gradient had been evaluated between ITPR locations. Although the general pattern is similar to the difference pattern presented in Fig. 26, the relative positions of the maximum values as well as the values themselves have changed.

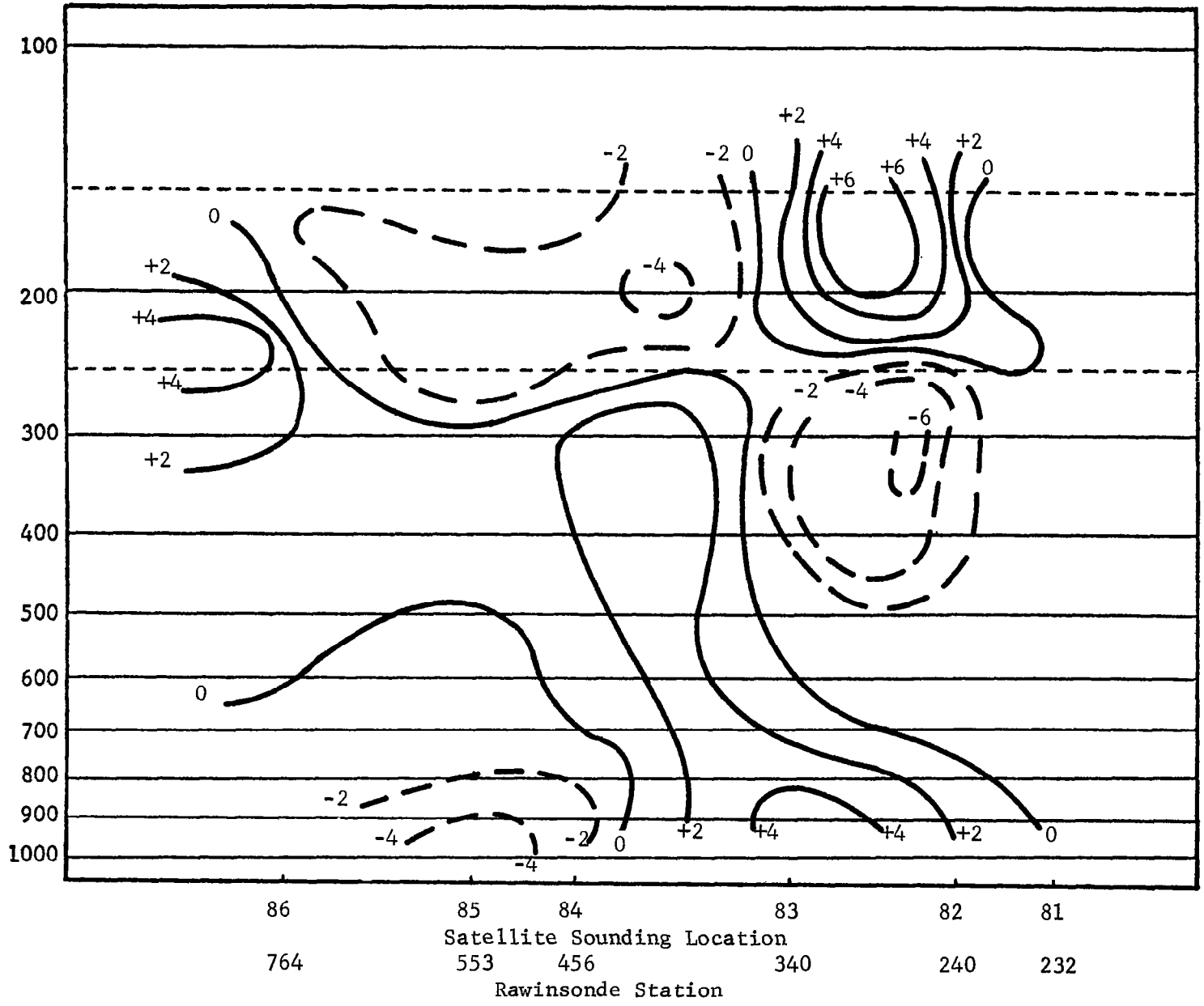

Fig. 25. Differences between satellite-derived horizontal temperature gradient (°C/4°lat) and RAOB temperature gradient at 1800 GMT, 11 May 1974, induced by differences at the individual sounding points along Orbit 6932.

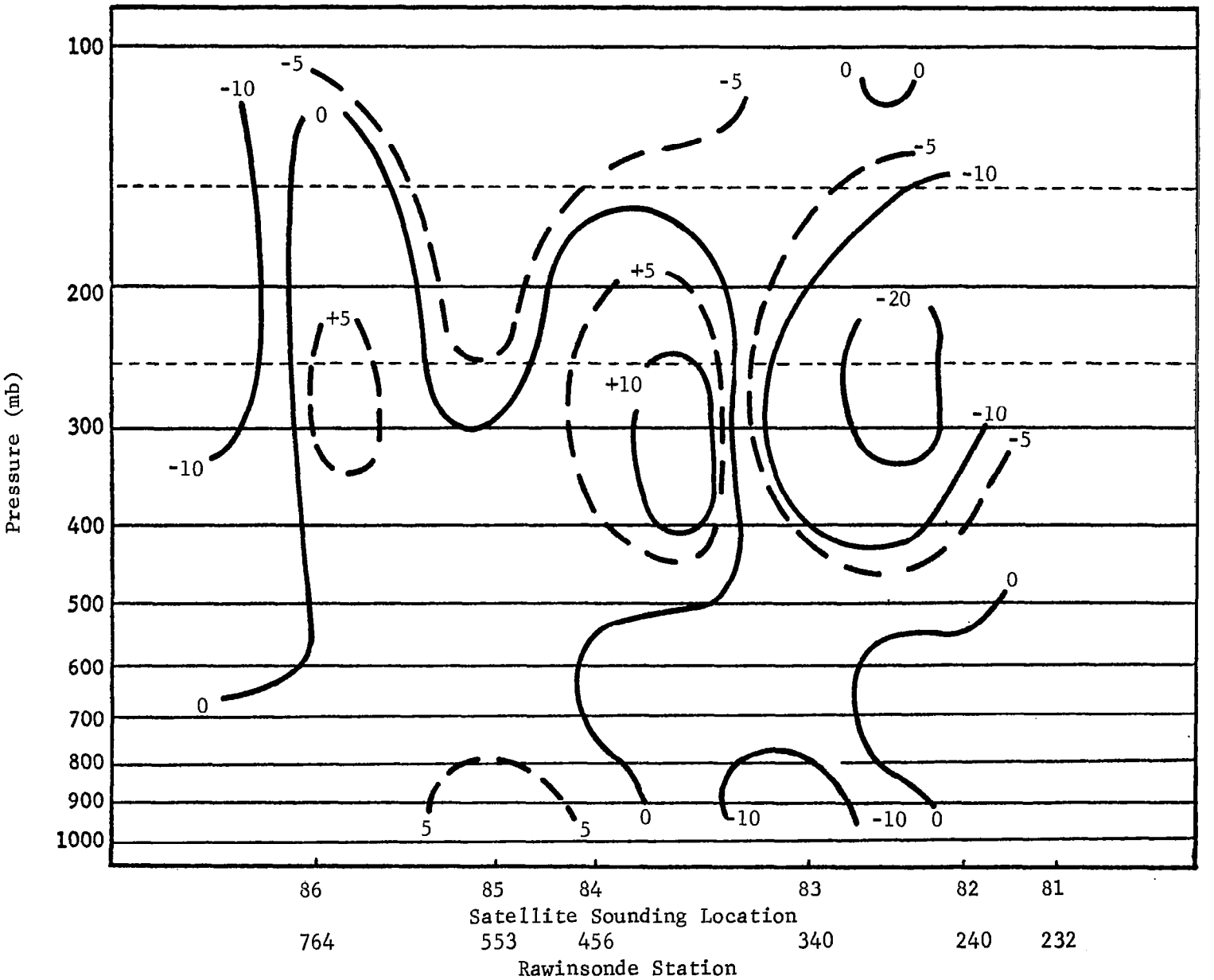

Fig. 26. Difference (V_{RAOB} - V_{SAT}) in the component geostrophic wind (m s^{-1}) normal to the Orbit 6932 cross section as a result of the difference between the satellite and RAOB-derived horizontal temperature gradient evaluated over a uniform interval of 4°lat. The 500-mb level was used as the tie-on level for the thermal wind buildup.

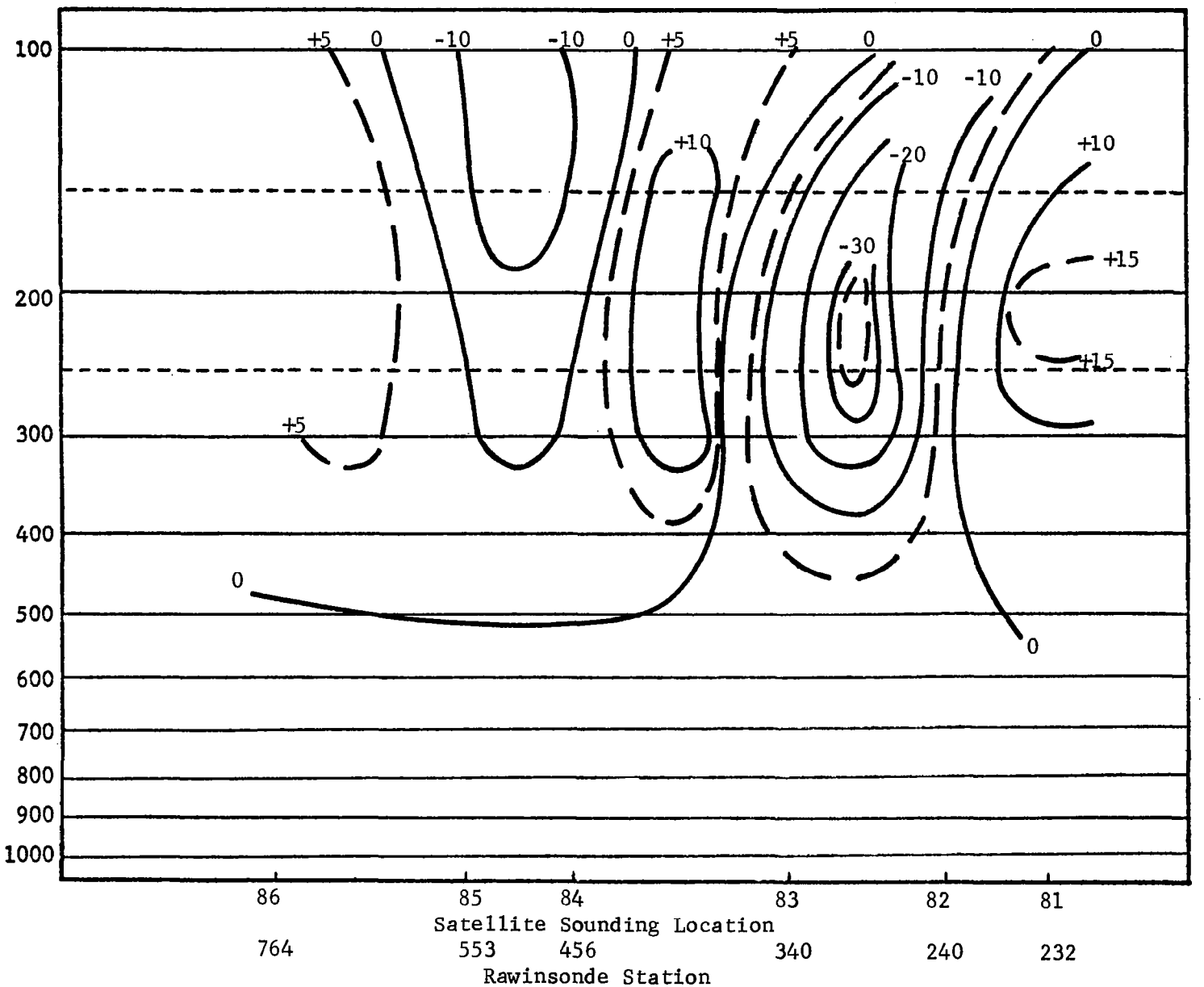

Fig. 27. Difference (V_{RAOB} - V_{SAT}) in the component geostrophic wind (m s^{-1}) normal to the Orbit 6932 cross section as a result of the difference between the satellite and RAOB-derived horizontal temperature gradient using actual sounding point separation as the distance over which gradients were evaluated. The 500-mb level was used as the tie-on level for the thermal wind buildup.

The differences in temperature gradient along the cross section of Orbit 6939 evaluated from the temperature difference distribution shown in Fig. 23 are presented in Fig. 28. Again, as was the case in Orbit 6932, a Solution 2 profile existed within the cross section at data point 105. This time, however, the associated differences were not as serious as in Orbit 6932 and the differences in gradient are not as localized. In the middle troposphere and lower stratosphere, the maximum difference between the temperature gradients evaluated from the ITPR and RAOB information over 4°lat were on the order of 2°C, and for the most part less, while in the lower troposphere gradient differences reached slightly in excess of 4°C/4°lat. The corresponding difference in the wind field, when built up and down from the 500-mb surface, is presented in Fig. 29. Above 600 mb the maximum difference was 4.4 m s^{-1} in tne upper troposphere. Below 600 mb the geostrophic wind difference becomes quite large, reflecting the large gradient differences presented in Fig. 28.

Again, if the gradient is evaluated between ITPR locations rather than using a uniform distance of 4°lat, a different geostrophic wind difference field is produced. As can be seen in Fig. 30 for Orbit 6939, geostrophic differences on the order of 10 m s^{-1} are present above 200 mb, and the area within the cross section where there are differences between the correct geostrophic wind and the erroneous geostrophic wind in excess of 5 m s^{-1} is quite large.

The preceding exploration of expected difference in the geostrophic wind as a function of the measured temperature differences and the associated difference in the temperature gradient revealed several interesting features. It is apparent that although the differences in the temperature data seem to be pressure dependent, there is a sufficient amount of difference variation at the same pressure levels that significant errors in a computed geostrophic wind will result. Although each of the orbits examined here had what might be termed a nonrepresentative profile in the data set, the fact that it occurred indicates that not all profiles within a data set of interest will be as good as desired.

The fact that in this case, minimum differences in the geostrophic wind occurred in the mid-troposphere is a result of the difference minimum in the temperature gradients in this region as well as from choosing the 500-mb wind as a tie-on wind. A different level of tie-on wind would have

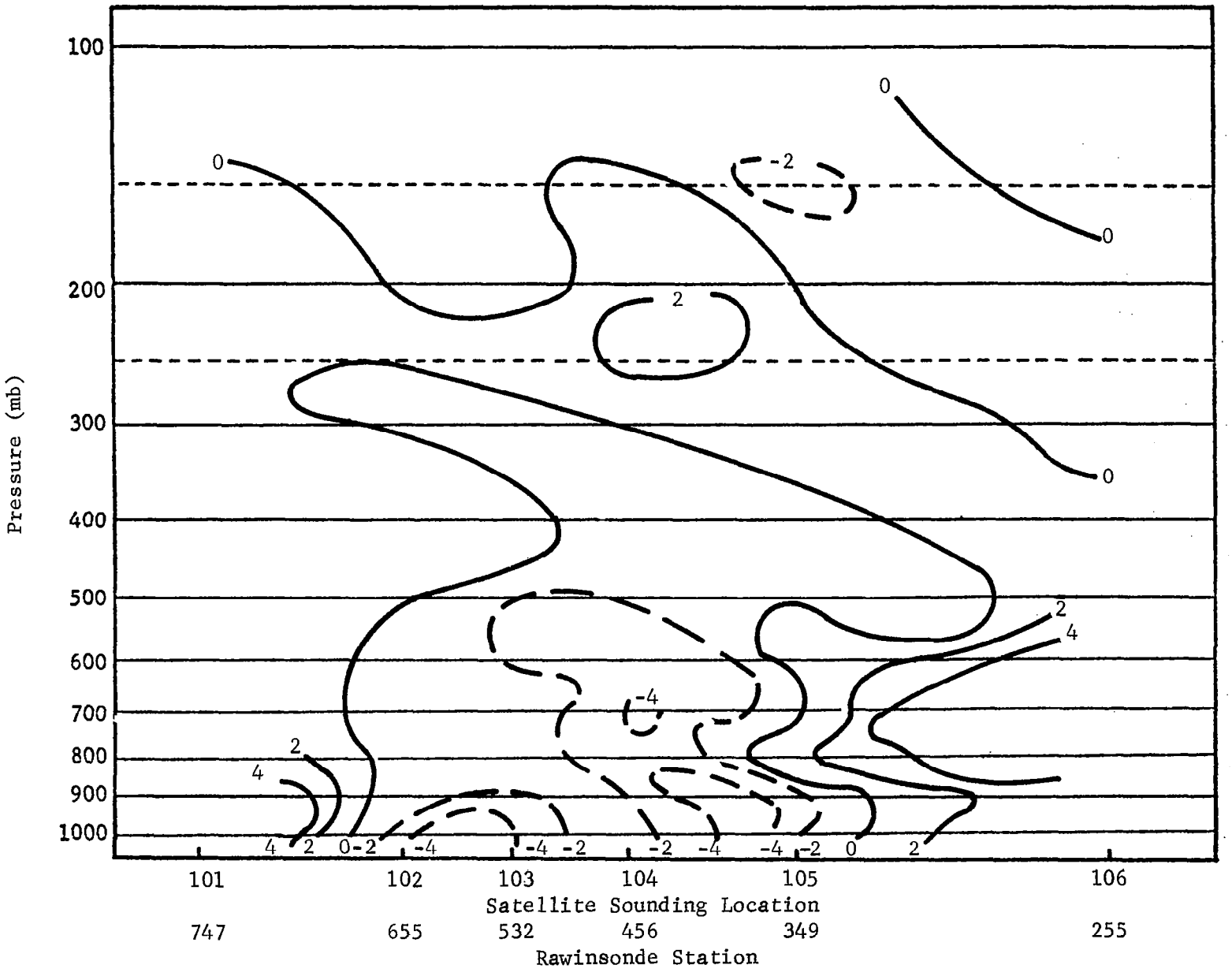

Fig. 28. Differences between satellite-derived horizontal temperature gradient (°C/4°lat) and RAOB temperature gradient at 0600 GMT, 12 May 1974, induced by differences at the individual sounding points along Orbit 6939.

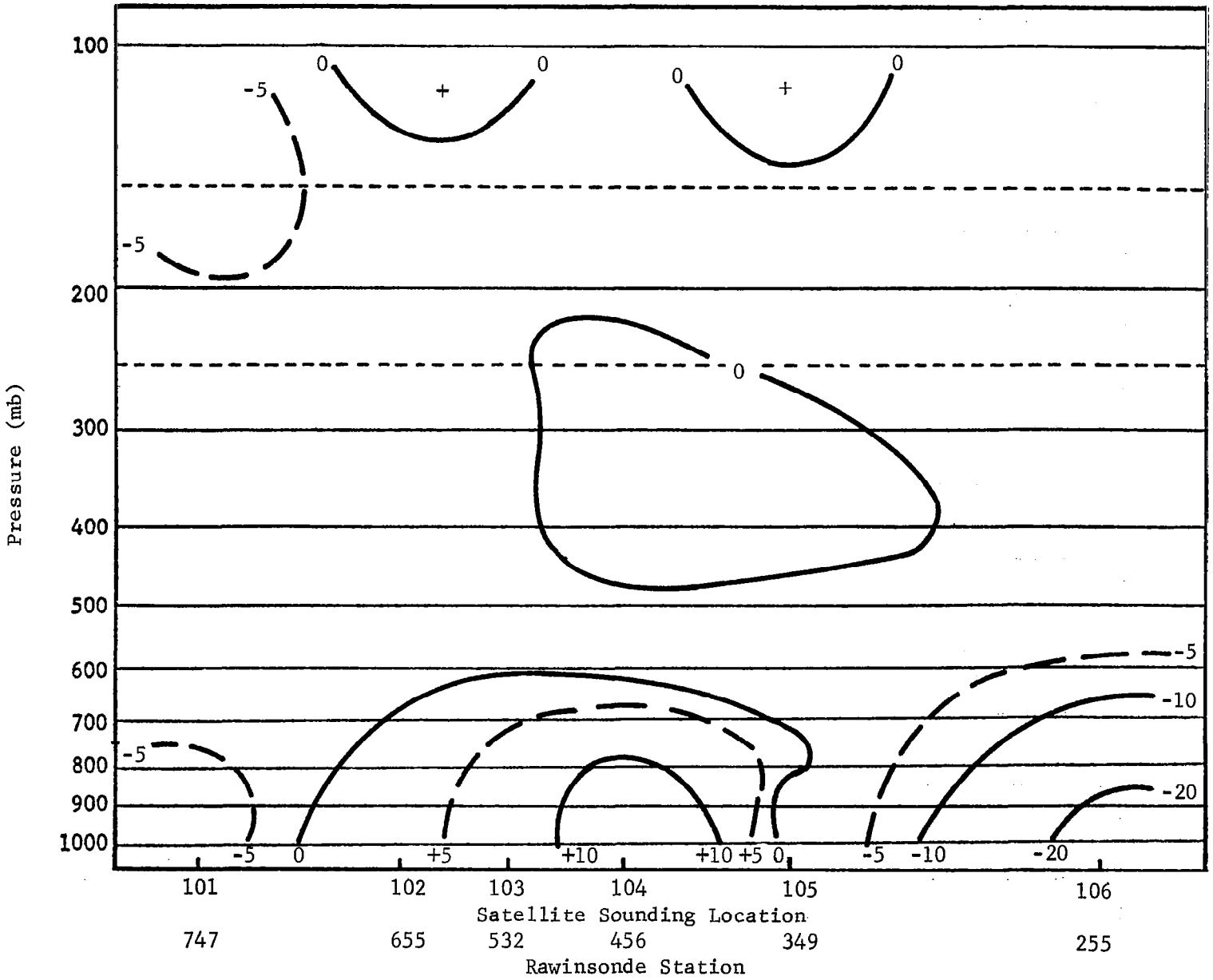

Fig. 29. Differences (V_{RAOB} - V_{SAT}) in the component geostrophic wind (m s^{-1}) normal to the Orbit 6939 cross section as a result of the difference between the satellite and RAOB-derived horizontal temperature gradients evaluated over a uniform interval of 4°lat. The 500-mb level is used as a tie-on level for the thermal wind buildup.

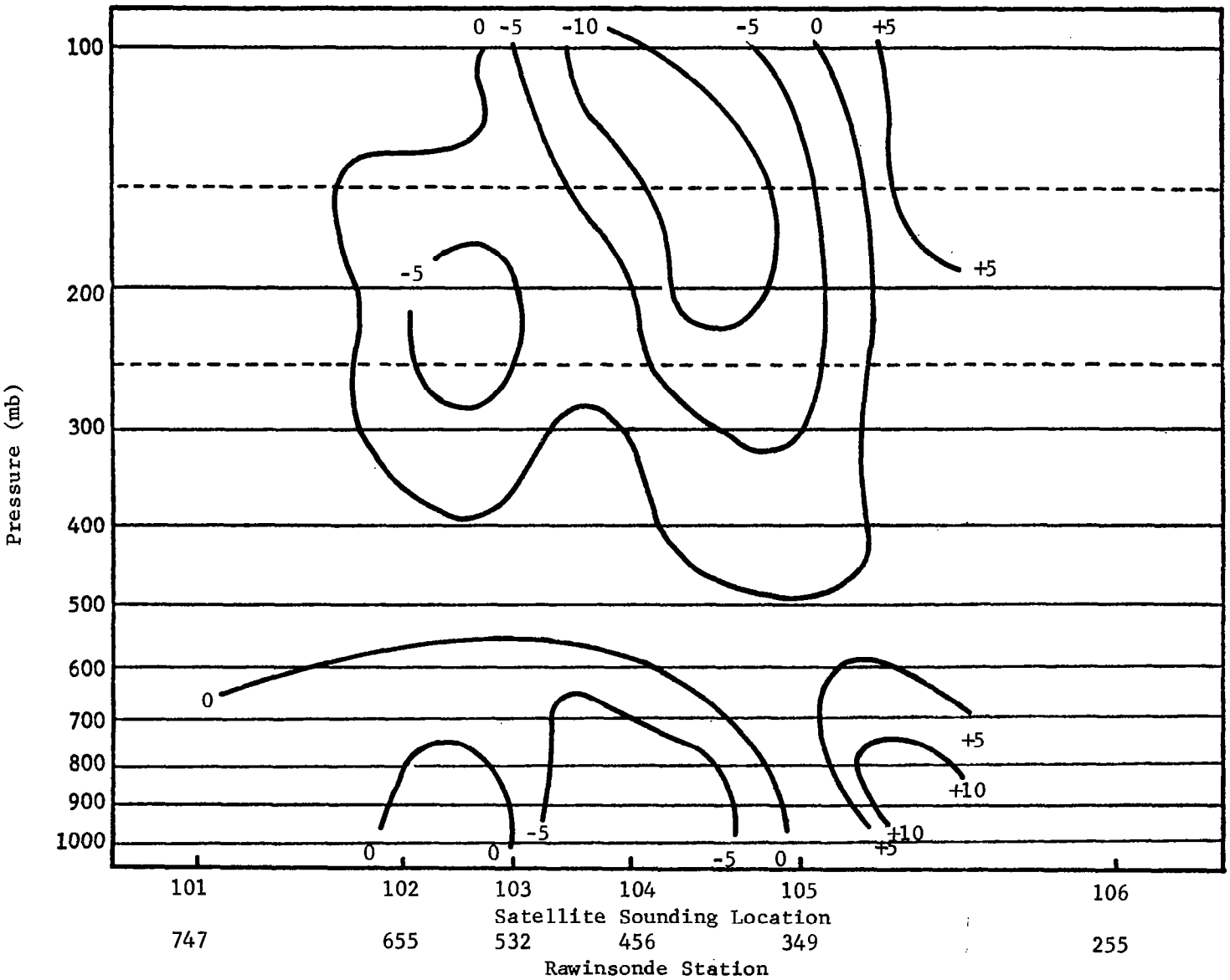

Fig. 30. Differences (V_{RAOB} - V_{SAT}) in the component geostrophic wind (m s^{-1}) normal to the Orbit 6939 cross section as a result of the differences between the satellite-derived horizontal temperature gradient using actual sounding point separation as the distances over which gradients were evaluated. The 500-mb level was used as a tie-on level for the thermal wind buildup.

changed the magnitudes of the differences but the patterns would have remained the same. As was pointed out previously, it would seem that two tie-on wind levels determined from cloud motion vectors and cloud levels would produce a more optimum solution approach. This could possibly minimize the differences developed by successively building from one level.

It is of interest to compare the geostrophic wind buildups determined from the ITPR satellite data and geostrophic wind buildups based on the radiosonde data. Using the thermal wind equation to evaluate the thermal wind between successive levels and using the 500-mb wind as a tie-on wind, a cross section of geostrophic wind normal to the satellite path was constructed for each of the two orbits using the radiosonde temperature data interpolated to the satellite sounding points. Figure 31 shows the resultant geostrophic wind cross section along Orbit 6932. A maximum wind component of 51 m s^{-1} from the west is present between points 84 and 85 at 300 mb with another maximum on the southern end of the cross section near data point 81. A deep minimum region in the component wind normal to the cross section is observed between points 82 and 83.

The geostrophic wind field normal to the 6932 orbital track derived from the ITPR data (including error) is presented in Fig. 32. The striking difference between this figure and Fig. 31 is the double maximum in the layer of 200-300 mb in the central portion of the cross section. In this particular case, the difference between the ITPR and RAOB temperature measurements have induced the secondary jet between stations 82 and 83 with the resulting misleading impression, based on the ITPR data, that two cores of maximum wind exist in this region. Within computational accuracy, the difference between Figs. 31 and 32 has already been illustrated in Fig. 27.

The geostrophic wind built up using the RAOB data coincident with Orbit 6939 is presented in Fig. 33. A maximum in the geostrophic wind occurs just above 300 mb between data points 103 and 104. The maximum component wind is 66.9 m s^{-1} with the axis of the maximum wind displaced slightly north at pressure levels below 700 mb and at 100 mb. At both the northern and southern ends of the cross section, the geostrophic wind normal to the cross section becomes less than 5 m s^{-1} with a shallow layer of eastward components near the surface on the southern end.

The ITPR data were used to construct a cross section of the component of geostrophic wind normal to Orbit 6939. The results are presented in

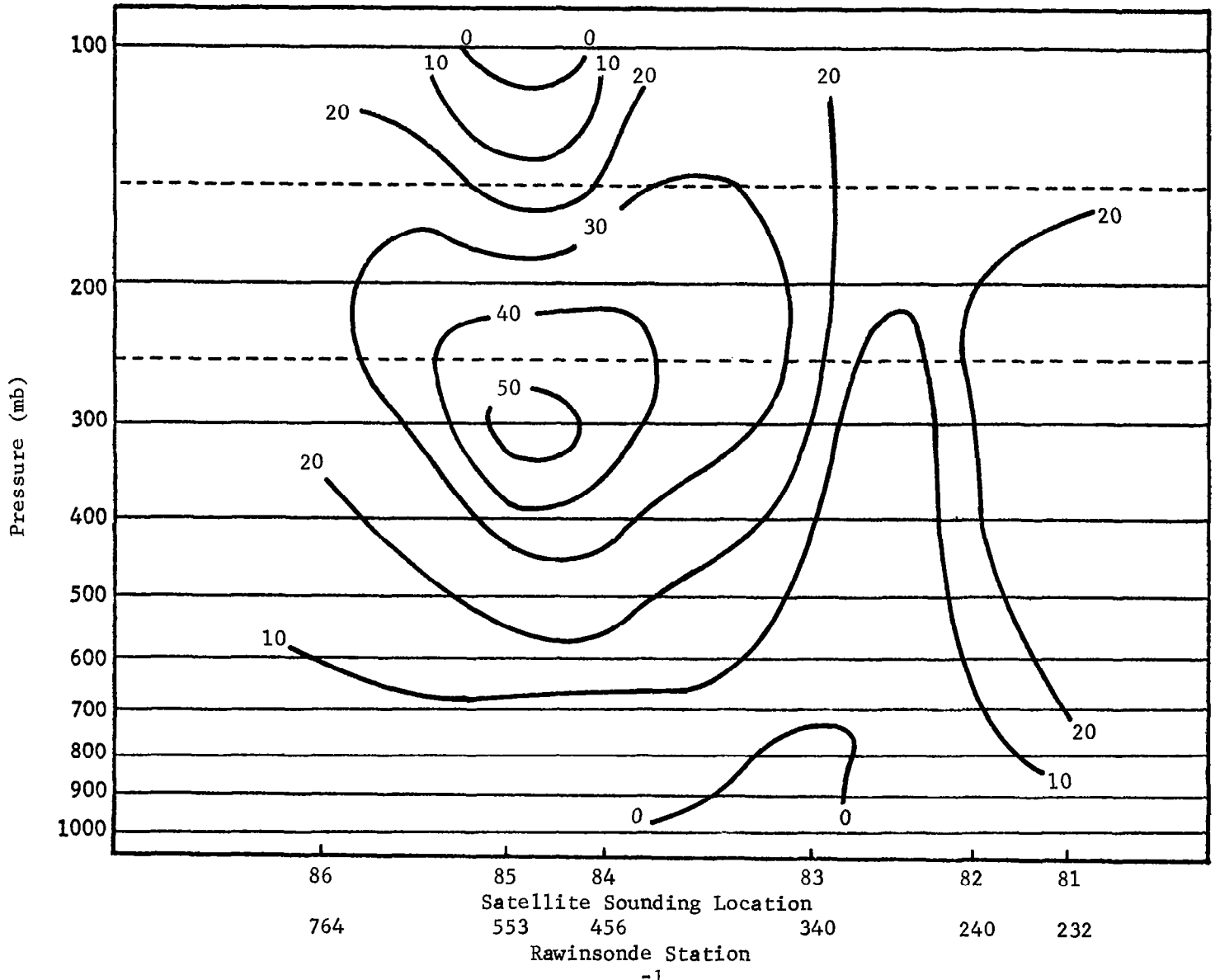

Fig. 31. The geostrophic wind component (m s^{-1}) normal to the Orbit 6932 cross section as determined from the radiosonde temperature data taken at 1800 GMT on 11 May 1974. The temperature profiles were interpolated to the position of the ITPR sounding point prior to the evaluation of layer temperature gradients. Positive values represent west to east flow.

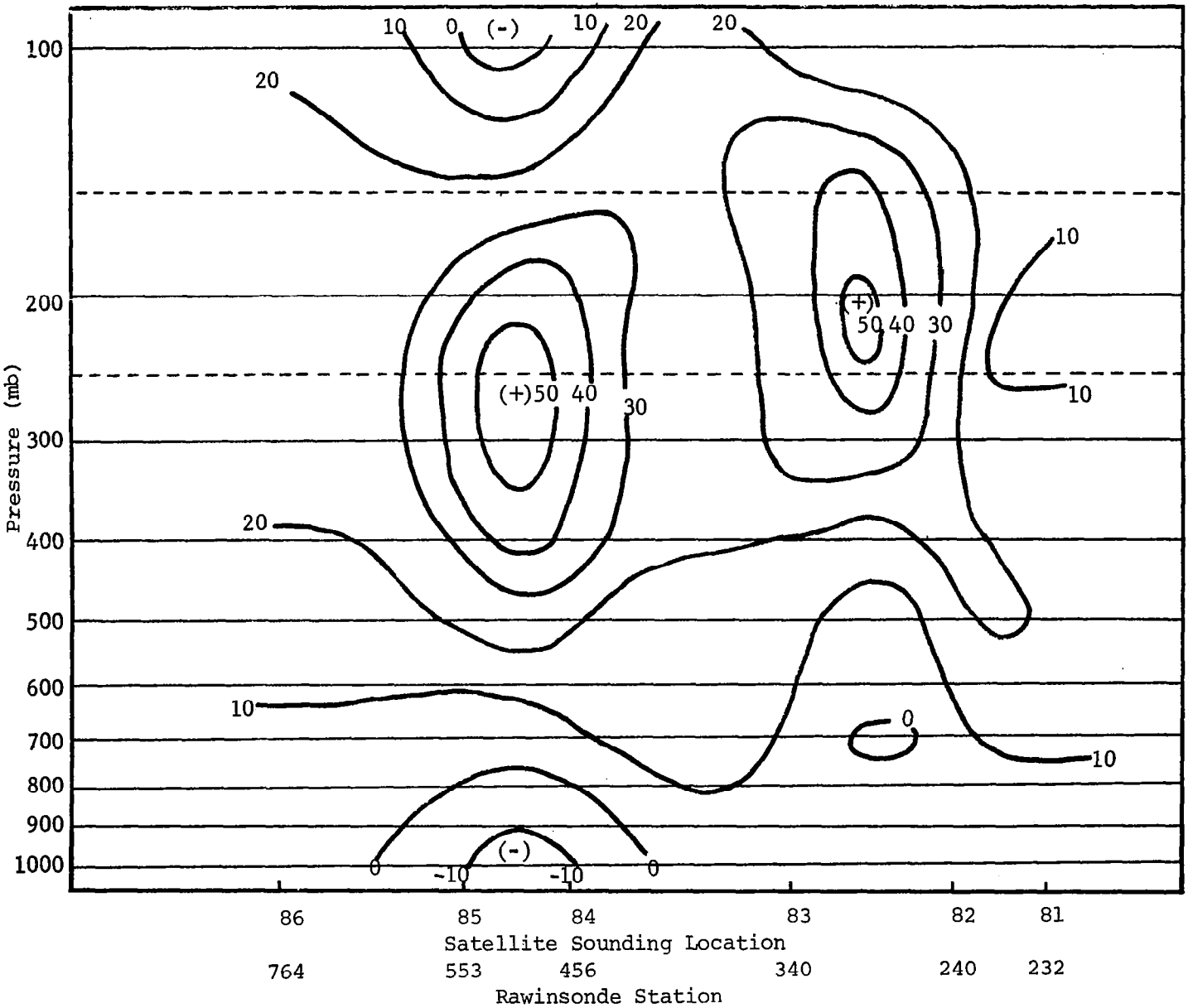

Fig. 32. The geostrophic wind component (m s^{-1}) normal to the Orbit 6932 cross section as determined from the temperature profiles determined from the Nimbus 5 ITPR. Layer temperature gradients were evaluated between sounding points.

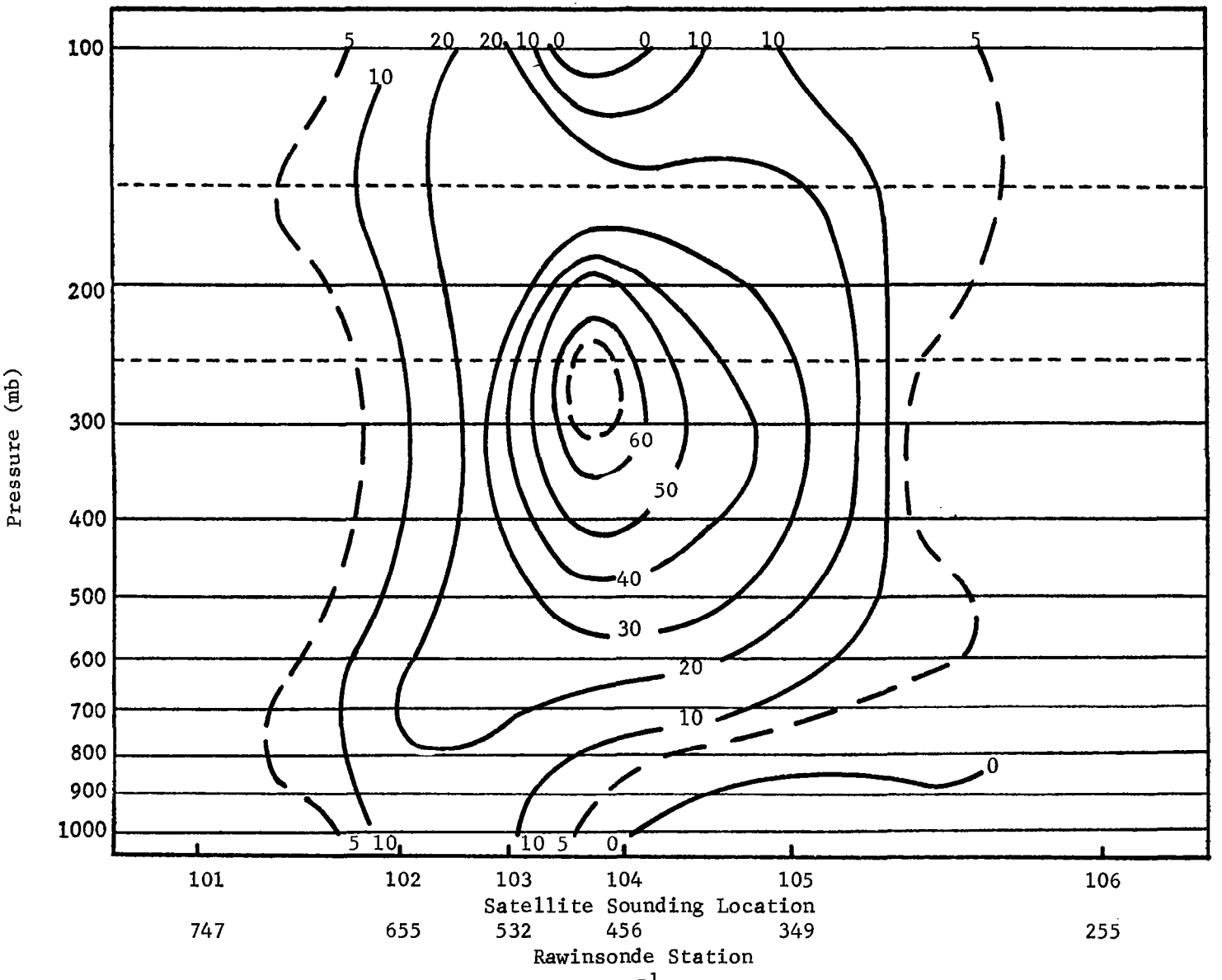

Fig. 33. The geostrophic wind component (m s^{-1}) normal to the Orbit 6939 cross section as determined from the radiosonde data taken at 0600 GMT on 12 May 1974. The temperature profiles were interpolated to the position of the ITPR sounding points prior to the evaluation of layer temperature gradients between stations. Positive values represent west to east flow.

Fig. 34. The ITPR-derived geostrophic wind field for Orbit 6939 shows the maximum geostrophic wind component occurring just above 300 mb between data points 103 and 104 with a maximum speed of 66 m s^{-1}. As in the RAOB cross section, the wind maximum is displaced northward at high and low altitudes. The low-level zone of easterly components also appears in the satellite-derived wind; however, it is shifted slightly north of the RAOB wind low-level easterlies. In both Figs. 33 and 34 there is a small area of easterly winds at 100 mb. The difference between the wind fields in these two figures has already been presented in Fig. 30.

The differences in the horizontal temperature gradients and the resulting differences in the geostrophic wind field within a given cross section will vary as a function of the gradient distance used in the evaluation. This is particularly true in cases such as have been examined here where the spacing of the ITPR data points corresponds to that spacing found in a normal radiosonde network. In fact, a noticeable wind difference has been shown to take place if actual sounding separation is used rather than a uniform distance corresponding to the mean sounding spacing. For this reason it is relatively difficult to place a numerical value on the mean gradient differences or wind differences determined from the ITPR and RAOB soundings.

Using the layer mean differences in temperature in individual ITPR soundings along the orbital cross section, an indication of the temperature gradient differences between bounding pressure values within each cross section can be determined. The distances over which the gradient was determined, and thus the gradient differences, were allowed to vary as a function of the actual distances between ITPR sounding points. ITPR stations averaged 3.8°lat apart on Orbit 6932 and 4.5°lat apart on Orbit 6939. The resulting temperature gradient differences observed between pressure levels on each of the orbits are shown in Table 6. The gradient difference data for Orbit 6932 shows a decrease up to the 700-500-mb layer followed by an increase at the 400-300-mb layer. The comparatively large difference in the temperature gradient at this level is due to large differences between the individual ITPR-RAOB profiles of different sign at these levels at data points 82 and 83 (see Fig. 16). The variation of the differences in the horizontal temperature gradients with height listed for Orbit 6939 are probably more representative of what should be

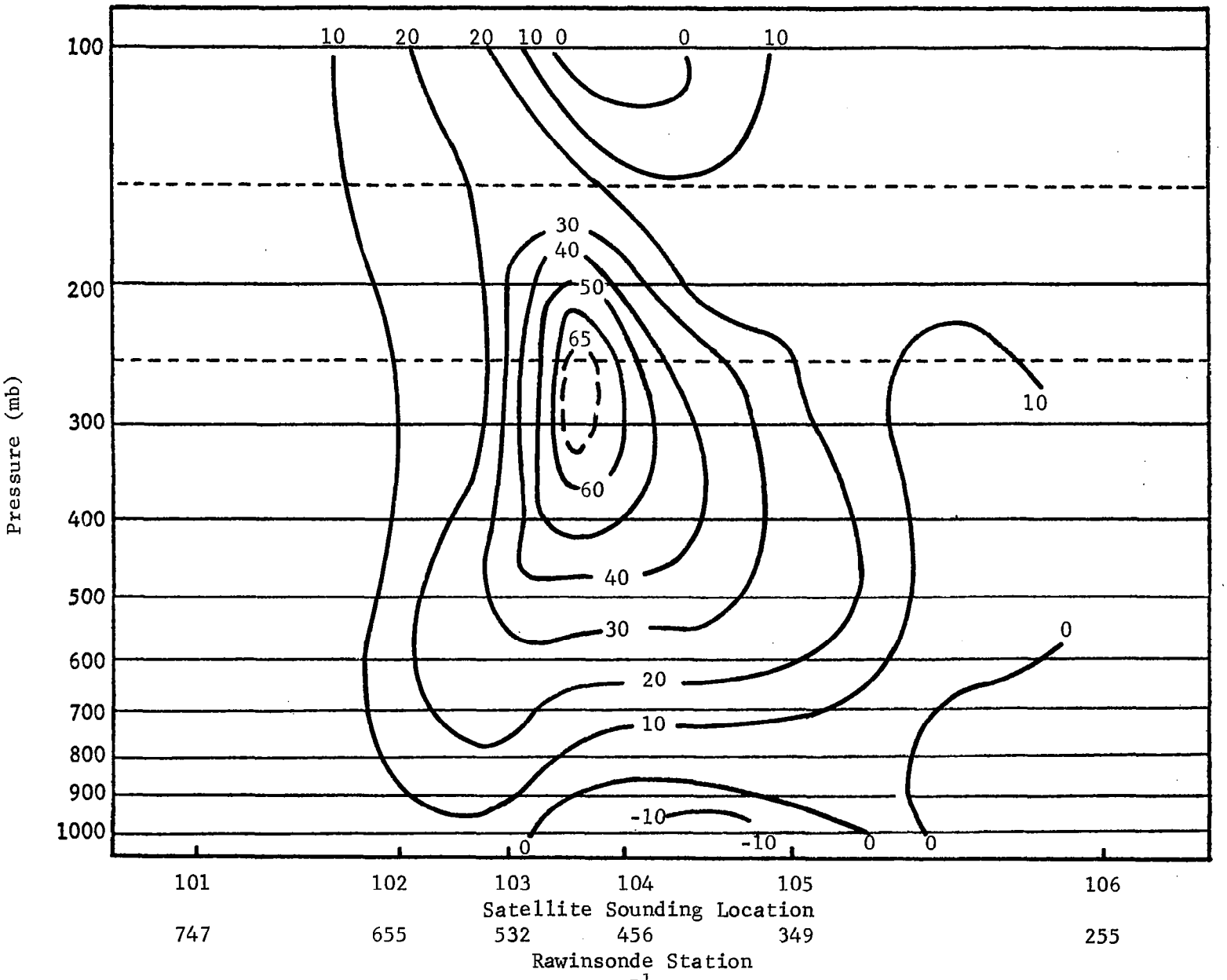

Fig. 34. The geostrophic wind component (m s^{-1}) normal to Orbit 6939 cross section as determined from the temperature profiles determined from the Nimbus 5 ITPR. Layer temperature gradients were evaluated between sounding points.

Table 6. ITPR layer temperature gradient differences (means of absolute value) between ITPR and RAOB temperature gradients. The gradient distance average was 4°lat, but specific distances were between adjacent ITPR data point.

Layer	Orbit 6932 Gradient Difference	Orbit 6939 Gradient Difference	Average Gradient Difference	Layer Thermal Wind Difference
920-850 mb	2.1°C/3.8°lat	2.1°C/4.5°lat	2.1°C/4.2°lat	1.3 m s^{-1}
850-700	1.5	2.3	1.7	2.5
700-500	1.0	1.7	1.4	3.6
500-400	1.8	0.9	1.3	2.2
400-300	3.2	0.8	2.0	4.4
300-250	2.9	1.4	2.1	2.9
250-200	1.6	1.3	1.4	2.4
200-150	3.8	0.9	2.4	5.3
150-100 mb	3.5°C/3.8°lat	1.2°C/4.5°lat	2.4°C/4.2°lat	7.5 m s^{-1}

expected. Here the layer horizontal temperature gradient difference decreases to 0.8°C/4.5°lat in the 400-300-mb layer followed by a slight increase. The vertical distribution of the temperature gradient in the plane of the cross section between layers for both orbits combined is also shown in Table 6. There is basically a trend toward minimum horizontal gradient differences in the mid-troposphere with a maximum at low and high levels. The average gradient distance here is 4.2°lat. Although it is tempting to normalize the gradient errors to 4°lat, such a manipulation would have little meaning.

The differences in geostrophic wind which would be present with the gradient temperature differences illustrated would depend on where the geostrophic wind buildup began. The thermal wind differences induced by the temperature gradient differences in the layers presented in Columns 2-4 of Table 6 are given in the last column of Table 6 if the gradient distance is assumed to be 4°lat. In most layers, the wind difference is approximately 3 m s^{-1}. The geostrophic wind differences at any one layer will be the sum of the individual thermal wind differences up to that level. A mid-tropospheric tie-on wind will produce a minimum magnitude difference at either extreme. A surface tie-on wind will produce a maximum magnitude difference at the top of the sounding if the gradient differences are of

the same sign throughout the profile. Usually, in individual cross sections, the sign of the gradient differences will change at least once in the vertical. For this reason, the maximum geostrophic wind difference usually occurs at some point below the top of the geostrophic wind profile or cross section.

Comparison of the geostrophic winds derived from the RAOB and ITPR cross sections with actual wind components would only be realistically possible if the flow in the vicinity of the cross section were straight and unaccelerated. In the two cases studied, the cross sections are nearly in the trough lines in the synoptic data where neither of the above conditions is met. In an effort to obtain some comparison with actual winds, however, rawinsonde winds normal to the cross sections were adjusted through the gradient wind equation to simulate a geostrophic wind field. The curvature of the flow was estimated from the contours in the vicinity of the cross section axis. This adjustment brought the observed winds within fair agreement with the geostrophic winds determined from the temperature data within the cross sections. The adjusted wind components are presented for 11 May, Orbit 6932, in Fig. 35 and for 12 May, Orbit 6939, in Fig. 36. In both cases the magnitude and the general pattern of the adjusted winds are similar to the geostrophic winds developed from the radiosonde temperature data.

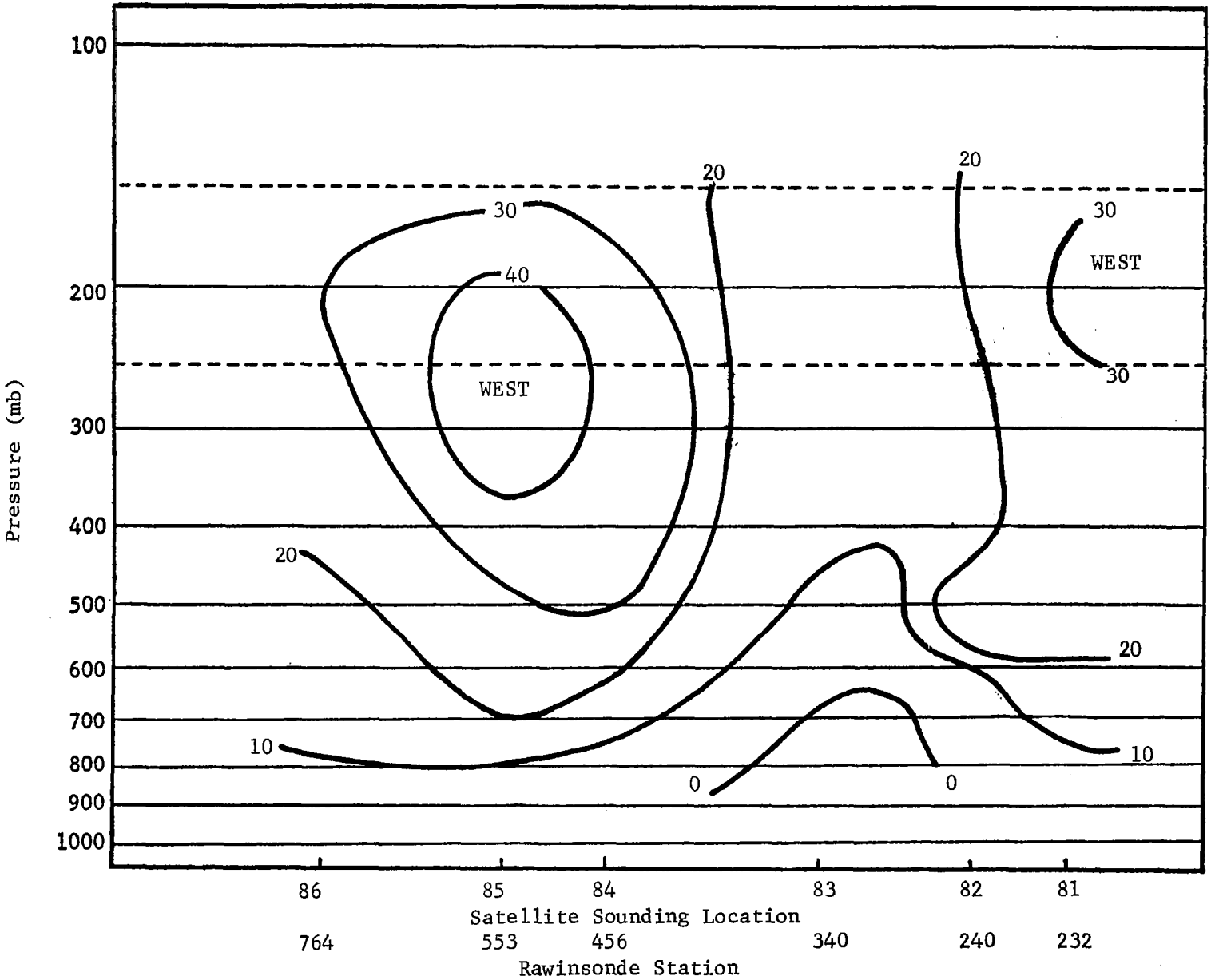

Fig. 35. Adjusted geostrophic wind component (m s^{-1}) normal to the orbital plane of Nimbus 5 Orbit 6932 at 1800 GMT, 11 May 1974. The geostrophic wind component was deduced from the actual wind by estimating the streamline curvature and using the gradient wind equation.

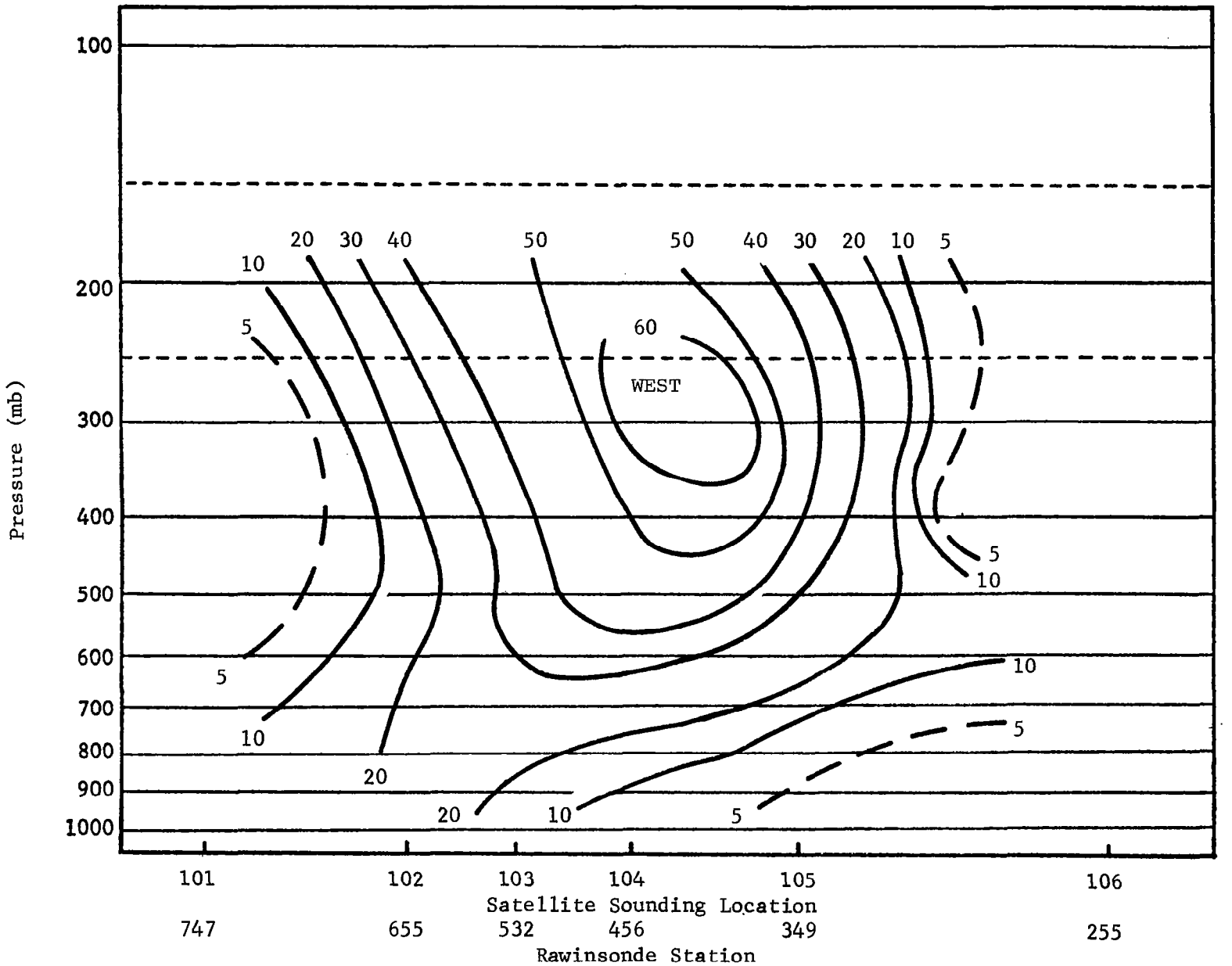

Fig. 36. Adjusted geostrophic wind component (m s^{-1}) normal to the orbital plane of Nimbus 5 Orbit 6939 at 0600 GMT, 12 May 1974. The geostrophic wind component was deduced from the actual wind by estimating the streamline curvature and using the gradient wind equation.

8. CONCLUSIONS

The purpose of this study was to examine some of the temperature fields derived from the Nimbus 5 THIR experiment over regions where clouds exist, to compare them with radar cloud-top observations, and to examine clear sky surface temperatures as determined from the THIR experiment and the ITPR experiment and to compare them with shelter temperatures. A second and significant portion of this study was to examine the accuracy of the ITPR data, and implicitly the reduction technique, based on coincident radiosonde observations. This accuracy analysis is projected into the area of geostrophic wind determinations using the satellite ITPR data. From the results of this study the following tentative conclusions were deduced:

1) Temperature mapping from the 11.5 micrometer THIR channel on a 1:10,000,000 scale produced a drastic smoothing of the temperature field; however, cloud-top heights assigned on the basis of temperature still agreed well with maximum radar-echo tops in regions of significant clouds.

2) Use of the 11.5 micron THIR channel on a 1:2,000,000 scale gave great detail in the cloud fields but agreement between cold cloud spots and radar echoes was only fair. Cloud-top contours using the THIR data would require detailed knowledge of the cloud emissivity, particularly in areas where cirroform clouds were present over large areas, as well as information about the vertical cloud distribution.

3) Comparisons between surface-shelter temperatures and the 11.5 micrometer temperatures from the THIR experiment as well as the ITPR-derived surface temperatures revealed that the radiometer temperatures averaged approximately 9°C warmer in the daytime and 4°C colder at night than the shelter temperatures. Although the differences were fairly uniform with temperature at night, during the daytime a large range of differences occurred. This observation remained basically true whether temperature data from scales of 1:10,000,000 or 1:2,000,000, or ITPR data were used. The differences did decrease, however, going from the 1:10,000,000 mapping down to the ITPR surface temperature determinations. The differences, however, were not unexpected since the air temperatures in the shelter are near the ground while the radiometers see the radiating ground surface itself.

4) On the basis of coincident time radiosonde data interpolated to

each ITPR sounding, it appears that derived temperature data from the Nimbus 5 radiance data is, in the mean, as accurate as would be expected on the basis of error in the present reduction technique. Minimum differences occurred from approximately 700 mb to 400 mb in the cases examined with the actual differences in this layer less than the standard error which would be expected on the basis of the individual errors in the reduction and comparison processes. Differences between the ITPR and RAOB data above 400 mb probably would have been less in this study than were found if all the ITPR profiles had been synthesized from the ITPR+NEMS+SCR data. As it was, some significant point differences occurred in the profiles where NEMS+SCR profiles were present.

5) Although temperature differences tended to be height dependent, differences at any one pressure level were large enough to induce significant temperature gradient errors in individual cross sections. This points out that although the mean difference of a collection of data may be small, there are still sufficient differences relating to specific features in a given cross section to influence horizontal temperature gradient determination.

6) Differences in temperature gradients on individual cross sections can be significant enough to greatly distort synthesized geostrophic wind profiles. In one of the cross sections examined in this study it was sufficient to induce a double jet core where none actually existed. Since a considerable amount of the major gradient differences occurred where abbreviated solutions were required by internal checks, such gradient differences and induced erroneous winds are probably likely in areas where significant weather exists.

7) In the cross sections examined in this study, the geostrophic wind developed from the ITPR data differed from the geostrophic winds developed from the radiosonde temperature data by an amount induced by the differences between the ITPR and RAOB data. In these particular cases, this finding is essentially required since ITPR spacing along the track was essentially the same as is found in the standard radiosonde network. Some significant wind differences were found when a fixed gradient distance over which temperature gradients were evaluated was used as opposed to gradient evaluation over actual station or sounding distances. Specific comparisons with actual wind data in the cross section were complicated by the fact that

geostrophic winds were computed while actual winds probably more nearly resemble gradient winds in their magnitude. Attempts to adjust actual wind to geostrophic wind using the gradient approximation indicated that cross-section computed geostrophic winds were at least reasonable.

8) Wind determination from the thermal wind buildup requires a tie-on or assumed wind somewhere in the profile. To avoid the accumulation of significant wind differences using a single tie-on wind, it seems logical to begin the buildup in the mid-troposphere under ideal conditions. In actuality, mid-tropospheric winds may not be known. It would seem that wind buildups and builddowns from wind vectors derived from cloud motions might possibly provide a worthwhile approach to arrive at a wind profile and wind cross section in data sparce areas.

REFERENCES

Allen, J. R., 1971: Measurements of Cloud Emissivities in the 8-13 μ Wave Band. J. Appl. Meteor., 10, 260-265.

Case, B. A., 1962: Root-Mean-Squar Error Analysis for Equations in Rawinsonde Evaluation Program. Report No. MTP-AERO-62-83, NASA Marshall Space Flight Center, Huntsville, Alabama, 40 pp.

Duncan, L. D. and M. Kays, 1974: Determining Nuclear Fallout Winds from Satellite-Observed Spectral Radiances. R. and D. Tech. Rept., ECOM-5529, Atmospheric Sciences Lab., U.S. Army Electronics Command, White Sands Missile Range, New Mexico, 16 pp.

Fuelberg, H. E., 1974: Reduction and Error Analysis of the AVE II Pilot Experimental Data. NASA Contractor Report CR-120496, Marshall Space Flight Center, Alabama, 140 pp.

Hodge, H. W. and C. Harmants, 1965: Compatability of United States Radiosondes. Mon. Wea. Rev., 93, 253-266.

Hubert, L. F. and L. F. Whitney, Jr., 1974: Compatability of Low-Cloud Vectors and Rawins for Synoptic Scale Analysis. NOAA Technical Report NESS 70, National Environmental Satellite Service, National Oceanic and Atmospheric Administration, U.S. Department of Commerce, Washington, D. C., 26 pp.

Lenhard, R. W., 1970: Accuracy of Radiosonde Temperature and Pressure-Height Determination. Bull. Amer. Meteor. Soc., 51, 842-846.

_____, 1973: A Revised Assessment of Radiosonde Accuracy. Bull. Amer. Meteor. Soc., 54, 691-693.

Poteat, K. O., 1973: A Comparison of Satellite-Derived Low-Level and Cirrus-Level Winds with Conventional Wind Observations. J. Appl. Meteor., 12, 1416-1419.

Platt, C. M. R., 1975: Infrared Emissivity of Cirrus-Simultaneous Satellite, Lidar, and Radiometric Observations. Quart. J. R. Met. Soc., 101, 119-126.

Scoggins, J. R. and R. E. Turner, 1974: Data for NASA's AVE II Pilot Experiment, Part I: 25-mb Sounding Data and Synoptic Charts. NASA Technical Memorandum TM X-64877, Marshall Space Flight Center, Alabama, 534 pp.

Shen, W. C., W. L. Smith and H. M. Woolf, 1975: An Intercomparison of Radiosonde and Satellite-Derived Cross Sections During the AMTEX. NOAA Tech. Report, NESS 72, National Environmental Satellite Service, National Oceanic and Atmospheric Administration, U.S. Department of Commerce, Washington, D. C., 18 pp.

Smith, W. L. and H. M. Woolf, 1974: An Intercomparison of Meteorological Parameters Derived from Radiosonde and Satellite Vertical Temperature Cross Sections. NOAA Tech. Report, NESS 71, National Environmental Satellite Service, National Oceanic and Atmospheric Administration, U.S. Department of Commerce, Washington, D. C., 13 pp.

Smith, W. L., H. M. Woolf, P. G. Abel, C. M. Hayden, M. Chalfant and N. Grody, 1974: Nimbus 5 Sounder Data Processing System; Part I: Measurement Characteristics and Data Reduction Procedures. NOAA Tech. Memorandum NESS 57, National Environmental Satellite Service, National Oceanic and Atmospheric Administration, U.S. Department of Commerce, Washington, D. C., 99 pp.

Togstad, W. E. and L. H. Horn, 1974: An Application of the Satellite Indirect Sounding Technique in Describing the Hyperbaroclinic Zone of a Jet Streak. J. Appl. Meteor., 13, 264-276.

NASA-Langley, 1976